Experimental investigation of timber-to-steel connection using self-drilling wing screws

Gowrava Mohanswamy

A thesis submitted in fulfillment of the requirements for the degree of

Master of Engineering

Main supervisor: Dr Zhiyuan (Arthur) Fang

Co-supervisor: Prof James Lim, Dr Kris Roy

School of Engineering

The University of Waikato

New Zealand

THE UNIVERSITY OF
WAIKATO
Te Whare Wānanga o Waikato

2024

Abstract:

Self-drilling wing screws are well-suited for hardwood and pressed material boards and are explored as an alternative connector to traditional bolts for connecting thick hot-rolled steel with timber. The wing avoids force-feeding of the screw into the timber which prevents the timber from cracking. However, limited studies were found on the timber-to-steel connection using self-drilling wing screws under shear loading. This paper investigates the shear behaviour and capacity of self-drilling winged screw connections between radiata pine timber and hot rolled steel plate through the experimental test. In addition, tensile coupon tests, screw bending tests, moisture content tests, screw pullout tests, and screw bearing tests were performed to determine the material properties of the steel, timber, and screws. A total of 70 experimental tests were conducted on the timber to steel connection connections with different steel thicknesses (8mm-20mm), timber thickness (15mm-45mm), numbers of screws (1-3), and screw axis angle (45°-90°). The failure mode is theoretically analyzed using Johansen yield theory. The resulting data from Eurocode 5 [24] was compared with experimental results as current AS/NZ standards lack adequate guidance in addressing timber-to-steel connections. From the above comparison, it was found that the Eurocode 5 [24] was under-conservative by 90%. Based on the experimental results, new design equations for calculating the shear capacity of self-drilling winged screws are proposed.

Keywords: Self-Drilling wing screw; Shear strength; MSG8 Radiata Pine H3.2; Hot rolled steel; Microscope; Digital Image Correlation; Single lap connections; Multiple screws; Screw axis; Euro-code 5.

Contents

List of Figures

List of table

Outline of the thesis

This thesis consists of seven chapters:

- Introduction – chapter 1 presents the background of steel-timber structural evaluation of connection methods used and the objectives of the study.
- Material Tests - chapter 2 describes the physical properties of the materials used in this study delivered from the performed material properties tests.
- Shear test setup and procedure - chapter 3 illustrates the testing methodology and procedure of self-drilling wing screws, in single shear connections for timber-to-steel arrangement.
- Steel-timber test results – chapter 4 provides observation during test and effect of parameters. Also, this chapter discusses the test's outcome together with the failure modes of the screw in timber to steel configuration.
- Comparative asswssments - chapter 5 provides a design comparision with Eurocode 5 and proposed design equations
- Conclusions and future study - chapter 6 provides conclusion of the current study and proposes some recommendations for future research.
- Acknowledgment – chapter 7.
- References – chapter 8.
- Appendix A. Shear test for single screw connection, Appendix B. Shear test for two screw connection, Appendix C. Shear test for three screw connection, Appendix D. Shear test for 110 mm length single screw connection screw connection, Appendix E. Shear test for incline screw connection, Appendix F. Eurocode 5 design equation, Appendix G Proposed design equation.

1 Introduction

1.1Yield Theory

1.1.1 *Introduction to Yield Theory*

The shear connection also known as the laterally loaded connection, is the load applied perpendicular to the length of the fastener. A key idea in materials science and engineering is yield theory, which focuses on understanding and predicting the behaviour of materials under stress. Its main goal is to determine the moment at which an object experiences irreversible deformation or yielding in response to external forces. When a material exceeds its yield strength under stress, it is said to have yielded, which results in profound changes to its structure or form.

1.1.2 Assumption of Yeild theory

Europe yield theory was 1st applied to timber fasteners by K.W. Johansen (1941). He assumed dowel connection strength depends on timber resistance to dowel bearing, and resistance of Dowel bending which he assumed that timber and dowel were ideally plastic under loading, the bearing strength of fasteners was dependent on the crushing strength of timber member and bearing strength varies with specific gravity of timber and load direction. The bending yield moment must also be determined to examine the process of screw lateral resistance forming in the metal-to-particleboard connection. Like the timber bearing strength, the fastener's bending yield strength is another important aspect that affects how screw plastic hinges form in timber connections. For conservative design practice, fastener friction and axial load could increase the effective load resistance, but all friction and axial load effects were ignored in Johansen’s theory. And there is no limitation on joint deformation. Based on these assumptions, Johansen used engineering mechanics approach to obtain the load capacity of the dowel connection formulations for both single- and double-shear joints. The basic assumptions in the generalized

Johansen's yield theory were the fundamental method which influencing fasteners lateral load prediction till now.

1.1.3 Yeild Failure Modes

Eurocode 5 classifies steel plates as thin plates with thickness lesser or equal to 0.5 times the screw diameter and steel plates of thickness greater than screw diameter. Based on metal thickness lateral connection failure mode has been defined:

Mode a: Localised crushing of timber.

Mode b: Single plastic hinge of fastener and localised crushing of timber.

Mode c: Uniform crushing of timber.

Mode d: Single plastic hinge of fastener and uniform crushing of timber.

Mode e: Localised crushing of timber with two plastic hinge of fastener.

1.2 Literature review

Self-drilling wing screws have gained increasing acceptance in the construction industry for connecting various composite constructions made of steel and timber. When comparing wing screws to traditional self-drilling screws, wing screws offer several advantages including ease of use, improved stability, and the elimination of the need for pre-drilling holes. However, when it comes to timber-steel connections, the design guidelines and structural behaviour of thick hot-rolled steel and timber are still not widely recognised.

Despite limited research on self-drilling wing screws for thin steel plates,[37] including in domestic, agricultural, and industrial constructions, their usage in linking steel components with timber offers a unique challenge and possible benefit.. This novel method tackles the requirement for effective and adaptable connections that may bridge the structural divide between steel and timber components. The primary focus in construction materials research has been on timber, concrete, and steel, typically studied separately rather than in combination.

Although timber-concrete composite buildings [38-39] have received considerable attention, there has been a noticeable lack of research on hybrid steel-timber composite systems. Timber and steel are two popular building materials extensively used in construction due to their unique advantages. Steel is known for its durability and high strength in tension it provides the necessary strength for long spans but timber on the other hand provides better aesthetics, is cost-effective, and high strength-to-weight ratio [1-3] but cannot be used for long spans due to its limitation [4,5]. Timber fiber orientation plays an important role in the transfer of load. The industry is utilizing timber-steel constructions, which blend the advantages of both materials. There is ample research in composite structures using timber [6-15] to improve bearing capacity. Other research has been conducted for timber-steel connections to examine the mechanical properties of these connections using various types of fasteners [17-20] and developed a design method for the strength predictions of steel-timber connections [21-23].

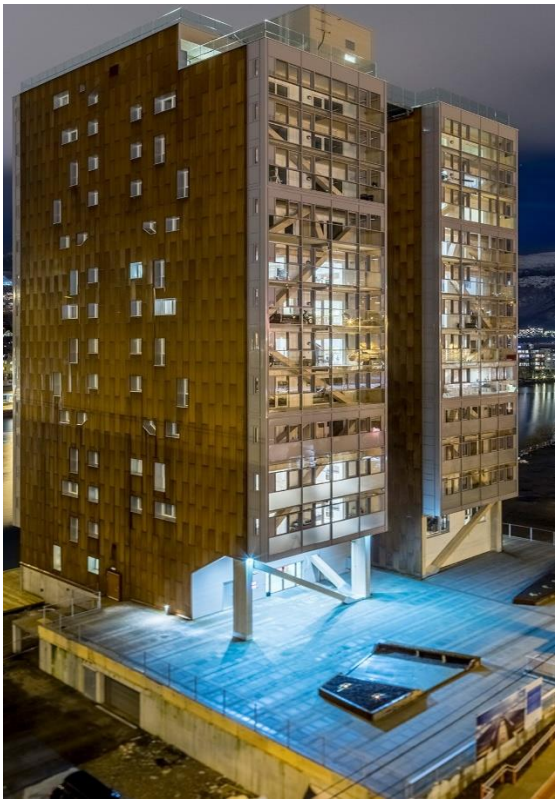

Figure 1 Treet—Timber tower apartment building in Bergen [16].

The most common way of joining timber to steel components is with self-drilling screws. Self-

drilling screws can be installed more quickly since they are typically also self-tapping, which eliminates the need for pre-drilled pilot holes or pre-tapping the steel element. The screws often have wings tips for screw installation from the timber side, which means driving the screw first into the timber and then into the steel because the wings are broader than the screw's threaded diameter, a pre-bored hole bigger than the screw diameter is created during installation, avoiding thread action between the screw and the timber material. Because the wings allow the screw to spin freely while drilling into the steel, there is no longer any chance that the screw tip breaks or timber bulges while drilling.

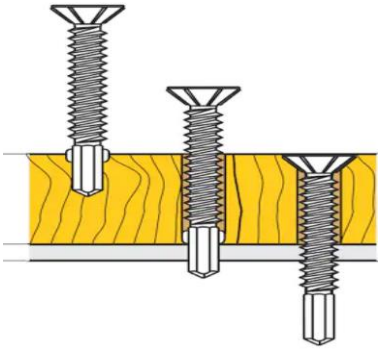

Figure 2: Self-drilling wing screw mechanism [35]

1.2.1 Shear Connection

There are studies on the shear behaviour of screw connections in steel-timber composite structures. Yang et al. [17] investigated steel H-section and timber, glulam. They highlighted the positive impact of increased bolt diameter on load-carrying capacity and the inverse relationship with bolt spacing and found that STC connections using SDS were 61% more ductile than connections using 6 mm bolts, and 55% more ductile than those using 8 mm bolts. Hassanieh et al. [18,22,45] used several connectors to connect steel-CLT and reported the failure mode and load-bearing capacity. Milewska [46] investigated the shear strength of connectors for power-actuated fasteners embedded into light gauge steel framing with various steel grades and gauges. 81 specimens of pined, overlapped connections were fabricated, and experimental tests were conducted using a single shear strength test method using a Universal

Testing Machine – Instron with 100 kN capacity to analyse shear connection strength and found that the capacity of the nailed connection is related to fastener diameter, steel plate thickness and steel sheet ultimate tensile strength and predominant mode of failure for all tested specimens were tiling and bearing, or head shearing induced by tilting of the fasteners. This result was utilized to numerically analyse shear strength using a tilting screw equation. Rogers et al. [47] investigated the bearing resistance of screwed connections that are loaded in shear and provided a summary of results detailing the behaviour of thin G550 and G300 sheet steel, single overlap, screwed connections and found that two different-thickness sheet steels are connected with screws, failure will probably result from bearing distress in the thinner of the connected elements and proposed method of analysis aims to provide a more accurate analysis of screw connections by considering the interaction of bearing and tilting failure modes. It introduces a gradated bearing coefficient that depends on the ratio of d/t [represents the ratio of the diameter of the screw (d) to the thickness of the sheet steel (t)], with the maximum and minimum values adjusted from existing standards. This approach is intended to improve the accuracy of predicting the behaviour of screw connections that are loaded in shear-predicted load resistance when two different-thickness sheets of steel are joined. Ng et al. [20] studied an experiment using plywood and Balau hardwood, and the thickness of the steel-1.2 mm, 1.6 mm, and 2.0 mm revealed that thicker cold-formed steel shifted failure modes from withdrawal to screw failure and the shear strengths obtained from experimental tests and Eurocode 5 [24] show that the Eurocode 5 is 7 % conservative for plywood and Balau hardwood specimens. Other research has been conducted on timber-steel connections to examine the mechanical properties of these connections using various types of fasteners [17-20] and developed a design method for the strength predictions of steel-timber connections [21-23].

1.2.2 Screw Arrangement

LaBoube and Sokol's research [48] on behaviour of screw connections in residential

construction investigated how the number of screws, group effect reduction, and screw spacing impact the strength of screw connections. Additionally, it was found that the strength per screw in a connection decrease as the number of screws in the connection increases. The decrease in strength is defined as the ‘‘Group Effect’’ reduction where connection strength did not increase as a direct multiple of the number of screws in a connection. That is, the strength of a connection with four screws is less than four times the strength of a similar connection with one screw. AS-1720.1-2010 [49] specifies limits on the spacing between the centre of the fastener in connection to not less than 3-times the outer diameter of the screw as spacing of screw less than 3-times the outer diameter of the screw caused the head of the screws to come very close to each other. Laboube and Sokol's research [48] on the effect of spacing showed that 3 times the outer diameter of screw spacing connection has greater connection strength than 2 times the outer diameter of screw connection spacing. Lu et al. [50] investigated the shear bearing capacity of self-drilling screw group connections of CFS sheets experimentally with 237 tests using G550 to verify the new design equation proposed which can be used to calculate the nominal shear capacity of self-drilling screw group connections, including high-strength steel such as G550 CFS sheets and the new design equation's unsafe rate is only 4.42%. Roy et al. [51] experimentally studied the screw pattern of self-drilling screw connections for high-strength cold-formed steel using G550 and CFS plates with 12- and 14-gauge screws. In studies, it was observed the connection strengths of the screw patterns for 3, 4, and 5 screws are 5.95%, 1.52%, and 3.91% lesser when compared to the number of screws. Screw arrangement does contribute to the connection strength. Further investigation on steel-timber screw arrangement helps us to determine connection strength which can be utilized as part of industrial practice.

1.2.3 Current Design standards

NZS 3603 [29] lays forth specifications and principles for the planning, designing, and

constructing of timber buildings and structures. Standard in section 4 discusses the design of fastener connections, such as bolts, screws, nails, and proprietary fasteners, between timber members and other materials like steel. It is important to note that NZS 3603 section 4.3 does not cover all types of fasteners, such as self-drilling winged screws. Similarly in Eurocode 5 [24] section 8.2.3 specifies the characteristic load-carrying capacity of Steel timber connection for screws, but no studies have been conducted for self-drilling winged screws. Lack of equations and formulae to evaluate the structural properties such as strength, stiffness, and deformation capacity from the current design standards for the timber to steel type connections, prevent structural engineers from specifying self-drilling winged screws in their designs.

Eurocode 5 estimates the design strengths of steel-timber screwed connections for different failure modes, as illustrated in the below figures. These estimates can be derived from Equations 1(a-e) from the Eurocode 5 [24], which are presented below:

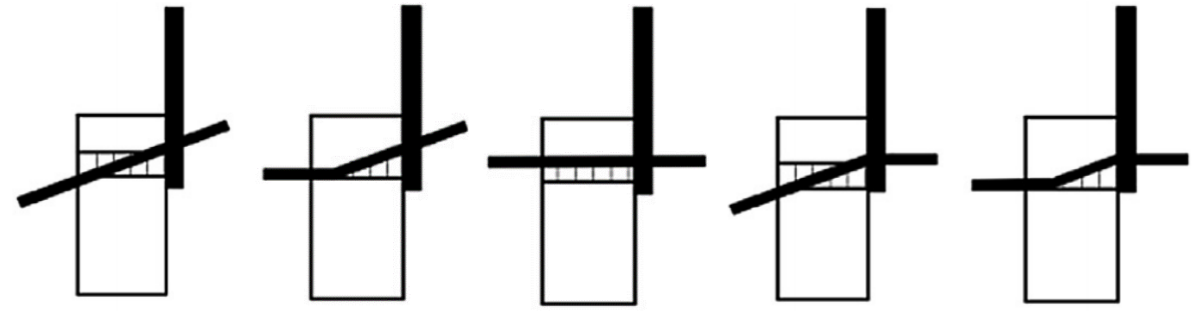

(a) (b) (c) (d)(e)

Figure 3 Failure modes from the Eurocode 5 [24]

$$F_{v,Rk} = \begin{cases} 0.4 f_{h,k} t_1 d \text{(a)} \\ 1.15\sqrt{2 M_{y,Rk} f_{h,k} d} + \frac{F_{ax,Rk}}{4} \text{ (b)} \\ f_{h,k} d t_1 \text{(c)} \\ f_{h,k} d t_1 \left[\sqrt{2 + \frac{4 M_{y,Rk}}{f_{h,k} d t_1^2}} - 1\right] + \frac{F_{ax,Rk}}{4} \text{(d)} \\ 2.3\sqrt{M_{y,Rk} f_{h,k} d} + \frac{F_{ax,Rk}}{4} \text{(e)} \end{cases} \quad (1)$$

$$F_{ax,\alpha,Rk} \begin{cases} f_{ax,k} d t_{pen} \\ f_{head,k} {d^2}_h \end{cases} \quad (2)$$

$$f_{ax,k} = 20 \times 10^{-6} \rho_k^2 \quad (3)$$

$$f_{head,k} = 70 \times 10^{-6}\rho_k^2 \quad (4)$$

$$M_{y,Rk} = 0.45 f_u d^{2.6} \quad (5)$$

$$f_{h,k} = 0.082(1 - 0.01\mathrm{d})\rho\mathrm{k} \quad (6)$$

In the above equation, t_1 is the smaller penetration depth value or timber thickness. f_{hk} is the characteristic embedment strength. The characteristic density of timber is displayed as ρ_k. $M_{y,Rk}$ is the characteristic yield moment of the screw. $f_{head,k}$ is the characteristic head side pull-through strength. d_h is the nail head diameter. t_{pen} is the point side penetration length. Diameter of screw d. $f_{ax,k}$ is the withdrawal strength perpendicular to the grain direction. For a laterally loaded screw, load carrying capacity is calculated using effective diameter d_{ef} taken as 1.1 times the treaded root diameter[24].

1.3 Advanced technology in connection testing using DIC and microscope

Researchers use modern techniques to observe internal damage with different approaches:

(a) High resolution photography: Failures in steel are captured using high-resolution photos, which reveal localized stress concentrations. Microscopic images display the patterns of damage progression for different steel and timber thicknesses. [40-41]

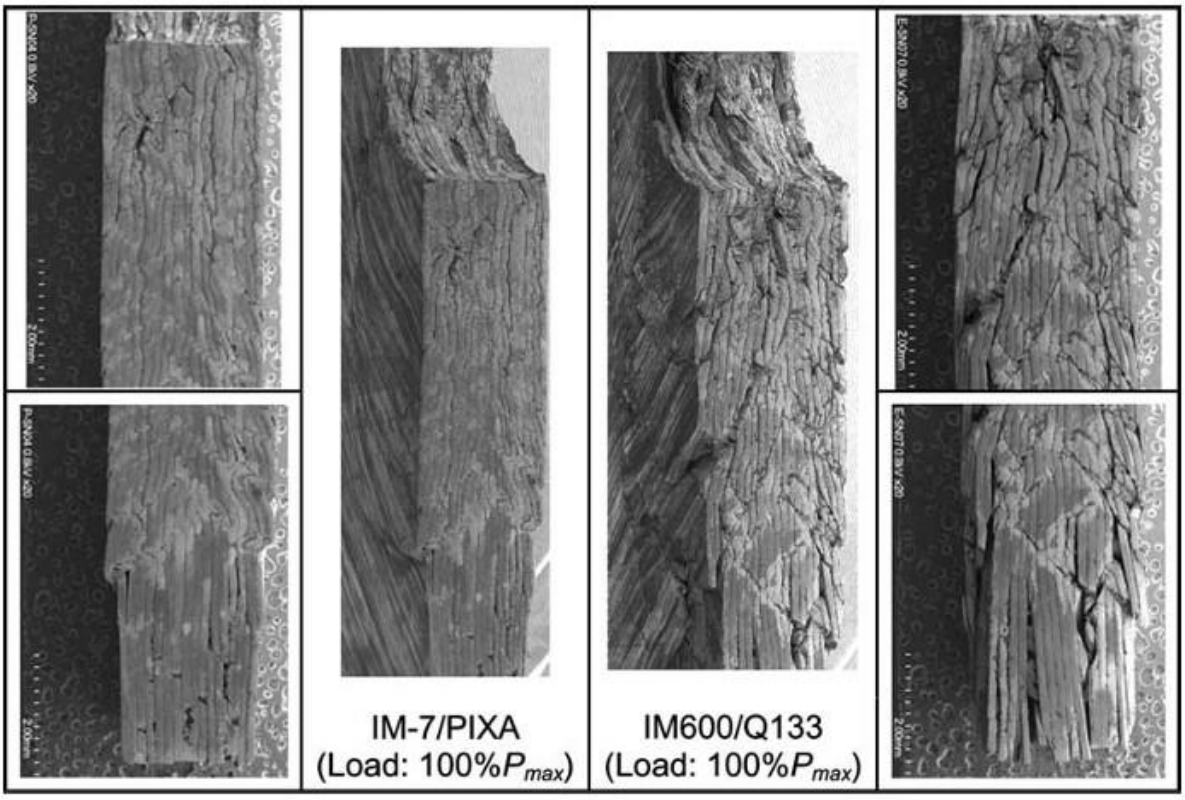

Figure 4 High-resolution photography of through thickness bearing damage, tested at 100% of maximum load.[40]

(b) Digital Image Correlation (DIC): Local damage in timber is identified using digital image correlation techniques, allowing researchers to examine its influence on the overall joint response [42-44]. Digital Image Correlation (DIC) is a commonly used optical technique in the field of experimental mechanics. Its purpose is to obtain a detailed understanding of the behaviour of materials. It does not serve as a standard for design but instead functions as a means of assessing or quantifying. European standards providing design advice. The outcomes of DIC analysis comprise strain maps that provide useful insights into the mechanical behaviour of materials under external stresses.

By combining high-resolution photography, DIC, and microscopic observations, researchers can gain a comprehensive understanding of the behaviour of connections under stress.

1.4 Research problem

In the current market, bolts are widely used for composite connections. However, this method is labor-intensive and time-consuming. Additionally, bolts often cause damage to timber surfaces during predrilling or bolt tightening. This drawback can be mitigated by using self-drilling wing screws, which eliminate the need for pre-drilled holes. This study investigates the use of self-drilling wing screws in timber to high-strength structural steel-to-timber connections.

This study investigates the use of self-drilling wing screws in timber to high-strength structural steel-to-timber connections. This approach reduces the risk of timber damage and decreases the time required for installation. Specifically, the novelty of this research lies in demonstrating that the investigated screws can be effectively used for thick hot-rolled steel, even when drilled manually. Such investigations for connections in timber-steel and steel-steel are currently lacking.

Current NZS 3603 [29] section 4 provides the design of fastener screws as general but no studies have been conducted for self-drilling winged screws. Lack of equations and formulae to evaluate the structural properties such as strength, stiffness, and deformation capacity from the current design standards for the timber to steel type connections, prevent structural engineers from specifying self-drilling winged screws in their designs.

The primary aim is to examine the structural behaviour of timber when connected to steel through self-drilling wing screw connections. This will involve analyzing the properties and composite systems of the three main components: timber, steel, and screw connections. The study will focus on various screw-connected material compositions, such as group screw connections, and will evaluate these connections according to both American and European guidelines [24,26-34].

2 Material Tests

2.1 Introduction

The material properties of steel, timber, and self-drilling wing screws were determined by conducting a series of material tests. These components were used to fabricate and test steel-timber connections in which the steel and timber geometry, screw type, inclination and number of screws were varied. All tests were carried out in the laboratory at the University of Waikato. Detailed information is provided in the sections below.

2.2 Material property of steel

For steel, three repetitive tensile tests were conducted per ASTM E8-21 [36]. The test steel coupons were extracted from a steel plate of 12.0 mm thickness as shown in Figure 4 the coupons of size 2.0 mm width, 2.0 mm thick, and 19.6 mm gauge length were prepared using Wire EDM. Tensile tests were carried out on a 50 kN Instron machine under displacement/force control at a displacement/loading rate of 1mm/min. Figure 6 and Table 1 present the stress-strain response and the main mechanical parameters for each tested coupon, such as the yield strength (σ_y), the ultimate tensile strength (σ_u), and the elongation at fracture (ε_f).

Table 1 Material property of steel

Steel coupon	Yield strength σy (MPa)	Tensile strength σu (MPa)	Elongation at fracture εf (%)	Average yield strength σy (MPa)	Average tensile strength σu (MPa)	Average elongation at fracture εf (%)
SC-01	422.88	565.53	12.11			
SC-02	445.60	569.02	16.7	433.66	568.23	14.77
SC-03	432.5	570.13	15.5			

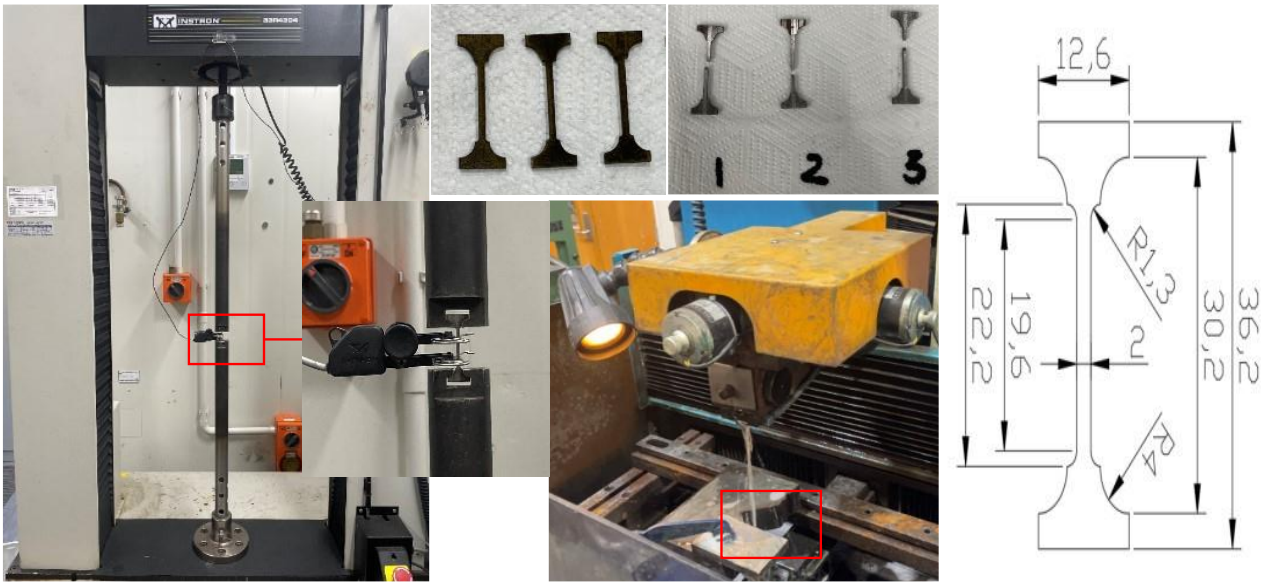

Figure 5 Steel coupon sample preparation.

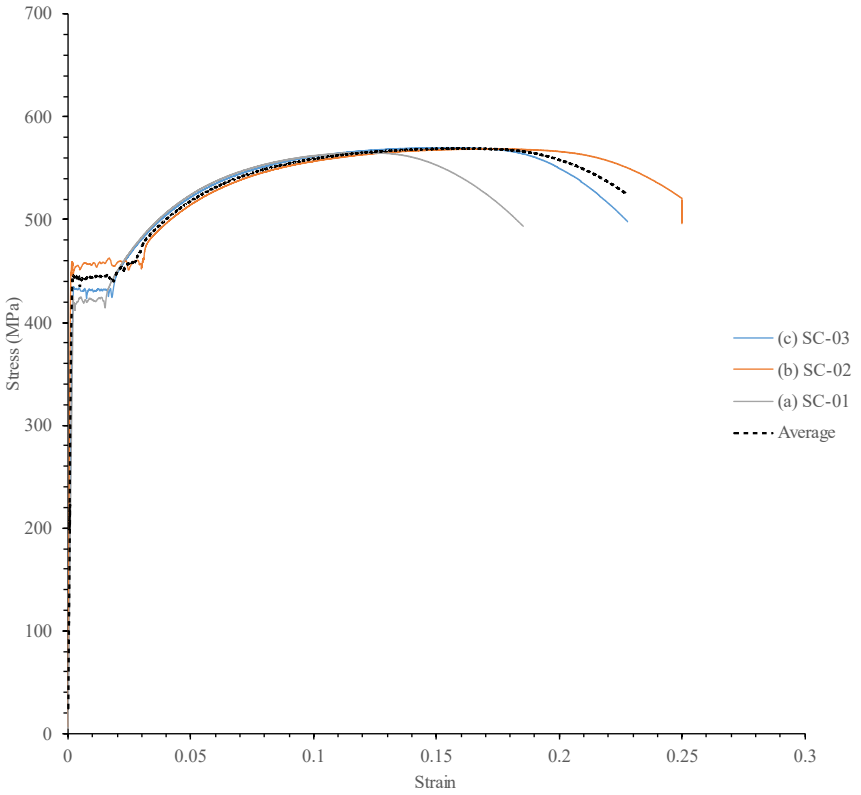

Figure 6 Stress-strain graphs for steel plates used in the experiments.

2.3 Material property of timber

For the steel-timber connection, grade SG08 [29] radiate pine timber was considered for the steel-timber connections. The nominal material properties of SG08 radiate pine timber according to NZ3404 [29] are elastic modulus 8 GPa, bending strength 14 MPa, tensile strength 6 MPa, and compressive strength 18 MPa, respectively. The dry density and moisture content of the specimens were determined by moisture content test in accordance with ASTM D2395-17 [27] as shown in Figure 7 the measured average density and moisture content were 494.97 kg/m^3 and 9.07%, respectively.

Figure 7 Moisture analyzer with test samples.

Table 2 Moisture content and specific gravity of timber

Test Number	Length (mm)	Width (mm)	Thickness (mm)	Weight before (g)	Weight after (g)	Moisture content %
1	50.33	49.52	5.11	6.58	5.95	9.56
2	50.33	49.06	5.22	6.59	5.93	10.1

3	50.43	49.38	5.04	6.33	5.74	9.31
4	50.18	50.26	5.23	6.46	5.96	7.74
5	50.14	49.35	5.25	6.10	5.56	8.77
6	50.42	49.73	5.07	6.53	5.99	8.27
7	50.27	49.53	5.34	6.50	5.92	8.93
8	50.16	49.38	5.30	6.10	5.49	9.89
					Average	9.07

2.4 Material property of screws.

The Self-drilling wing screw with a countersunk milling head had a screw diameter of 6.3 mm, a length varying from 80-130 mm, and a screw head diameter of 20 mm, as illustrated in Figure 8.

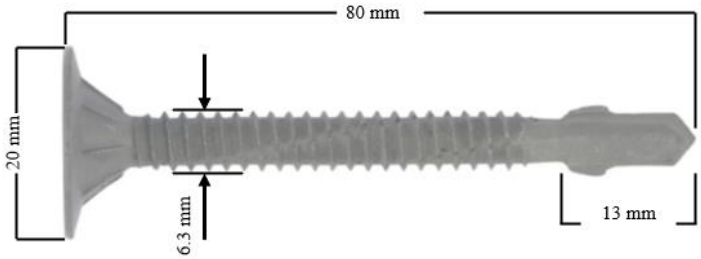

Figure 8 Self-drilling wing screw dimension [35].

Figure 9 provides the stress v/s strain response showing three curves representing Specimen 01, 02, and 03 and their behaviour characterized by elastic and plastic regions, as expected. Each curve exhibits initial elasticity, followed by plastic deformation until failure. The x-axis represents strain, and the y-axis represents stress (in MPa). The stress was evaluated by dividing the machine load in N to the cross-sectional area in mm^2, and the strain was calculated by screw length and elongation in mm.

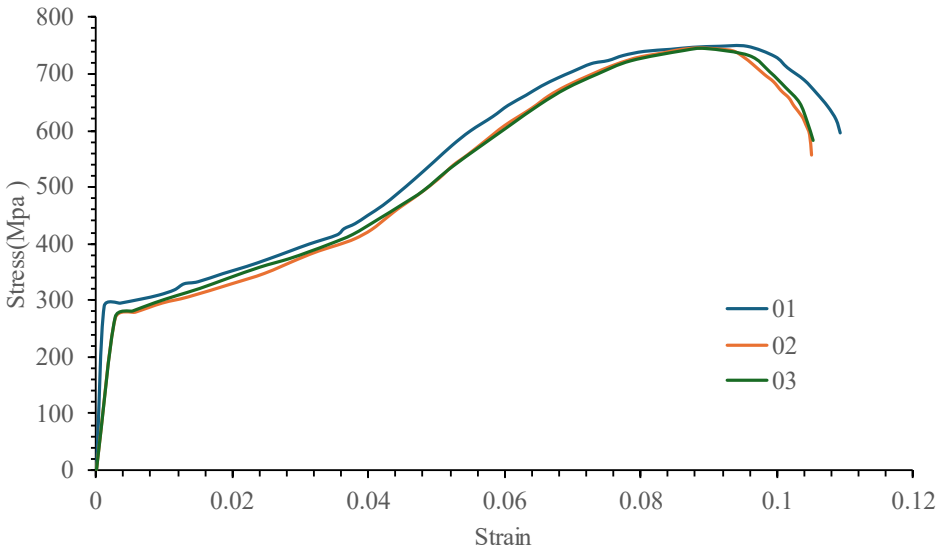

Figure 9 Stress v/s strain graph for screw tensile test

2.4.1 Screw Shear Test

Screw shear was carried out in accordance with DIN EN ISO 6892-1 [31] by Wurth company on a self-drilling wing screw for a screw of 6.3 mm diameter and the peak load in shear and tension is displayed in below Table 3.

Table 3 Summary of measured 6.3 mm nominal diameter self-drilling screws shear capacity.

Number of tests	Ultimate shear force, P_u (kN)	Mean Ultimate shear force, P_u (kN)
1	13.2166	
2	13.0026	
3	12.5900	
4	12.6392	13.0726
5	13.1611	
6	12.9919	
7	13.2651	
8	13.7146	

Figure 10 Testing of screw shear capacity

2.4.2 Screw Tensile Test

Screw tensile capacity was carried out in accordance with EN10002 [30] by Wurth company on a self-drilling wing screw for a screw of 6.3 mm diameter and the peak load in shear and tension is displayed in below Table 4.

Table 4 Summary of measured 6.3 mm nominal diameter self-drilling screws tensile capacity.

Number of tests	Ultimate tensile force, F_m (kN)	Mean Ultimate tensile force, F_m (kN)
1	23.1398	23.3873
2	23.4226	
3	23.2434	
4	23.6176	
5	23.3468	
6	23.4514	
7	23.4514	
8	23.4260	

Figure 11 Testing of screw tensile capacity

2.4.3 Screw Bending Test

2.4.3.1 Screw bending test for 80 mm screw length.

A total of 14 screw bending tests were carried out for a fully threaded 80 mm screw length with a shank diameter of 5.2 mm in accordance with ASTM F1575 [32], the span length S_{bp} is 60 mm. The test was conducted at a constant rate of loading at 6.35 mm/min using a 5 kN load cell in a 100 kN Instron testing machine resulting in an average maximum bending moment of 27100 N.mm as shown in Table 5. Figure 13 represents the relationship between midspan load and midspan displacement. Multiple tests are represented by different lines, with an average indicated by a dashed line. Initially, there's a linear increase in load with displacement (elastic deformation), followed by a plateau representing the yield point and plastic deformation. The x-axis represents strain, and the y-axis represents stress (kN).

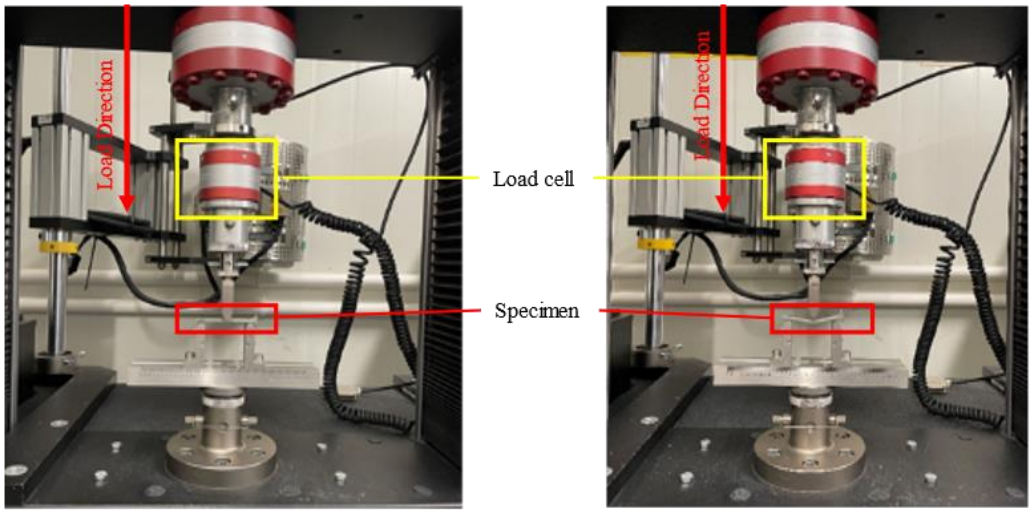

(a) Screw bending setup

(b) Post-testing of screw bending

Figure 12 Screw bending test result for 80 mm screw length.

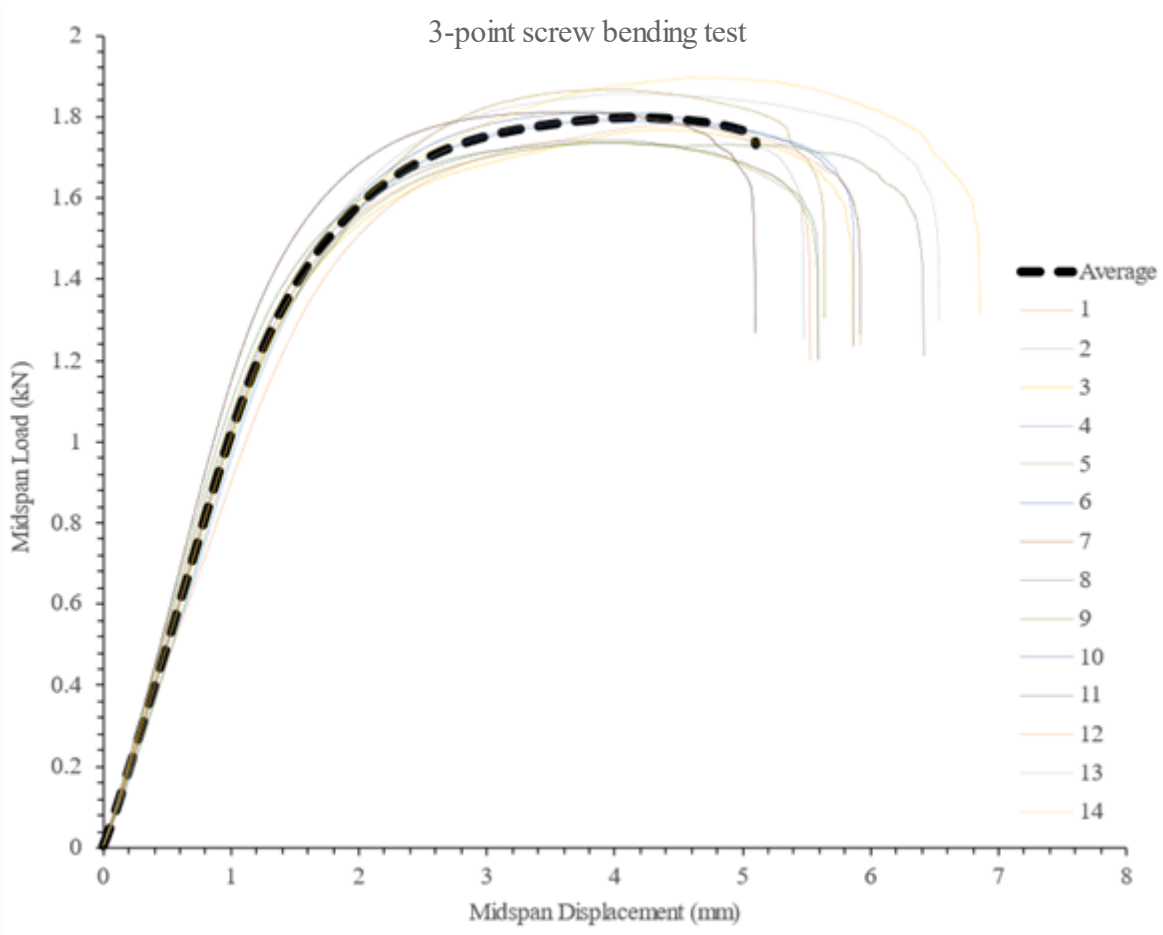

Figure 13 80 mm length screw bending load-displacement curve.

Table 5 Screw bending capacity for 80 mm screw length.

Test Number	Screw Diameter (mm)	Loading Rate (mm/min)	Bending Load (kN)	Displacement (mm)	Bending Moment (N.mm)
1	5.24	6.35	1.74	4.03	26100
2	5.20	6.35	1.80	4.04	27000
3	5.25	6.35	1.77	4.35	26550
4	5.20	6.35	1.79	3.99	26850
5	5.23	6.35	1.74	3.95	26100
6	5.19	6.35	1.80	4.12	27000
7	5.18	6.35	1.81	3.67	27150
8	5.24	6.35	1.74	3.81	26100
9	5.22	6.35	1.87	4.00	28050
10	5.18	6.35	1.81	3.97	27150
11	5.21	6.35	1.74	3.97	26100
12	5.2	6.35	1.95	5.74	29250
13	5.19	6.35	1.78	4.47	26700
14	5.17	6.35	1.86	4.08	27900
Average	5.20	6.35	1.81	4.19	27100
COV	0.02				0.03

Figure 14 Tested specimen for 80 mm length screw

2.4.3.2 Screw bending test for 110 mm screw length.

A total of 15 screw bending tests were carried out for a partially threaded 110 mm screw length with a shank diameter of 5.2mm in accordance with ASTM F1575, the span length S_{bp} is 60 mm. The test was conducted at a constant rate of loading at 6.35 mm/min using a 5 kN load cell in a 100 kN Instron testing machine resulting in an average maximum bending moment of 27100 N.mm as shown in Table 6. Figure 16 represents the relationship between midspan load and midspan displacement. As shown in the result bending capacity remains the same for both the length of screws within the engineering limit.

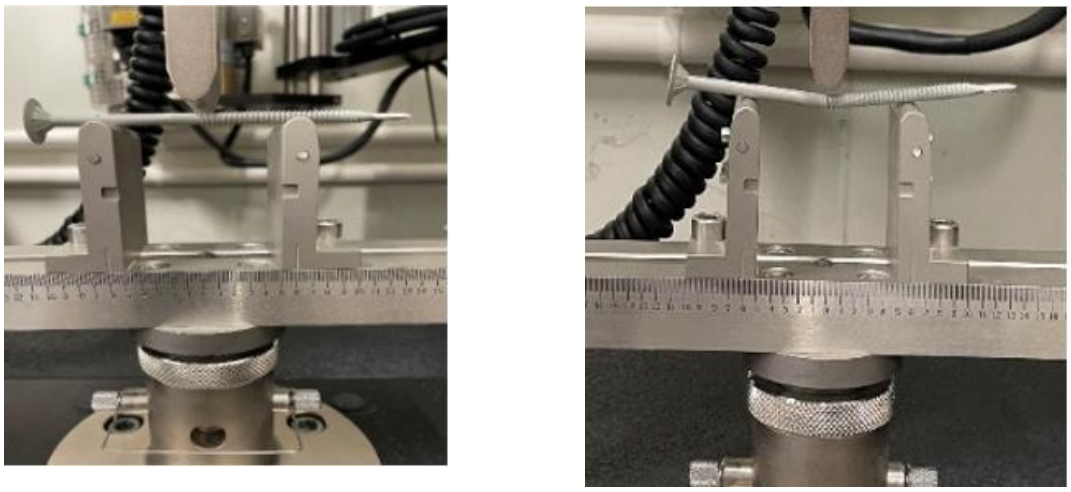

(a) Screw bending test setup (b) Bending failure of screw

Figure 15 Screw bending test for 110 mm screw length

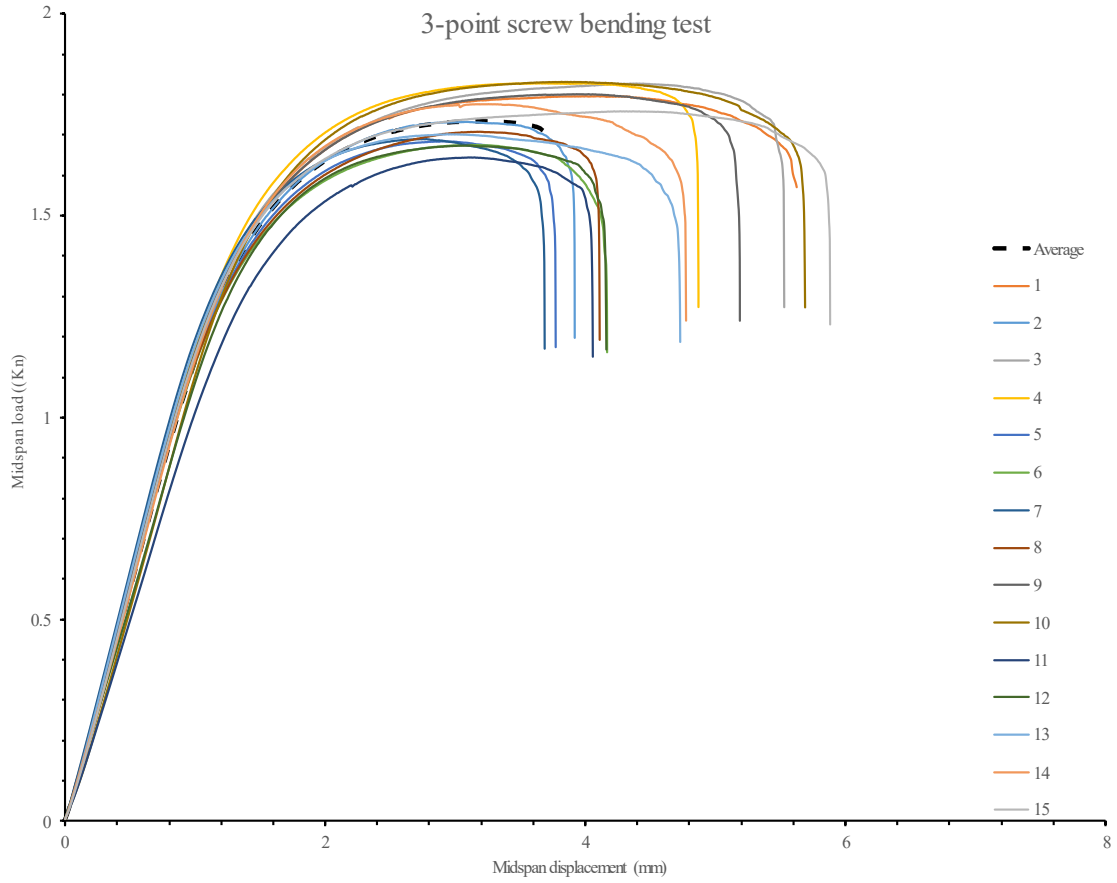

Figure 16 Load-displacement curves for 110 mm length screw from the bending test results

Table 6 Screw bending capacity for 110 mm screw length.

Test Number	Screw Diameter (mm)	Loading Rate mm/min	Bending Load (kN)	Displacement (mm)	Bending Moment (N.mm)
1	5.19	6.35	1.8	4.09	27000
2	5.2	6.35	1.73	3.09	25950
3	5.2	6.35	1.83	4.39	27450
4	5.19	6.35	1.83	3.99	27450
5	5.19	6.35	1.68	2.89	25200
6	5.2	6.35	1.68	3.12	25200
7	5.19	6.35	1.69	2.78	25350

8	5.19	6.35	1.71	3.17	25650
9	5.2	6.35	1.8	4.02	27000
10	5.2	6.35	1.83	3.82	27450
11	5.2	6.35	1.64	3.15	24600
12	5.2	6.35	1.67	3.11	25050
13	5.19	6.35	1.7	2.94	25500
14	5.2	6.35	1.78	3.26	26700
15	5.2	6.35	1.76	4.27	26400
Average	5.20	6.35	1.74	43.47	26130
COV	0.00				0.0378

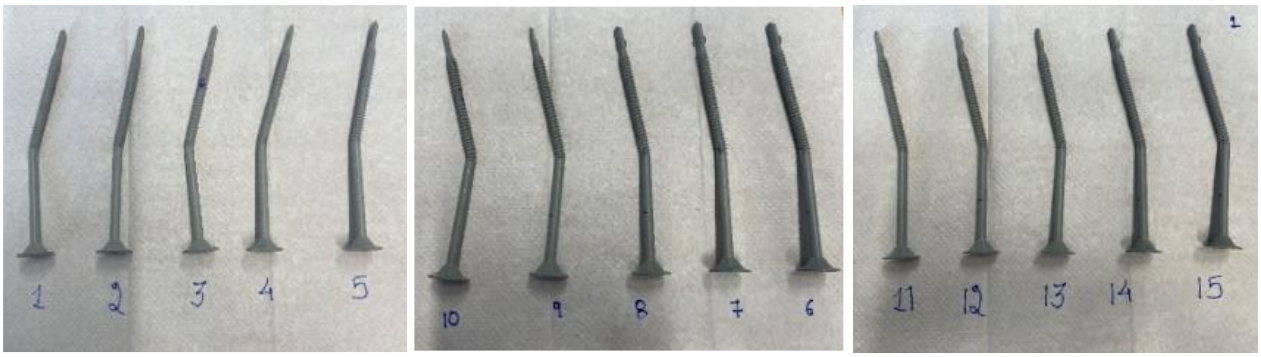

Figure 17 Bending failure of 110 mm screw length.

2.4.4 Screw Bearing Test

The bearing strength is one of the important system properties dependent on the characteristics of both the fastener and the timber material. The bearing test results determine the static load resistance and deformation of connections in timber and timber-based products resulting from applying a load transmitted by a fastener inserted. Ideal load-displacement curves are shown below in Figure 18.

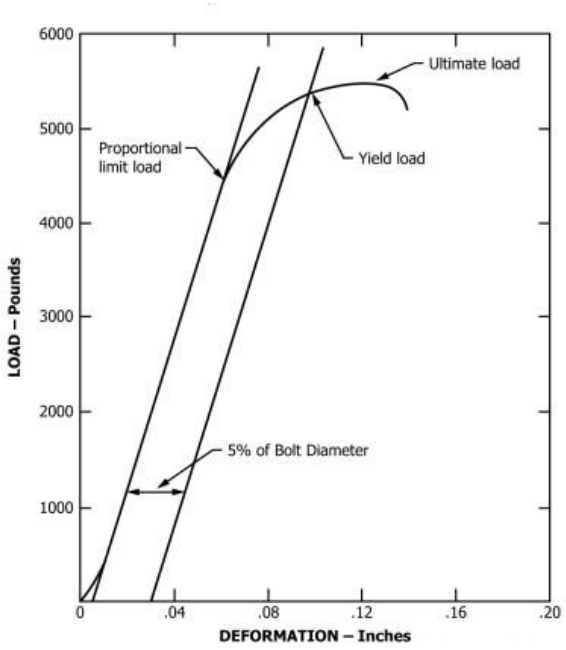

Figure 18 Definition of loads obtained from the load-deformation curve [34]

The screw bearing test was carried out in accordance with ASTM D5764-23a [34] for 3 timber samples with orientation positioned parallel to the grain direction. A half-hole configuration was used with a constant load rate of 1mm/min using a 100 kN Instron machine as shown in below Figure 19. The yield load and ultimate load are represented in Table 7. The load-displacement curve for specimens E1, E2, and E3 is shown in Figures 21, 22, and 23 respectively. For all the specimen yield load is calculated by fitting a straight line to the initial linear portion of the curve and the intersection at which the offset line equal to 5% of the fastener diameter intersects. The timber embedded strength is calculated using the max applied force (N), screw diameter (mm), and timer thickness (mm). Experimental results show that all the timber specimens failed due to localized crushing of timber by a screw with an average embedded depth of 5.62 mm.

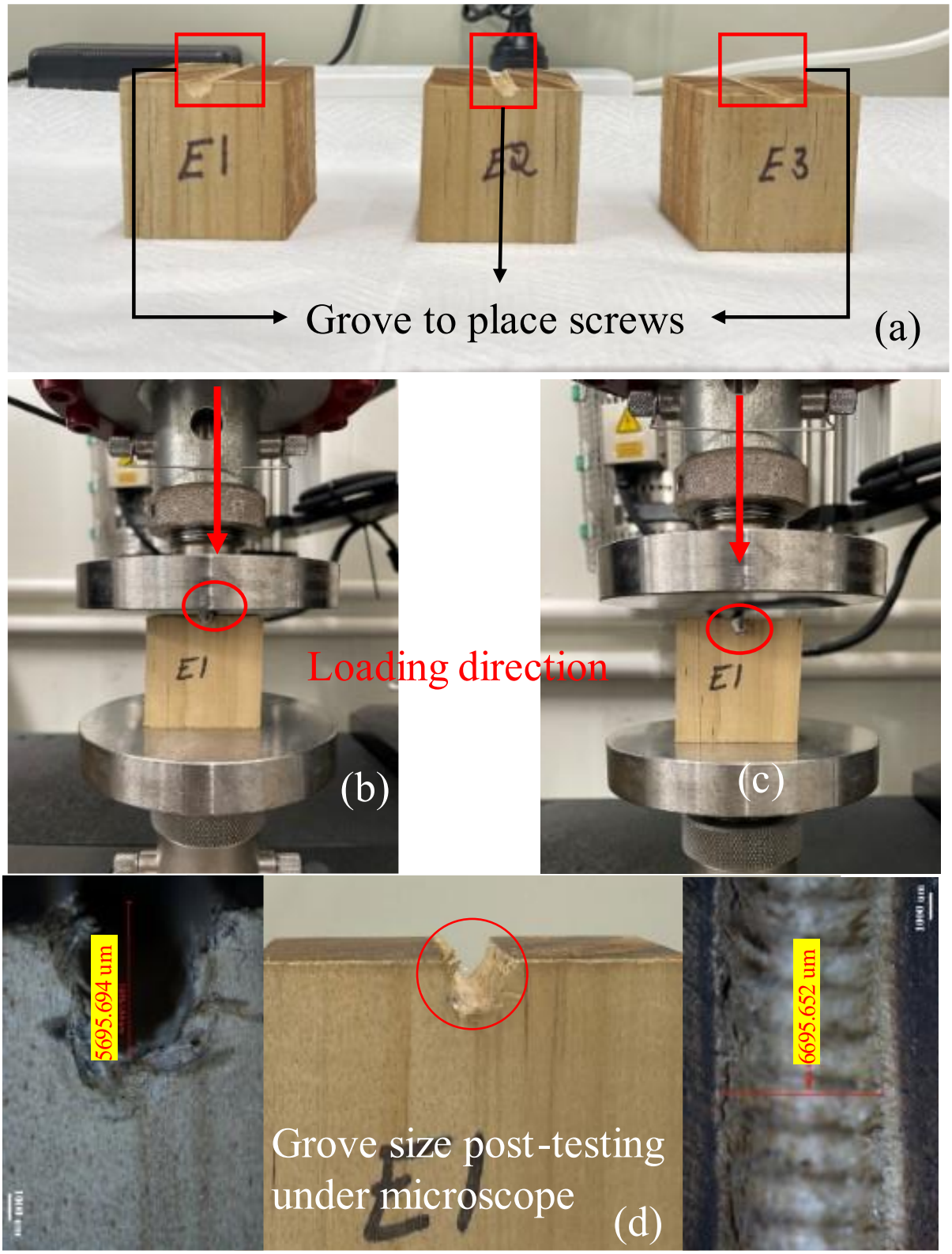

Figure 19 Screw bearing test

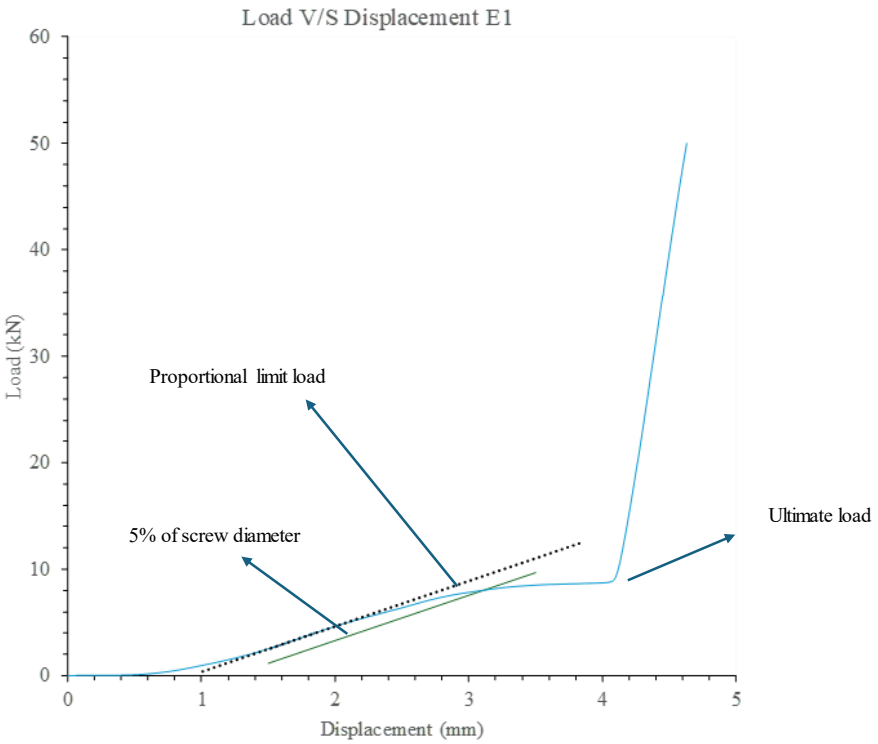

Figure 20 Load v/s displacement graph for specimen E1

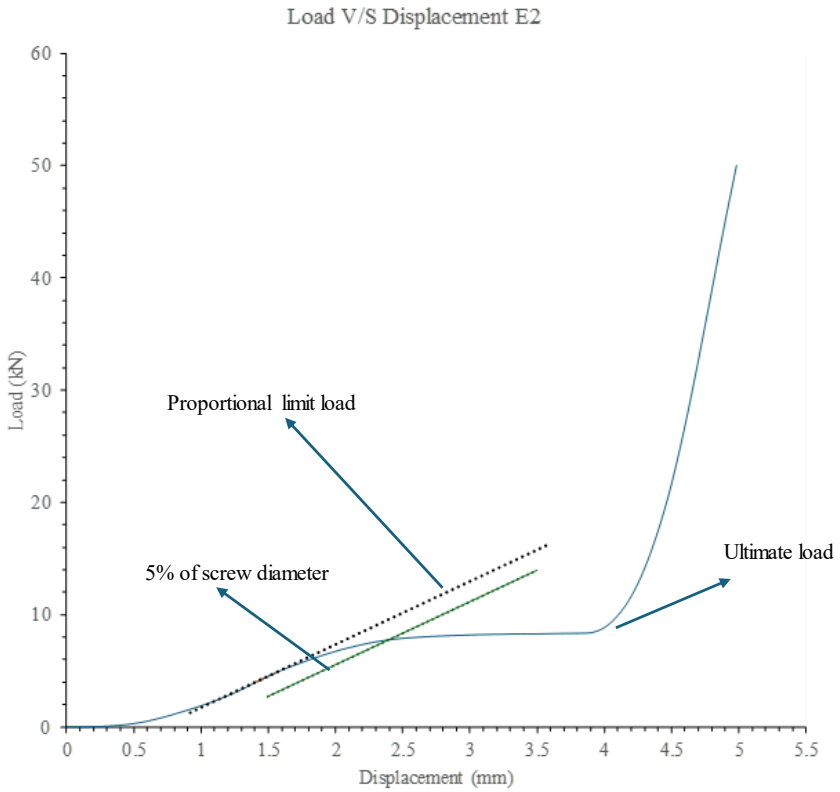

Figure 21 Load v/s displacement graph for specimen E2

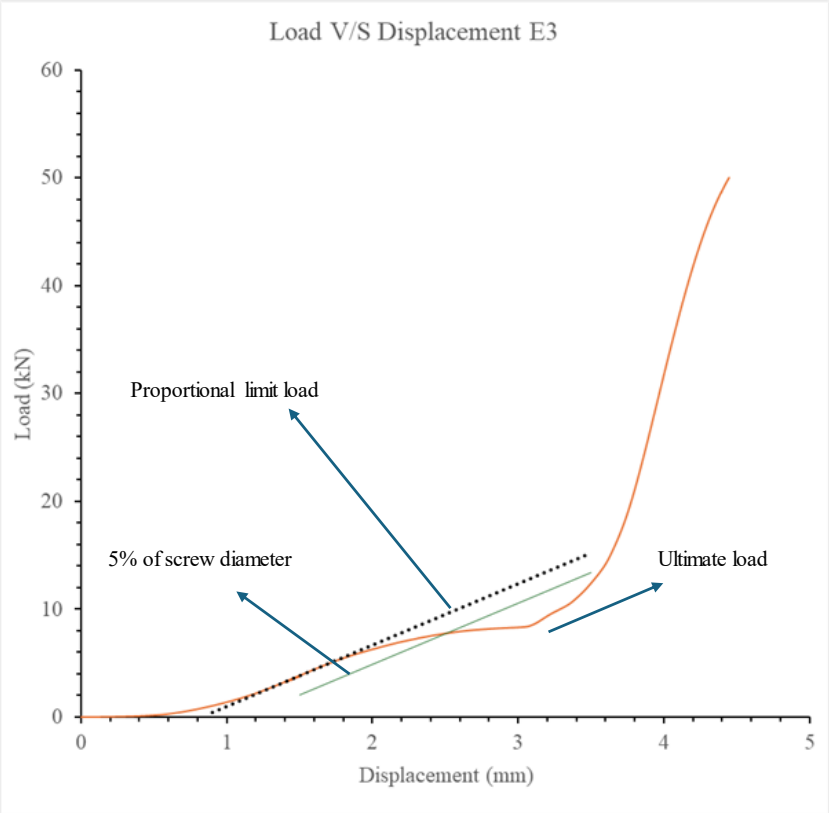

Figure 22 Load v/s displacement graph for specimen E3

Table 7 Screw bearing yield and maximum load.

Specimen	Yield load (kN)	Ultimate load (kN)
E1	8.02	8.91
E2	8.06	8.72
E3	7.77	8.43
Average	7.95	8.69
Standard Deviation	0.13	0.20
Embedded strength (MPa)	18.05	19.72

2.4.5 Screw thread withdrawal capacity.

The connection behaviour test between screw thread and steel was assessed through a series of withdrawal tests following ASTM-D1761-20 [33] for the steel thicknesses 12.0 mm, 16.0 mm, and 20.0 mm with 3 repetitive for each. The tests were conducted in a 100 kN Instron testing machine at a constant rate of 2.54 mm/min [33]. The load-displacement curve is

displayed in Figure 24 which was directly extracted from the instron and results are given in Table 8 . Initially there is a shallow stiffness due to the bolts in the attachment rigs. For steel thicknesses 16 mm, and 20 mm before screw pullout, the screw failed resulting in similar ultimate capacity.

Table 8 Ultimate load and corresponding displacement for different steel thicknesses.

Specimen No.	Maximum Force (kN)	Average Maximum Force (kN)	Displacement at Maximum Force (mm)	Average Displacement at Maximum Force (mm)
12mm-1	16.97		5.71	
12mm- 2	15.88	16.45	4.46	4.9
12mm- 3	16.49		4.53	
16mm-1	21.43		5.79	
16mm-2	21.80	21.59	8.58	6.57
16mm-3	21.53		5.34	
20mm-1	21.85		5.85	
20mm-2	22.02	21.69	5.55	5.50
20mm-3	21.18		5.11	

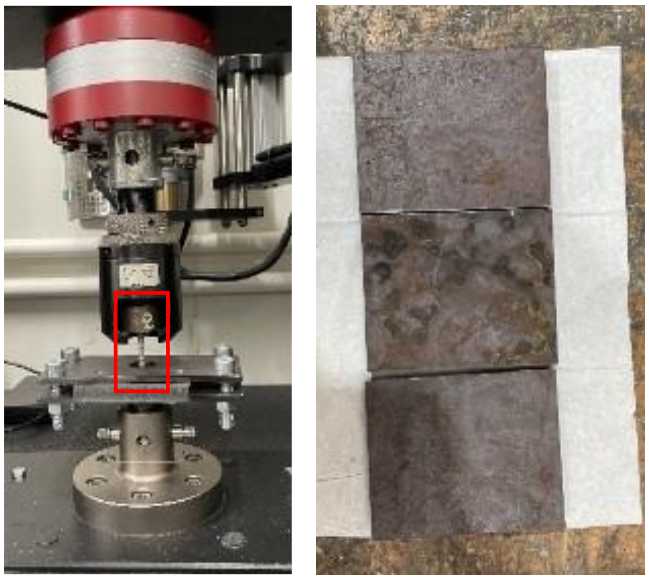

(a) Test setup (b) Test specimen under preparation

Figure 23 Test assembly of screw pullout test.

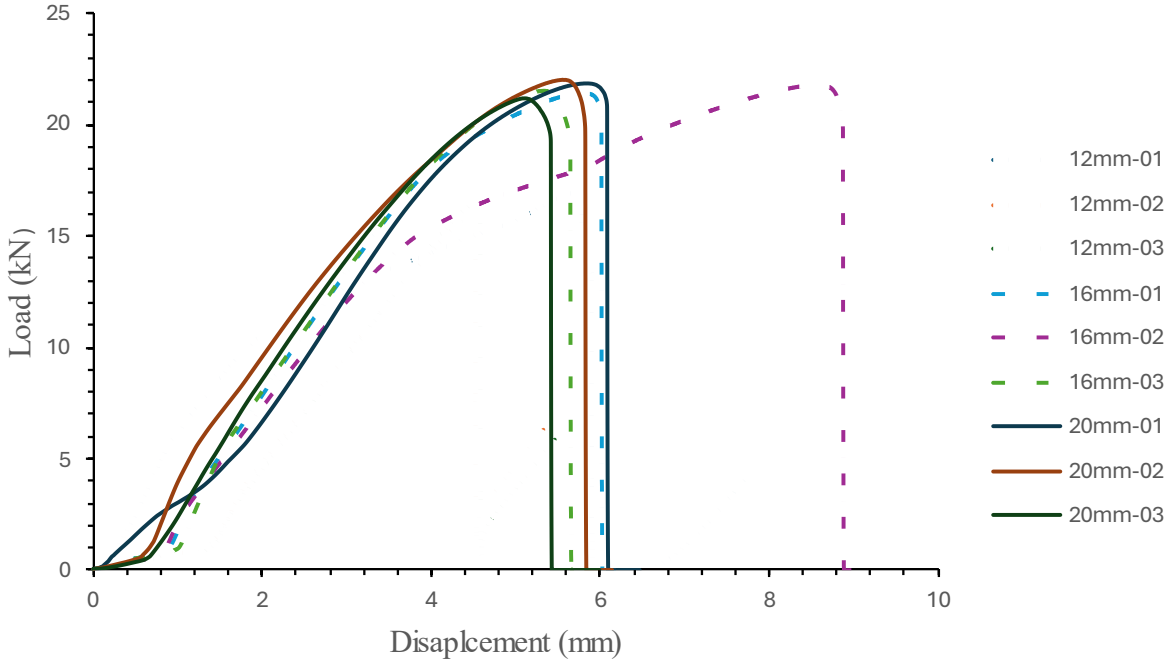

Figure 24 Screw pull-out load-displacement curve.

2.5 Summary

The objective of Chapter 2 was to confirm the material properties of all components of composite connection because the performance of the screw connections depends on the physical properties of the steel plate, screw, and timber.

3 Shear test setup and procedure

3.1 Introduction

The purpose of this chapter is to present the experimental investigation program for the shear strength of self-drilling wing screws in timber-to-structural steel. Shear tests were performed to investigate the design values of shear connections. The tests included a comprehensive set of combinations of different steel, and timber thicknesses in the most suitable configuration. An arrangement of the single lap joint with the screws was chosen to follow Eurocode 5 requirements for assessment and D1761 – 20 [33] for test verification.

3.2 Shear test

3.2.1 Specimen details

The shear tests were conducted on specimens incorporating structural steel and timber materials and screws described before. In all configurations, screws were employed to establish a connection between the timber and steel. The 6.3 mm diameter screw heads were aligned with the top of timber elements and the threaded part passed through the timber element. The screw was drilled into the composite structure keeping the screw head in contact with the timber. The parameters evaluated in the tests were: (i) timber thickness, (ii) steel plate thickness, (iii) number of screws, and (iv) screw inclination.

Three timber plate thicknesses were 20 mm, 40 mm, and 50 mm, whilst the length and width were 300 mm and 100 mm, respectively. The steel plates had four different thicknesses of 8 mm, 12 mm,16 mm, and 20 mm, and a length of 300 mm and a width of 100 mm. To evaluate the screw group effect, two to three screws were utilized as shown in Figure 25. For a single screw connection, the screw was positioned 100 mm from the end of the timber plate in the center of the lap joint. For a two-screw connection, two screws were positioned 60 mm pitch distance and 70 mm from the end of the timber, respectively, to ensure equal spacing. In three

screw arrangements, the screws were positioned equally (70 mm from the end of the timber and 50 mm from the center to the center as shown in Figure 25). For M16 bolts, which were used to connect to the rig, two predrill holes were made at a distance of 35 mm from one end (Figure 25).

The specimens are labeled according to steel thickness (8, 12, 16, 20 mm), timber thickness (15, 30, 45 mm), number of screws and then screw angle or length. For example, S08-T30-N1-45 indicates: S08 is for the steel with a thickness of 8 mm, T30 means timber with 30 mm thickness, N1 is one screw of diameter 6.3 mm, and 45 standards for a 45-degree angle. Two types of screws Type A and Type B were selected from the current new zealand market as shown in Figure 30.

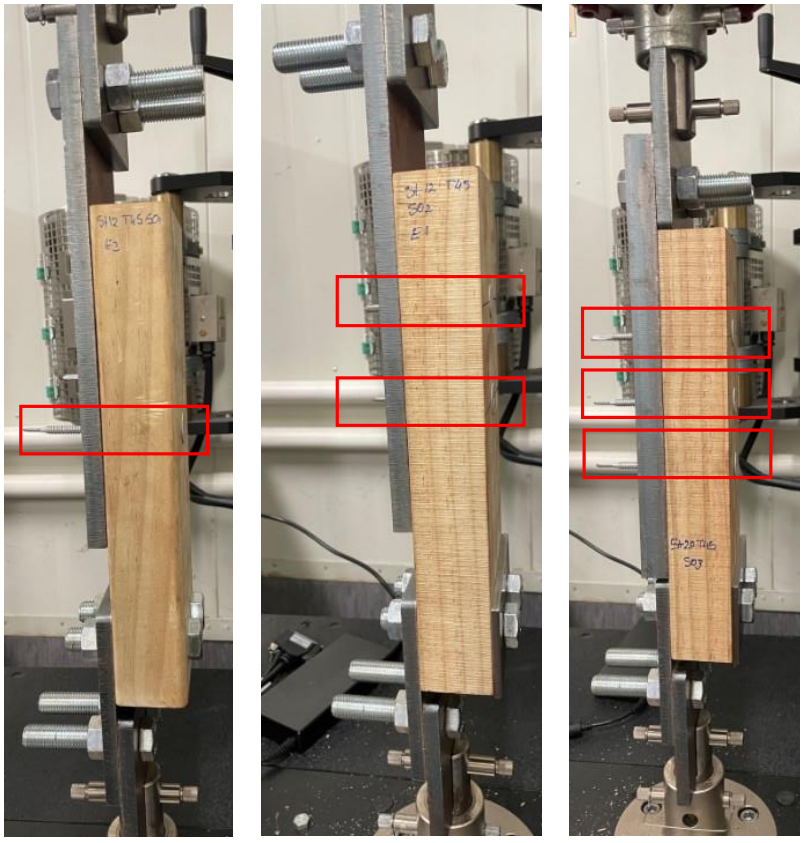

One screw Two screw Three screw

Figure 25 Screw arrangement

3.2.2 Testing arrangements and instrumentation

Two custom test rigs were constructed to replace the grips of the machine and to enable the test specimens to be bolted to the 100 kN Instron. The steel-timber specimens were fastened to the rigs using M16 bolts, in which the steel plate was connected to the top rig, while the timber panel was connected to the bottom test rig. A test specimen and schematic diagrams of the test rigs for the shear test are shown in Figure 26. In each test, the specimens were subjected to loading at a rate of 2.54 mm/min as per ASTM D1761-06 until failure [33]. The screw and loading cells of the Instron were aligned with the pulling axis. The tests were conducted in an Instron of 100 kN capacity and the ultimate capacity and corresponding displacement were obtained.

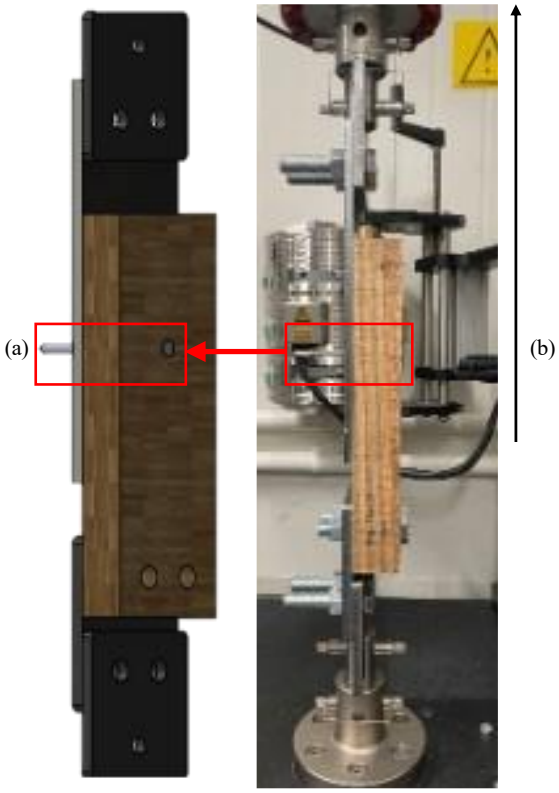

(a) Test screw specimen

(b) Load direction

Figure 26 Experimental test setup for Timbe to steel connection under shear.

Table 9 Test matrix

Type of test	Test group	Screw arrangement	Component	Position of the screw head
Shear	1	Single screw	Timber-Steel	Timber
	2	Multiple Screw	Timber- Steel	Timber
	3	Screw rotation	Timber- Steel	Timber

Figure 27 Test Samples post-sample preparation.

3.3 Digital Image Correlation (DIC) instrumentation

DIC was used to monitor the strain distribution across the surfaces of the specimens. Before data acquisition, the surfaces of the specimens were prepared by smoothing and cleaning them. Subsequently, a random black-on-white speckle pattern was uniformly applied to each face of the sample using opaque spray paint which forms an area of interest (AOI). The DIC system was calibrated following the specifications outlined for the VIC-3D calibration, using a calibration target of 10 mm spacing between the calibration dots. The cameras equipped with a lens of 35 mm focal length were adopted to acquire digitalized images. The sampling rate of the camera was set to be five images per second and was oriented towards the specimen

surfaces, in-plane (frontal). The location of this module was also determined by the recommended calibration distance to the timber specimen of thickness 15 mm, 30 mm, and 45 mm, resulting in an angle of 21.32°, 21.33°, and 25.59° between cameras with the precision error of 0.095%,0.099%, and 0.126%. Figure 28 shows the DIC setup with specimen assembly.

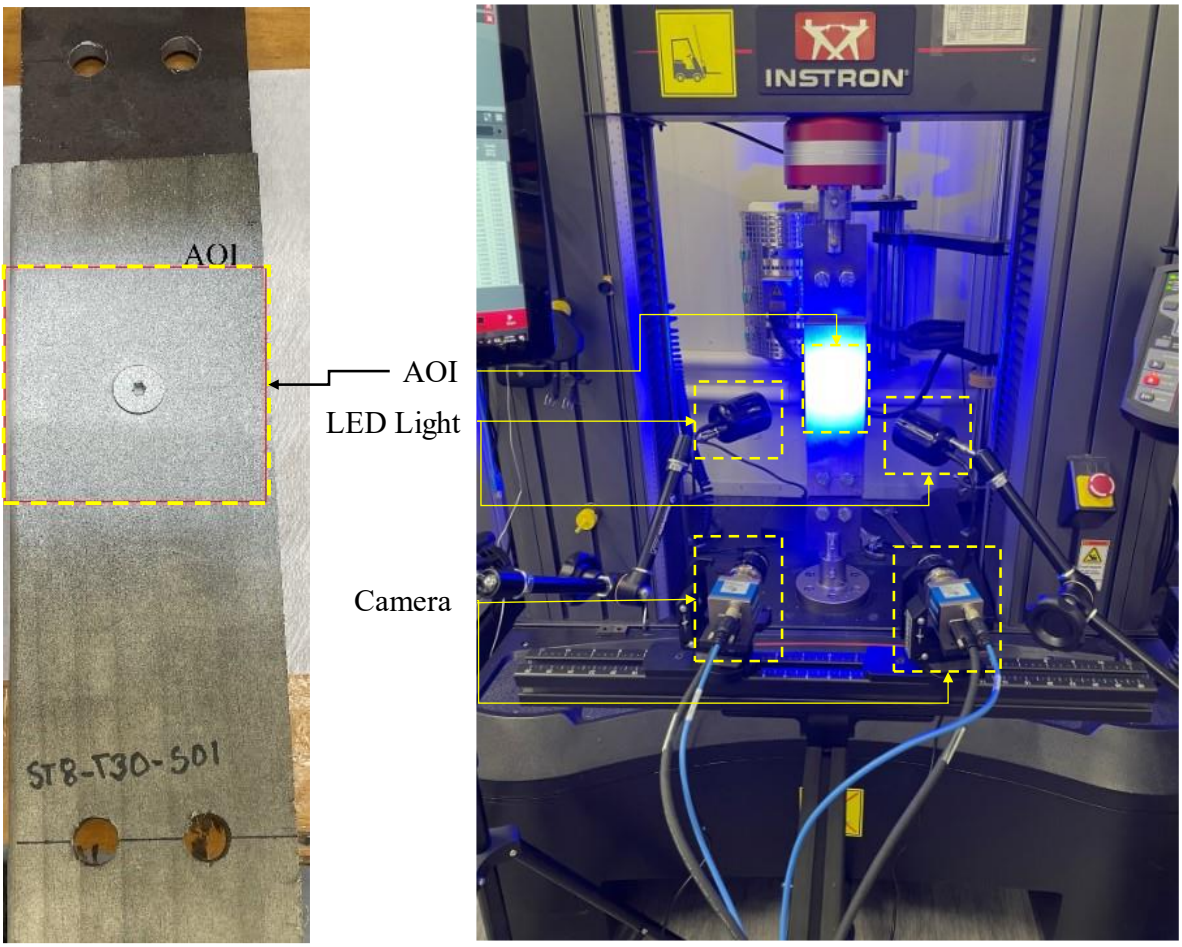

Figure 28: Preprocess of the samples and DIC test setup.

4 Steel-timber test results

This section presents the experimental investigation program for the shear strength of self-drilling wing screws in timber-to-structural steel. Shear tests were performed to investigate the design values of shear connections. The tests included a comprehensive set of combinations of different steel, and timber thicknesses in the most suitable configuration. An arrangement of the single lap joint with screws was chosen to follow Eurocode 5 requirements for assessment and D1761 – 20 [33] for test verification.

4.1 Influence of screw parameters

4.1.1 Screw length

To investigate the effect of screw length on shear capacity, the curve in Figure 29 shows the average response observed across three experiments conducted for each screw length. A 6.3 mm screw diameter was utilized for a steel thickness of 8 mm and timber thickness of 45 mm. Table 10 provides a summary of all test results for the maximum force (kN) and related displacement at maximum force (mm) values. The test findings indicated that the screw with a length of 80 mm had a force of 6.5 kN, while the screw with a length of 110 mm had a force of 6.47 kN. When comparing the total stiffness, it is observed that the 110 mm screw has a higher stiffness with a secant stiffness (k0,4) of 0.67 kN/mm, whereas the 80 mm screw has a stiffness of 0.53 kN/mm. However, during the experiment, it is observed that the initial stiffness of an 80 mm length screw is high, which decreases as the displacement increases. The fact that the screw's capacity remains unchanged indicates that varying the screw's length cannot affect the shear connection capacity

Table 10 Test results for different screw length

Sl. No.	Screw specimen of length 110 mm	Maximum Force (kN)	Displacement at Maximum Force (mm)	Screw specimen of length 80 mm	Maximum Force (kN)	Displacement at Maximum Force (mm)
01	S08-T45-N01	6.91	8.72	S08-T45-N01	6.11	12.7
02	S08-T45-N01	6.32	8.62	S08-T45-N01	6.96	11.96
03	S08-T45-N01	6.18	11.47	S08-T45-N01	6.42	11.97
	Average	6.47		Average	6.5	
	Standard Deviation	0.29		Standard Deviation	0.35	

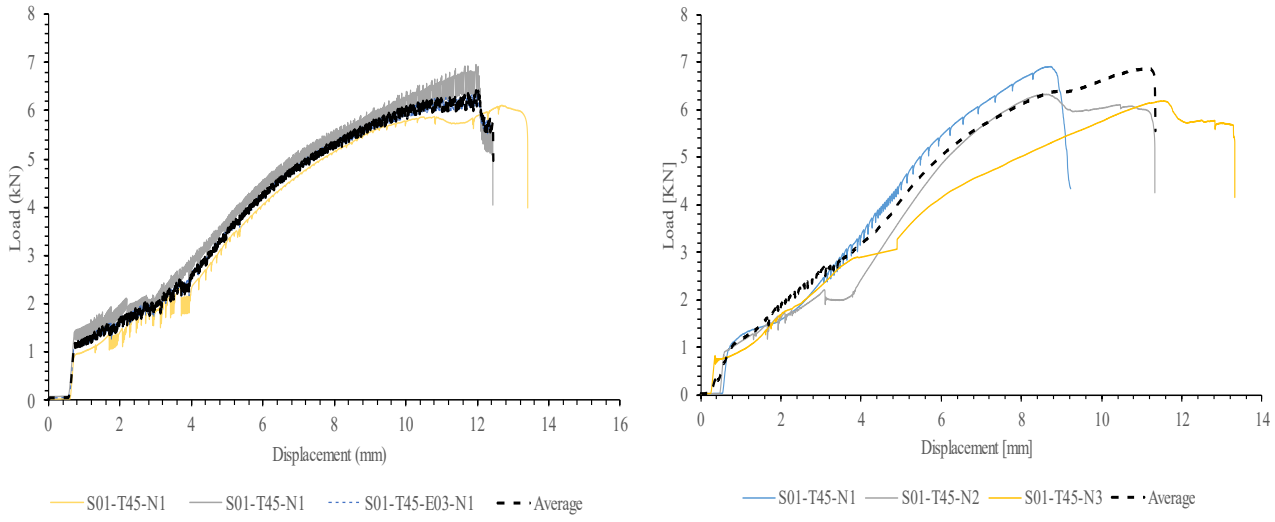

(a) 80 mm screw length

(a) 110 mm screw length

Figure 29: Average load v/s dispalcement curve for different screw length

4.1.2 Screw type

To examine the impact of different screws on shear capacity, the graph in Figure 31 illustrates the average results obtained from three separate experiments done for each screw. A screw with a nominal diameter of 6.3 mm was used for steel with a thickness of 8 mm and timber with a thickness of 45 mm. Table 11 presents a comprehensive overview of the test results for the Maximum Force (kN) values. The variability in the screw type can impact the shear connection capacity, as shown in this scenario the capacity increases by 60% for Type A screws when compared with Type B screws. It is observed that Type A screws are less ductile and more stiffer than Type B screws.

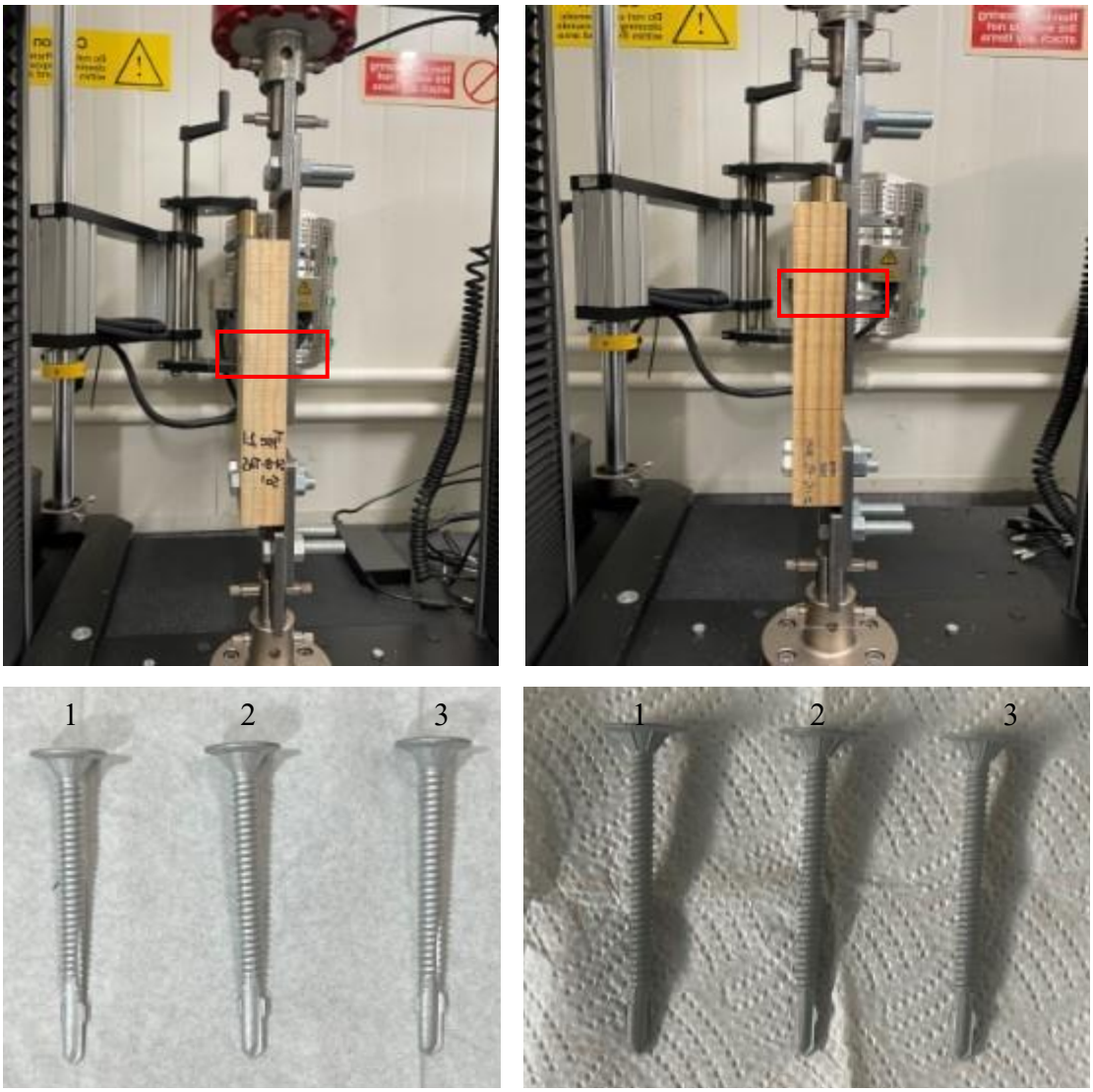

Figure 30 Different types of 6.3 mm screws

.

Table 11 Shear capacity for different types of 6.3 mm screws

Specimen label	Maximum force (kN)	Tensile displacement at maximum force (mm)
Type A-1	11.07	21.77
Type A-2	10.25	18.87
Type A-3	9.67	18.32
Average	10.33	

Type B-1	6.11	12.70
Type B-2	6.96	11.96
Type B03	6.42	11.97
Average	6.50	

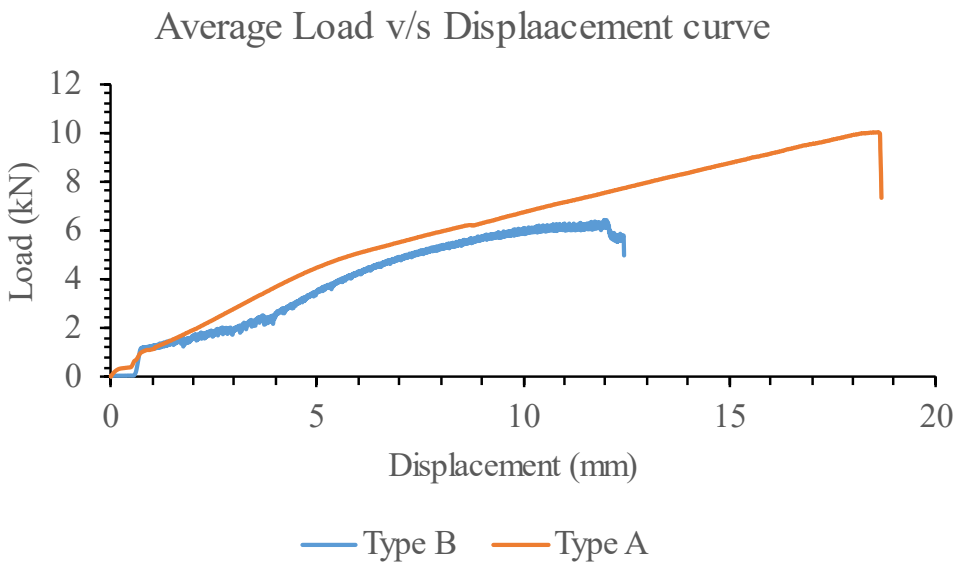

Figure 31 Average load v/s displacement curve for different types of screw

4.1.3 Screw inclination

To examine the influence of the screw inclination on shear capacity, the graph in Figure 33 illustrates the results obtained from experiments conducted for a 45-degree screw inclination which was achieved by using an angled washer of 45-degree with a nominal diameter of 6.5 mm. A screw with a diameter of 6.3 mm was used for steel with a thickness of 8 mm, 12 mm, 16 mm, and 20 mm, and timber with a thickness of 45 mm.

Figure 33 (a) illustrates the load-displacement curve for 8 mm steel thickness and 45 mm timber thickness and the effect of the screw inclination on shear capacity. Table 12 presents a comprehensive overview of the test results for the maximum force (kN) values. When comparing specimens with equal thickness but varying screw inclination angles (45 degrees vs. 90 degrees), differences in peak load are observed. Specifically, the ultimate capacity is

higher for the 45-degree screw inclination compared to the 90-degree screw inclination. Additionally, as the steel thickness increases, the capacity increases for 12 mm thickness but decreases for 16 mm and 20 mm thickness. For a screw axis with a 45-degree angle, the capacity trend is similar to that of a 90-degree angle. However, there is an exponential increase in capacity specifically for steel thicknesses of 20 mm. The experimental results of the screw's shear capacity on average increase by 140% because an axial component is developed when force is no more acting perpendicular to the screw axis as shown in Figure 34. This indicates that the shear connection capacity is influenced by the change in the screw's axis, which could be a potential area for future study.

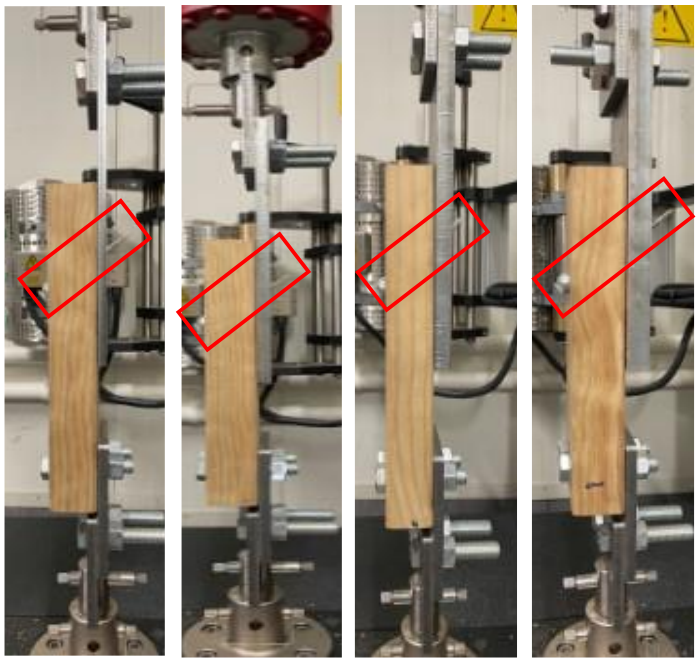

Figure 32 Single screw connection at an angle of 45-degree

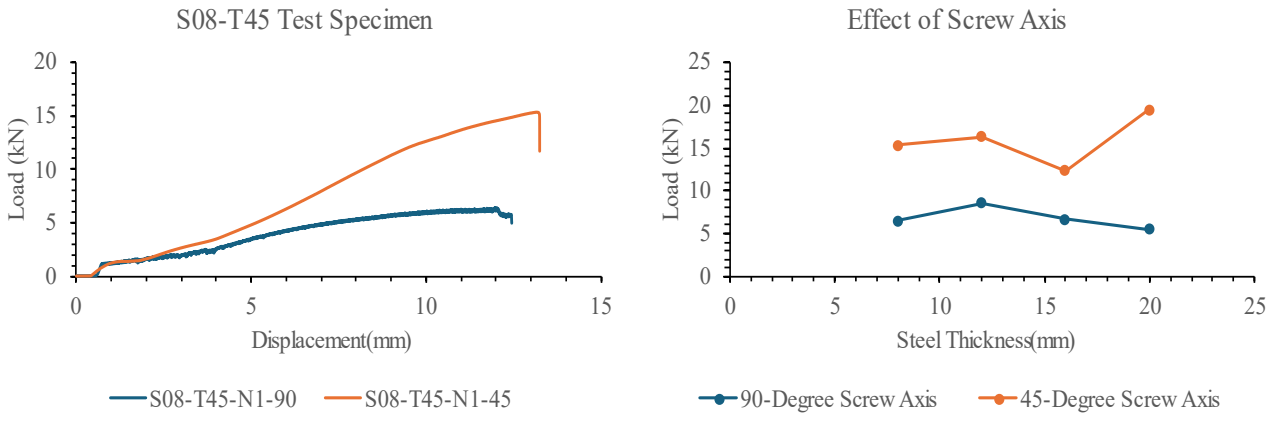

(a) (b)

Figure 33 (a) Comparison of 45-degree & 90-degree screw axis (b) Effect of screw axis

Table 12 Shear capacity for 45&90-Degree screw axis

Specimen	Ultimate Capacity (kN)	Specimen	Ultimate Capacity (kN)
S08-T45-N1-90	6.5	S08-T45-N1-45	15.35
S12-T45-N1-90	8.54	S12-T45-N1-45	16.33
S16-T45-N1-90	6.64	S16-T45-N1-45	12.34
S20-T45-N1-90	5.53	S20-T45-N1-45	19.5

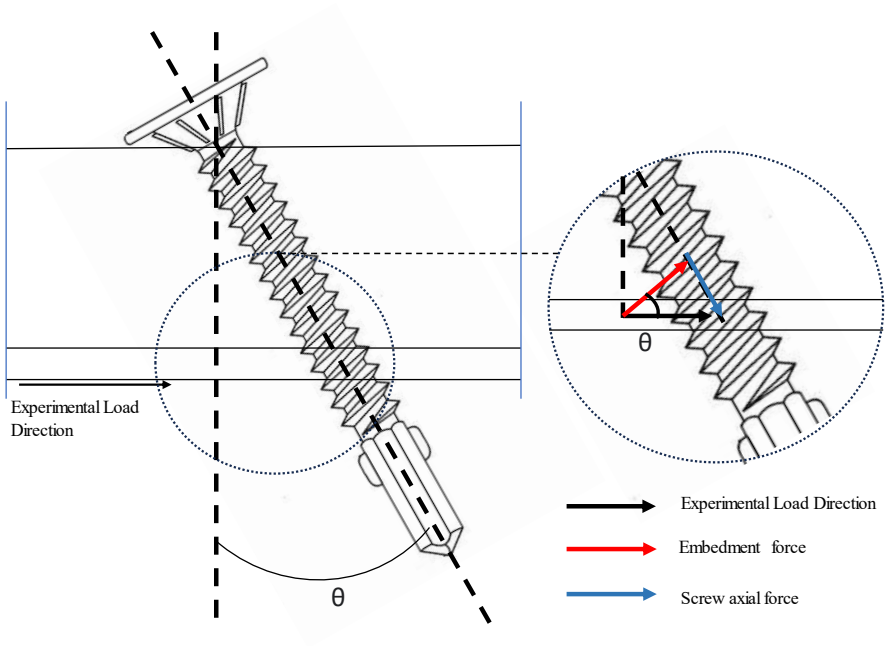

Figure 34 Different force components acting on inclined screws

4.1.4 Number of screws

All the test results of the experiments of shear connection were recorded and are presented in Table 13 including the type of failure mode that occurred for each specimen together and the corresponding ultimate capacity. All three failure modes related to thick steel plates were observed.

For all the tests, timber embedment failure was noticeable. The screw plastic hinge formation was dominant for 30 mm and 45 mm timber thickness. Even though the test specimens exhibited different failure modes, all the specimens ultimately failed in shear. Based on this observation and in conjunction with the fastener shear strengths investigated it can be concluded that for the timber-steel type of connection, fastener failure is governed by majorly on timber thickness.

Table 13 Shear test result

Steel thickness	Timber thickness					
	T15		T30		T45	
	Ultimate Load (kN)	Displacement (mm)	Ultimate Load (kN)	Displacement (mm)	Ultimate Load (kN)	Displacement (mm)
S08-N1	6.4	7.76	7.02	10.01	6.5	12.21
S12-N1	5.75	8.32	8.1	15.02	8.54	16.12
S16-N1	6.55	12.48	5.85	11.46	6.64	12.48
S20-N1	6.27	9.65	7.79	13.31	5.53	8.07
S08-N2	9.47	7.15	9.54	8.55	14.19	9.21
S12-N2	10.9	8.9	13.11	9.84	14.62	11.6
S16-N2	10.89	8.1	13.42	11.97	12.52	10.98
S20-N2	15.14	11.84	15.39	12.57	12.87	12.44
S08-N3			24.01	10.93	24.17	11.1
S12-N3			17.08	9.7	23.09	13.77
S16-N3			13.53	11	23.5	11.02
S20-N3			16.38	11.78	21.32	10.91

S12-T15-N1 S12-T30-N1 S08-T45-N1

S16-T15-N2 S12-T30-N2 S16-T45-N2

S16-T30-N3 S20-T45-N3

Figure 35 Photo of post-tested specimens

4.2 Influence of steel-timber connection parameters

4.2.1 Timber thickness

In timber-steel connection, the change in timber thickness is shown to be associated with a change in the failure mode. Based on Figures 36, 37, 38, and 39 it is indicated that the capacity of 1 and 2 screw connections increases when the increase in timber thickness from 15 mm to 30 mm. However, the capacity falls when the timber thickness goes from 30 mm to 45 mm. There is an average increase of 17% capacity in timber thickness when using one screw, from 15 mm to 45 mm. There is an average increase of 32% capacity in timber thickness when going from 15 mm to 45 mm using two screws. However, The capacity of the 3-screw connection increases from 30 mm to 45 mm due to the efficient distribution of the load. There is an average increase of 35% capacity in timber thickness from 30 mm to 45 mm for three screws.

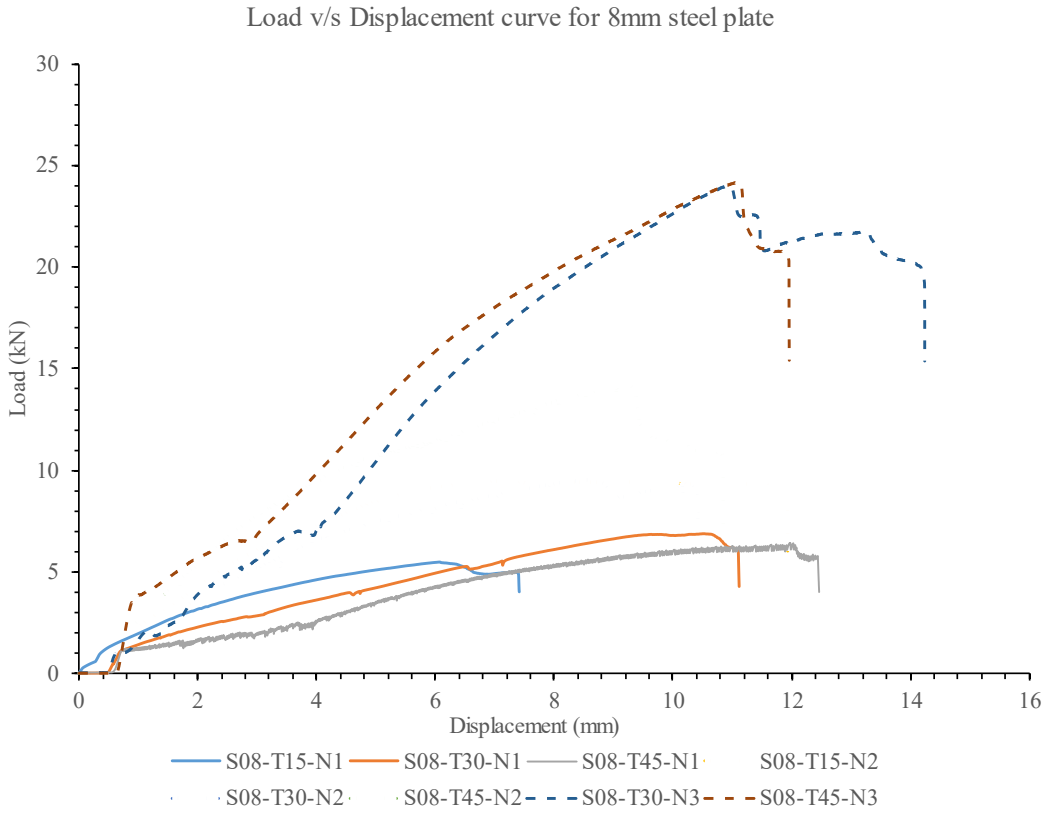

Figure 36 The load-displacement curve for 8 mm steel plate

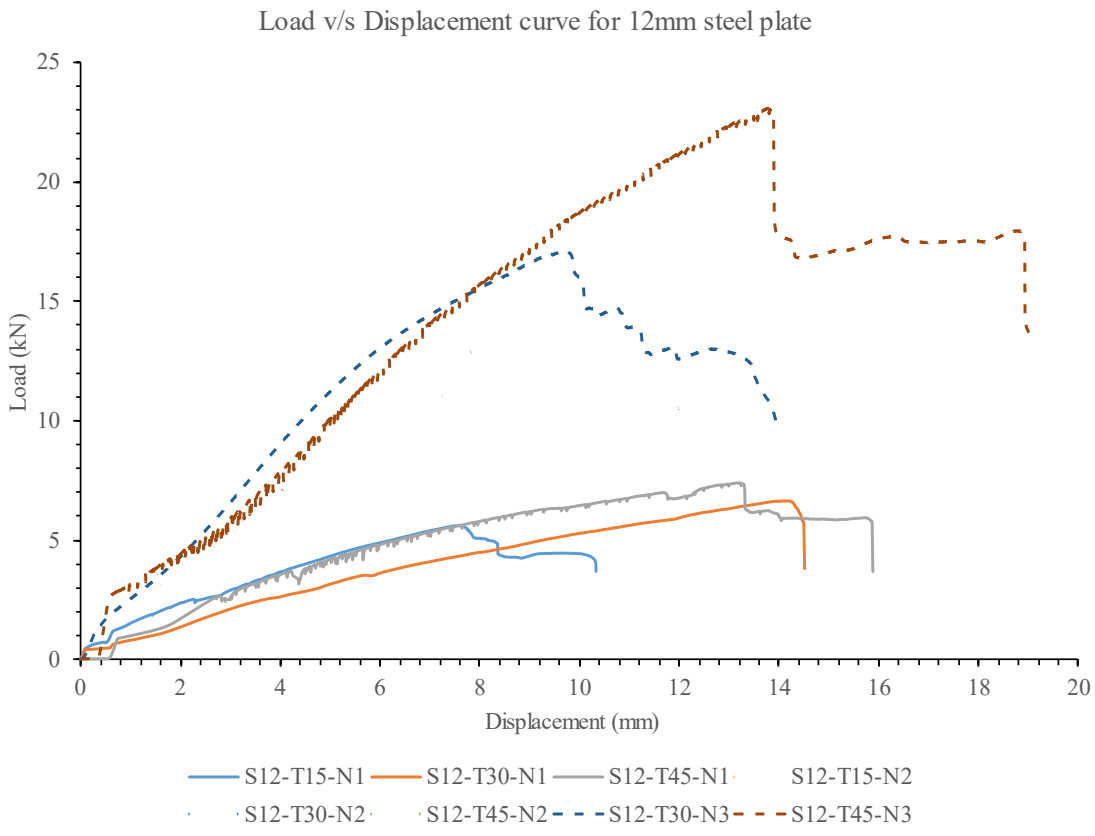

Figure 37 The load-displacement curve for 12 mm steel plate

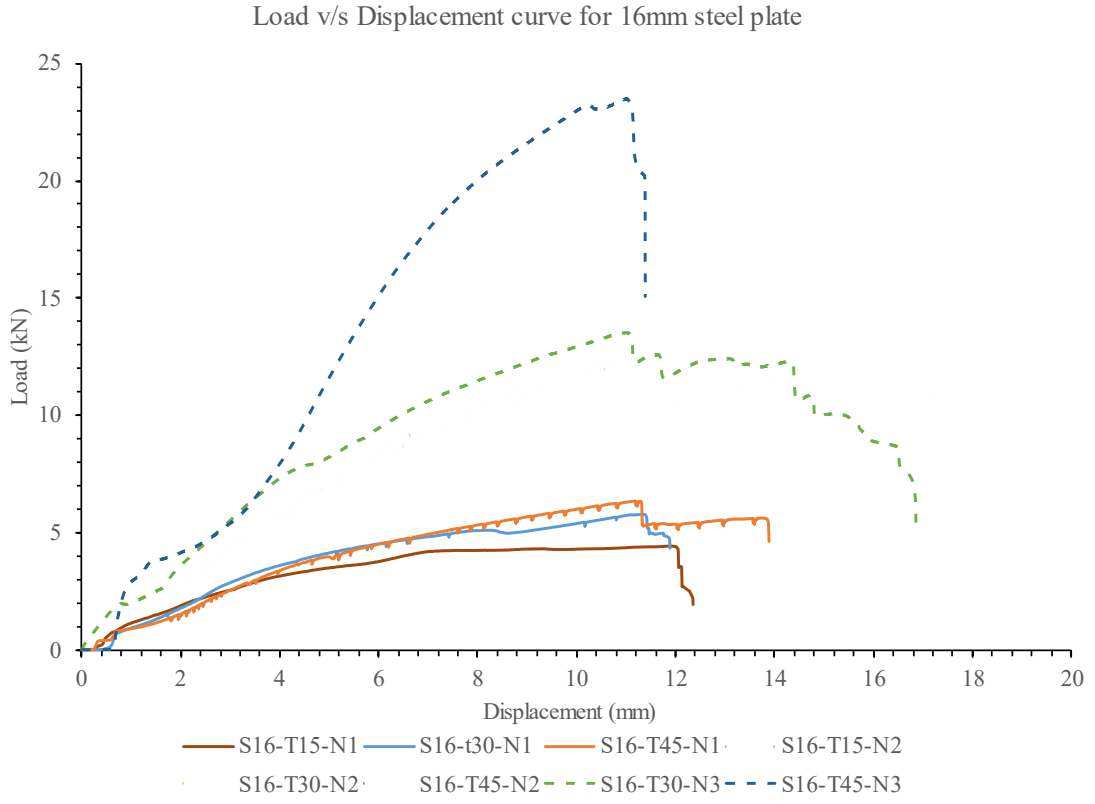

Figure 38 The load-displacement curve for 16 mm steel plate

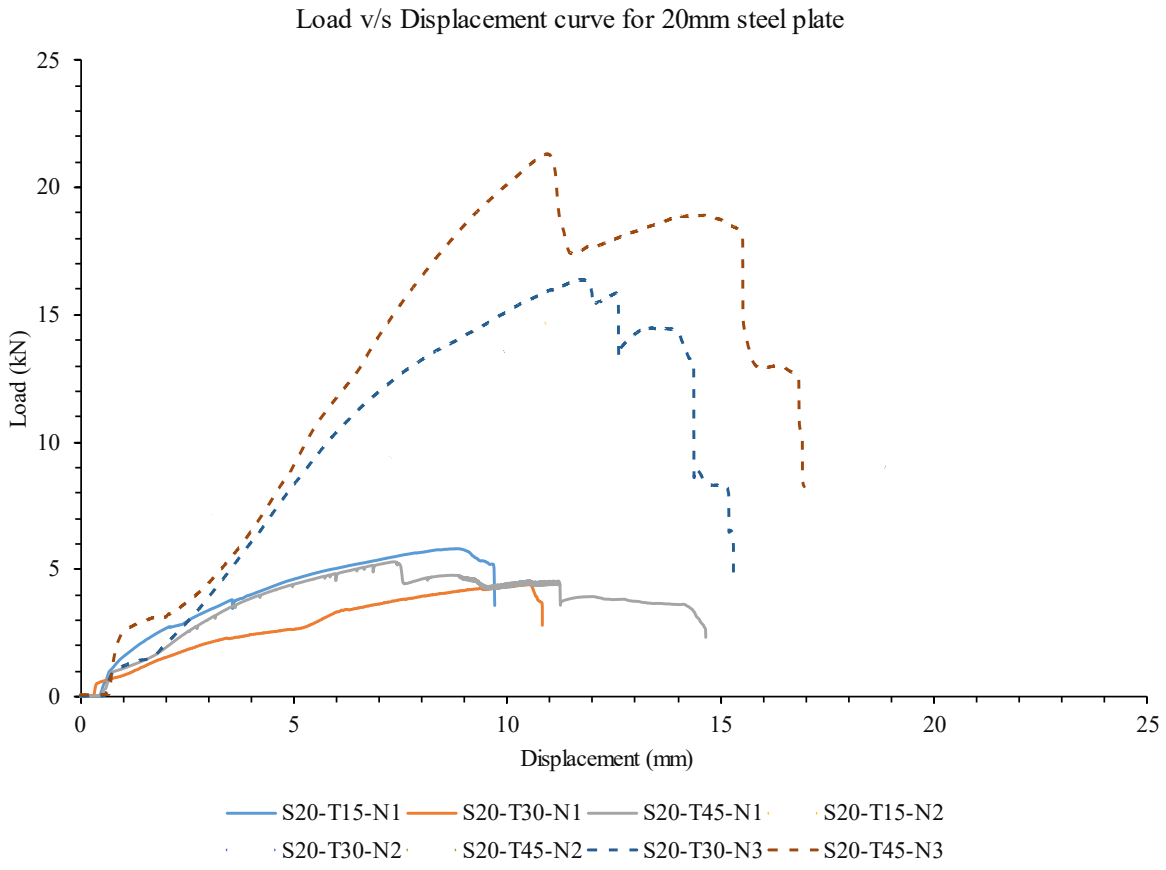

Figure 39 The load-displacement curve for 20 mm steel plate

4.2.2 Effect of steel thickness

An effect in either peak load or stiffness has been found in timber-to-steel connections when thicker steel is used. According to the graphs in Figures 40, 41, and 42, there is an average reduction of 14% in capacity as the steel thickness increases from 8 mm to 20 mm for a single screw. The capacity of two screws decreases by an average of 9% as the steel thickness changes from 8 mm to 20 mm. There is a consistent decrease in capacity for steel thickness from 8 mm to 20 mm across three screws, with an average decrease of 11%. Additionally, for timber thicknesses of 15 mm and 45 mm, as steel thickness increases there is an average decrease in stiffness by 22%.

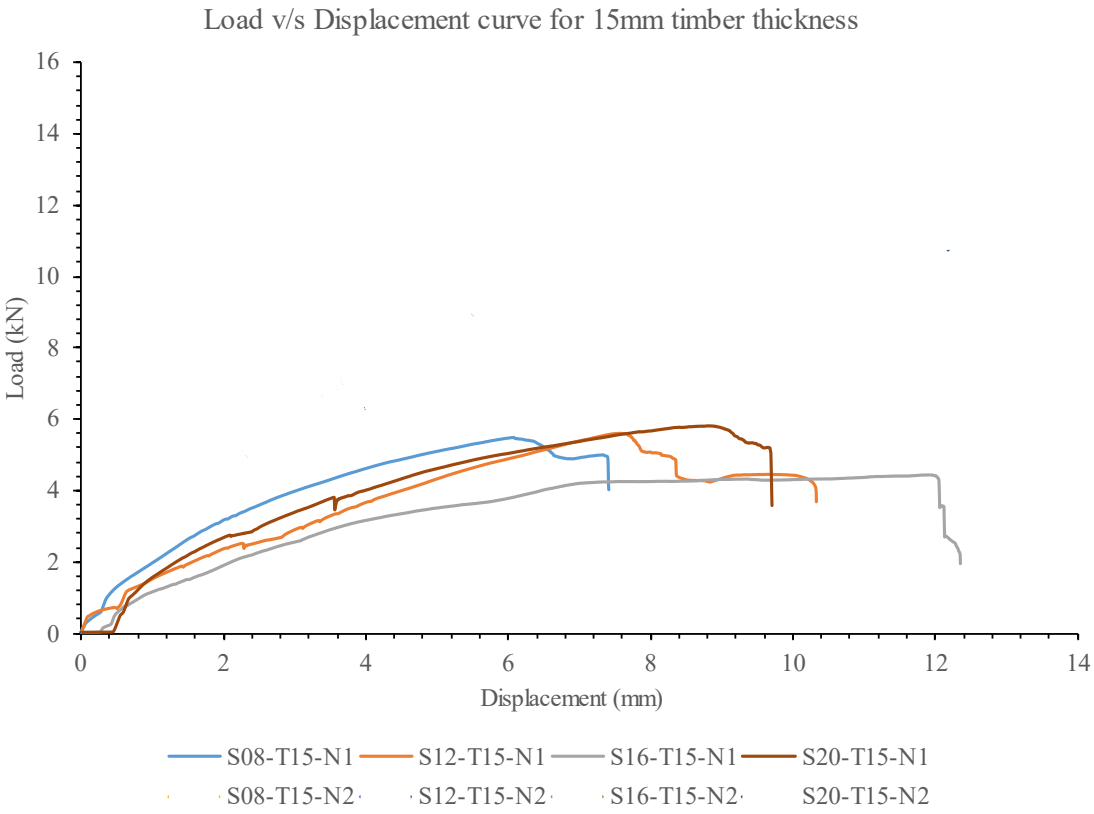

Figure 40 The load-displacement curve for 15 mm timber thickness

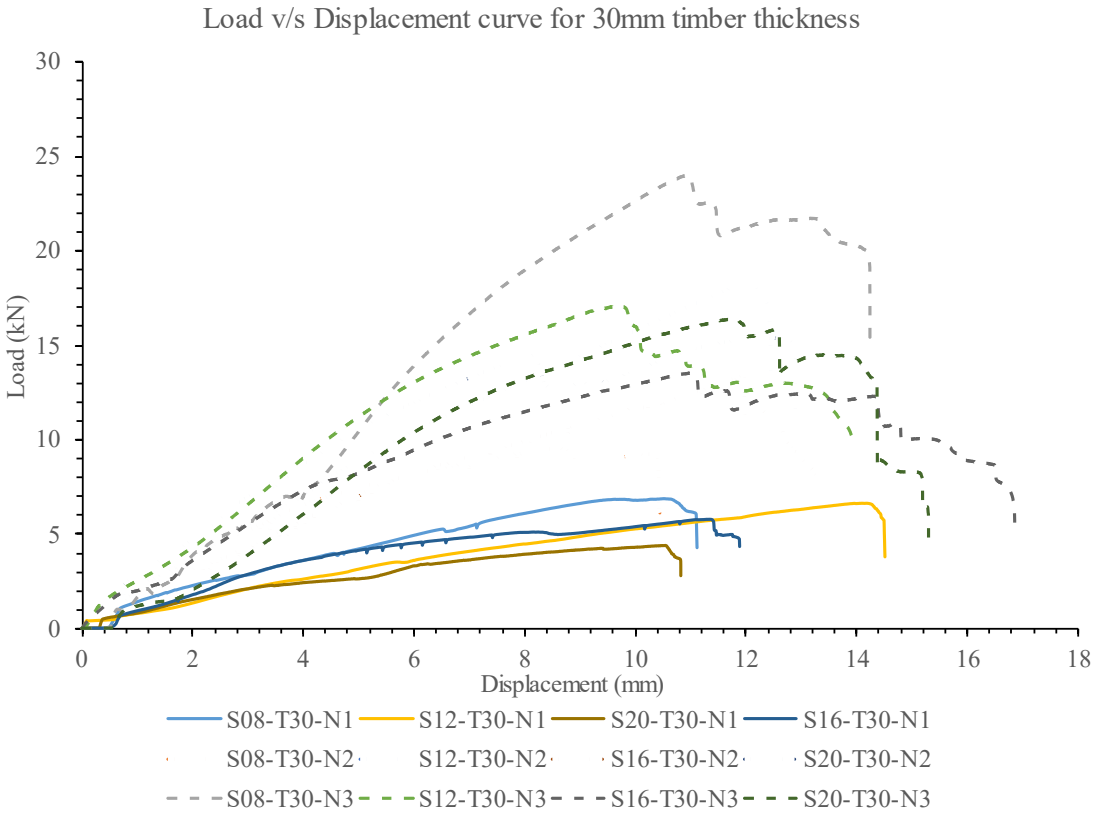

Figure 41 The load-displacement curve for 30 mm timber thickness

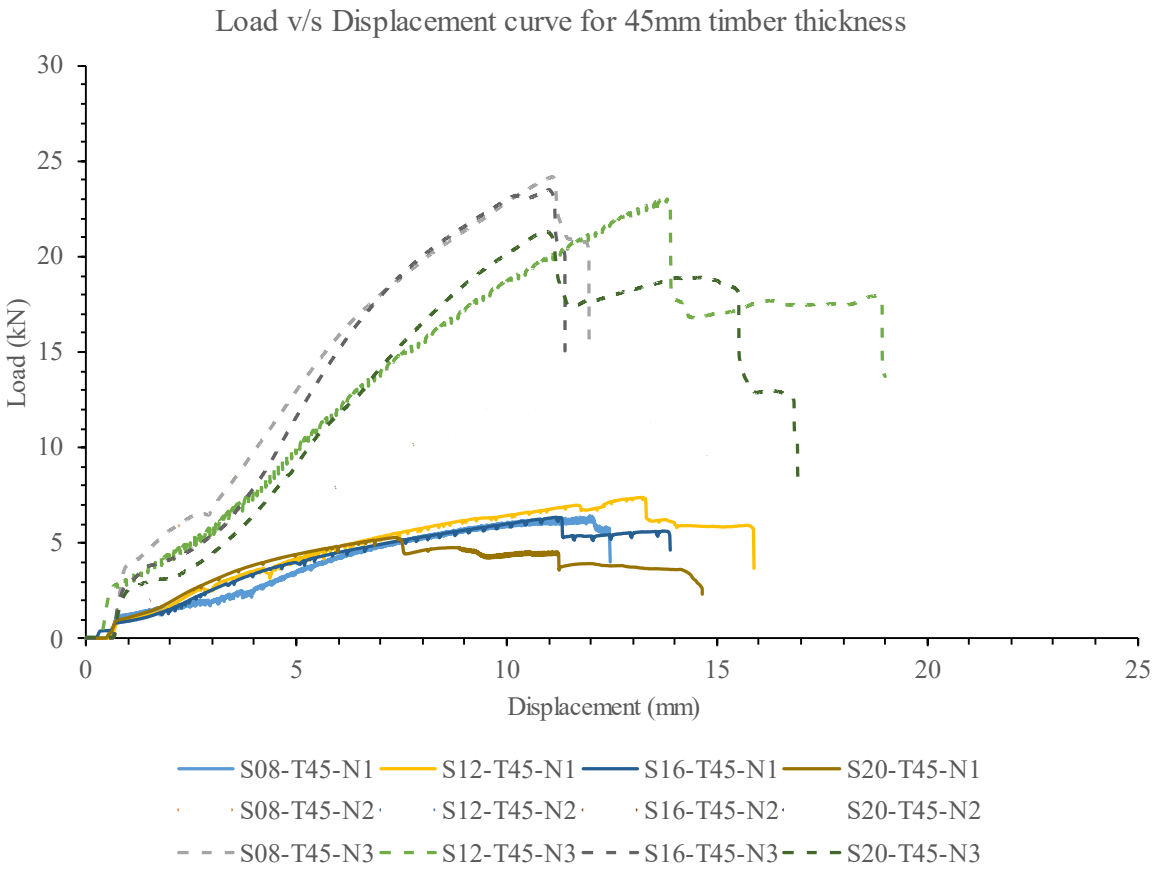

Figure 42 The load-displacement curve for 45 mm timber thickness

4.2.3 Load-displacement relationship

For the loading stages of all the test specimens, the initial slip was observed because of the rig's bolt resulting in a small flat line before elastic deformation. The specimen showed elastic deformation up to the maximum strength after which non-linear behaviour was observed. At an average displacement of 11 mm, most of the specimens failed. Due to the formation of the plastic hinge of the screw, several peaks were observed in the load-displacement curve.

4.2.4 Group effect on strength

The group effect is defined as the ratio of the strength per screw for a connection to the average strength of a single screw connection, as indicated in Table 14. According to the data shown in Table 14, the group effects of using 2-screws connection drops by 6.8% and 9.4% on average for timber thicknesses of 15 mm and 30 mm, respectively. However, there is an average rise of 1.3% in the group effect for a timber thickness of 45 mm.

The group effect for a 3-screw connection drops by an average of 17% for a timber thickness of 30 mm. However, for a timber thickness of 45 mm, the group effect increases by an average of 15%. The total connection capacity increases as the number of screws increases but the main reason for shear capacity to decrease on average for 15 mm and 30 mm timber thickness is because of different displacements of each screw at the maximum load whereas, in 45 mm timber thickness, there is less timber embedment failure resulting in less displacement of the screw. This combined effect leads to different failure modes as shown in Table 15. Therefore, the Group effect does affect the shear capacity.

Table 14 Screw connection group effect

Specimens	Experimental results	Experimental results/N	Group effect ratio
S08-T15-N1	6.4	6.4	1
S08-T30-N1	7.02	7.02	1
S08-T45-N1	6.5	6.5	1
S12-T15-N1	5.75	5.75	1
S12-T30-N1	8.1	8.1	1
S12-T45-N1	8.54	8.54	1

S16-T15-N1	6.55	6.55	1
S16-T30-N1	5.85	5.85	1
S16-T45-N1	6.64	6.64	1
S20-T15-N1	6.27	6.27	1
S20-T30-N1	7.79	7.79	1
S20-T45-N1	5.53	5.53	1
S08-T15-N2	9.47	4.74	0.74
S08-T30- N2	9.54	4.77	0.68
S08-T45-N2	14.19	7.1	1.09
S12-T15-N2	10.9	5.45	0.95
S12-T30-N2	13.11	6.56	0.81
S12-T45-N2	14.62	7.31	0.86
S16-T15-N2	10.89	5.45	0.83
S16-T30-N2	13.42	6.71	1.15
S16-T45-N2	12.52	6.26	0.94
S20-T15-N2	15.14	7.57	1.21
S20-T30-N2	15.39	7.7	0.99
S20-T45-N2	12.87	6.44	1.16
S08-T30-N3	24.01	8	1.14
S08-T45-N3	24.17	8.06	1.24
S12-T30-N3	17.08	5.69	0.7
S12-T45-N3	23.09	7.7	0.9

S16-T30-N3	13.53	4.51	0.77
S16-T45-N3	23.5	7.83	1.18
S20-T30-N3	16.38	5.46	0.7
S20-T45-N3	21.32	7.11	1.29

4.3 Failure modes and observations

4.3.1 Failure modes

During experimental testing, the behaviour of the connections was captured using a video camera. Figure 43 depicts the cross-sectional view of the timber section post-testing for samples S08-T45, S12-T15, and S16-T30 showing all three failure modes: Mode C with screw shear failure &timber bearing, Mode D with timber embedment failure & negligible screw shank deformation as plastic deformation occurs in timber fibers resulting in the formation of one plastic hinge in the screw which is evident in Figure 43 for 30 mm timber thickness, and Mode E with screw head deformed, timber embedment failure of timber along steel surface where plastic deformation occurs in both the element resulting in two plastic hinge formation in the screw. Table 15 provides a summary of the specimens categorized by the failure mode observed under shear for all the screw connections. The failure mode depends on timber thickness. As the timber thickness varies from 15 mm to 45 mm, the failure mode transitions

from C to D to E.

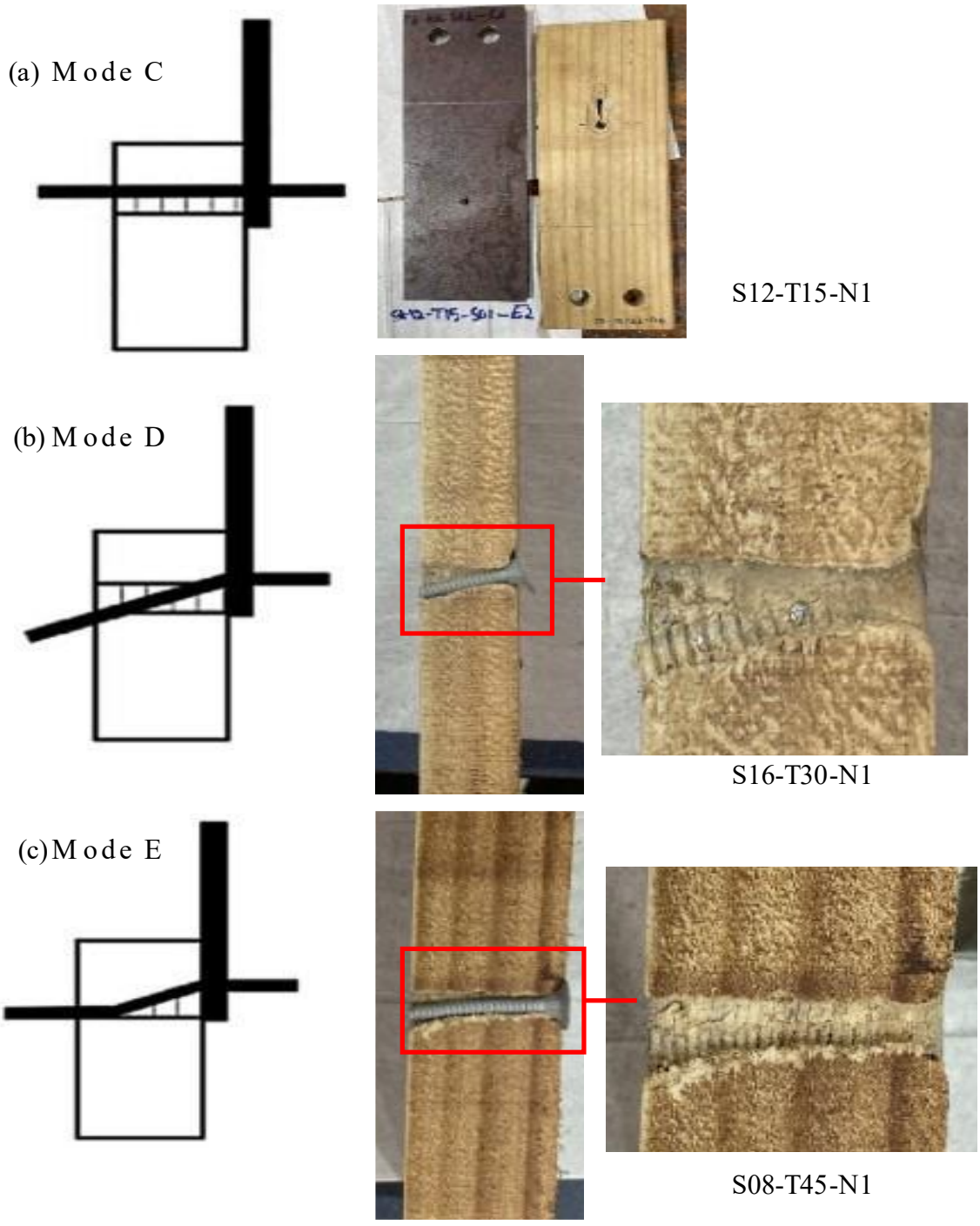

Figure 43 Failure modes of one-screw connection according to Eurocode-5

Table 15 Specimen classification based on failure mode

Specimens	Failure Mode C	Failure Mode D	Failure Mode E
Single Screw	S12-T15	S08-T15	S08-T45
	S16-T15	S08-T30	S12-T45
		S12-T30	S16-T45
		S16-T30	S20-T45
		S20-T15	
		S20-T30	
Two Screw	S08-T15	S08-T30	S08-T45
	S16-T15	S12-T15	S12-T45
	S16-T30	S12-T30	
		S16-T45	
		S20-T15	
		S20-T30	
		S20-T45	
Three Screw		S12-T30	S08-T30
		S16-T30	S08-T45
		S20-T30	S12-T45
			S16-T45
			S20-T45

4.3.2 DIC analysis for different failure mode

The failure mode of timber was captured utilizing Digital Image Correlation (DIC), showcasing the strain contour along the longitudinal strain (e_{yy}) where tensile strain is depicted in red and compressive strain in purple and the respective ultimate load and corresponding displacement

are obtained in Table 16.

All test specimens exhibited clear strain concentration around the screw head as shown in Figure 44. At a timber thickness of 15 mm, there was a localized increase in strain at the upper and lower parts of the screw head. One of them was created due to a tensile strain of 0.00127 at the lower half of the screw head, while the other was made due to a compressive strain of 0.00072, indicated by the purple section. When timber is subjected to bearing stress, it experiences the development of w-shaped strain, with compressive strain spreading through the timber from the top to the bottom of the screw with 0.003 tensile and compressive strain.

For a timber thickness of 30 mm, the initial strain behaves similarly to a 15 mm timber thickness. However, as the stress increases, the timber experiences bearing stress due to the increased thickness. This causes the screw head to crush the timber with a compressive strain of 0.00095, resulting in a higher concentration of tensile strain of 0.00485 at the bottom of the screw head and the formation of cracks in the timber.

With a timber thickness of 45 mm, the high density of the timber and the production of two plastic hinges in the screw lead to the development of tensile strain at the top and bottom of the screw head. As a result, the likelihood of the timber surface being crushed by a screw is reduced with a compressive strain of 0.0022, and a tensile strain of 0.0103 as shown in Figure 44.

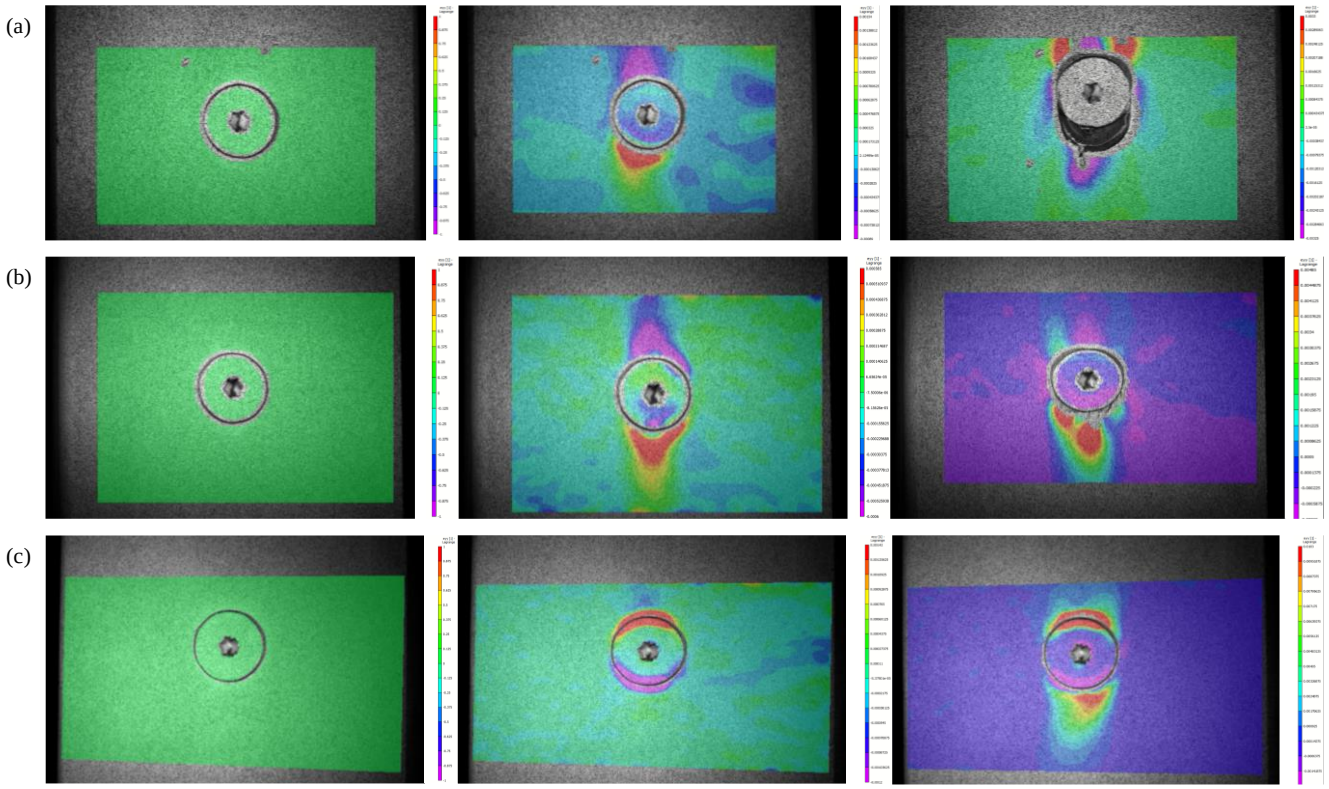

Figure 44 DIC strain contours (a) Failure mode C (b) Failure mode D (c) Failure mode E

Table 16 Load-displacement values for specimens used for DIC analysis

Specimen	Ultimate Load (kN)	Displacement (mm)	Failure Mode
S16-T15-N1	6.33	10.01	C
S8-T30-N1	6.4	16.11	D
S8-T45-N1	7.25	10.32	E

4.3.3 Microscope photographs

A microscope was utilized to acquire a detailed photograph of the damage on the steel surface. The microscope was adjusted to a magnification of 6.4x, and all measurements were calibrated

in micrometers. Image-pro software was utilized to capture photographs of all the specimens. It can be seen from Figure 45 that the bearing of the steel surface for thicknesses 8, 12, 16, and 20 mm grows as the thickness of the timber increases from 15 mm to 45 mm. When the timber thickness is 30 mm irrespective of steel thickness, the screw breaks due to shear without causing any damage to the steel surface.

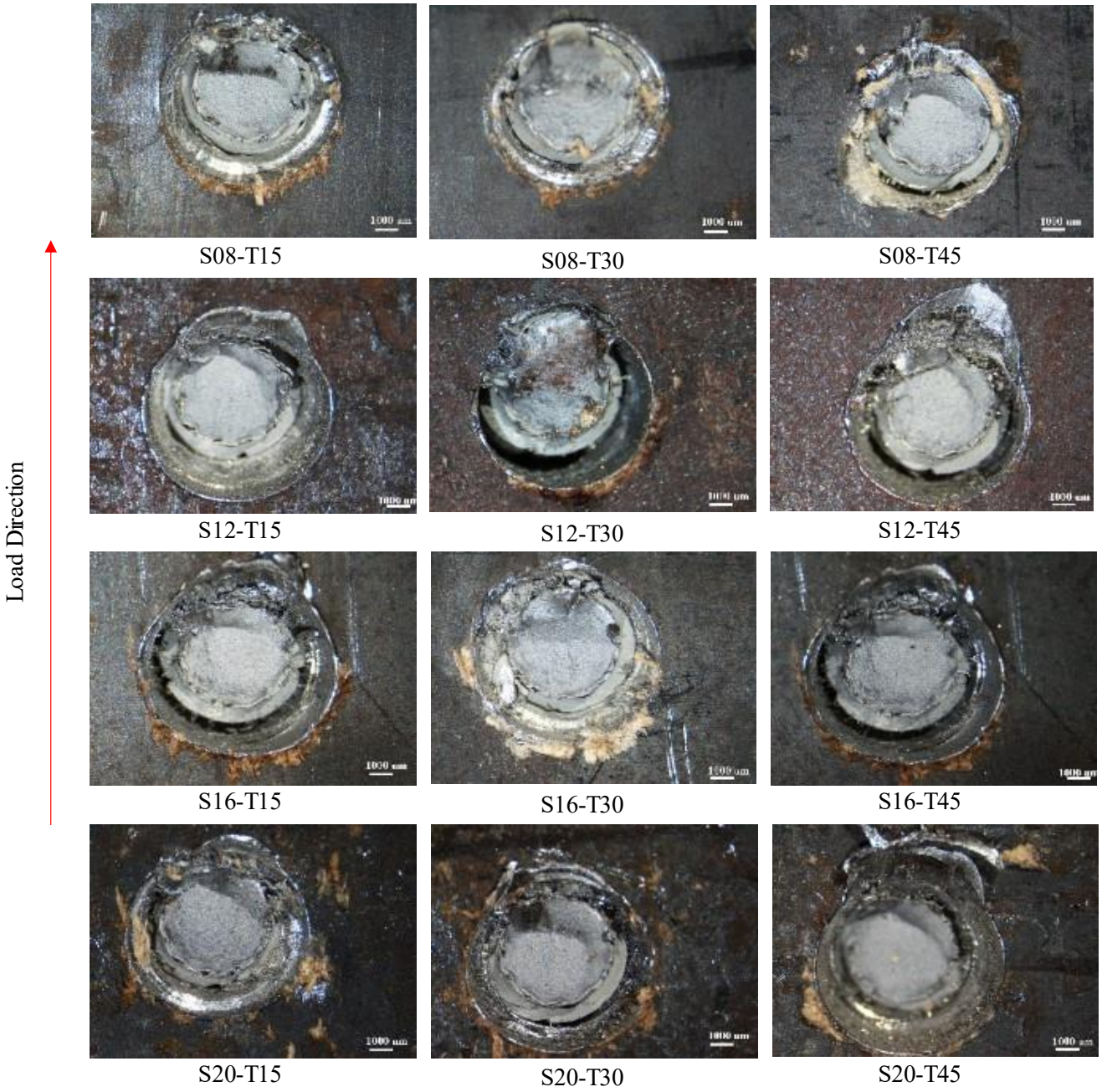

Figure 45 Microscopic image of test steel specimens

5 Comparative assessments

5.1 Eurocode 5 design rules

Eurocode 5 estimates the design strengths of steel-timber screwed connections for different failure modes, as illustrated in the below figures. These estimates can be derived from Equations 1(a-e) from the Eurocode 5 [24], which are presented below:

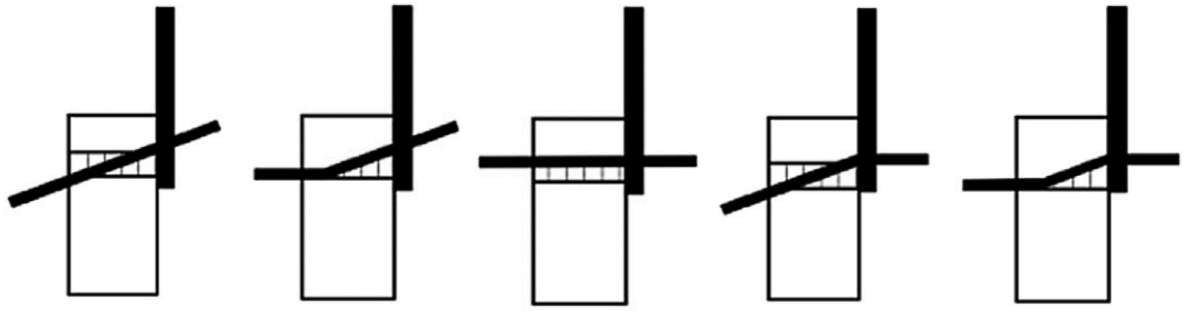

(a) (b) (c) (d) (e)

$$F_{v,Rk} = \begin{cases} 0.4 f_{h,k} t_1 d \text{(a)} \\ 1.15\sqrt{2 M_{y,Rk} f_{h,k} d} + \frac{F_{ax,Rk}}{4} \text{ (b)} \\ f_{h,k} d t_1 \text{(c)} \\ f_{h,k} d t_1 \left[\sqrt{2 + \frac{4 M_{y,Rk}}{f_{h,k} d t_1^2}} - 1\right] + \frac{F_{ax,Rk}}{4} \text{(d)} \\ 2.3\sqrt{M_{y,Rk} f_{h,k} d} + \frac{F_{ax,Rk}}{4} \text{(e)} \end{cases} \quad (1)$$

Where,

$$F_{ax,\alpha,Rk} \begin{cases} f_{ax,k} d t_{pen} \\ f_{head,k} d^2{}_h \end{cases} \quad (2)$$

$$f_{ax,k} = 20 \times 10^{-6} \rho_k^2 \quad (3)$$

$$f_{head,k} = 70 \times 10^{-6} \rho_k^2 \quad (4)$$

$$M_{y,Rk} = 0.45 f_u d^{2.6} \quad (5)$$

$$f_{h,k} = 0.082(1 - 0.01 d)\rho k \quad (6)$$

In the above equation, t_1 is the smaller penetration depth value or timber thickness. f_{hk} is the characteristic embedment strength. The characteristic density of timber is displayed as ρ_k. $M_{y,Rk}$ is the characteristic yield moment of the screw. $f_{head,k}$ is the characteristic head side pull-

through strength. d_h is the nail head diameter. t_{pen} is the point side penetration length. Diameter of screw d. $f_{ax,k}$ is the withdrawal strength perpendicular to the grain direction. For a laterally loaded screw, load carrying capacity is calculated using effective diameter d_{ef} was taken as 1.1 times the treaded root diameter [24].

5.2 Comparison of experimental strengths with design strengths

A comparison of the strengths obtained from the different timber-to-steel connection configurations with the design strengths calculated according to Eurocode 5 [24] is tabulated in **Error! Reference source not found.** 17. For screw connection as per the design calculation, the shear capacity remains the same irrespective of steel thickness resulting in 3 different failure modes i.e Failure mode C for 15 mm timber thickness, and Failure mode D for 30 mm and 45 mm timber thickness but for single screw, two screws, and three screws connection the failure mode and shear capacity changes based on connection thickness. Results show that the overall design strength estimated using Eurocode 5 [24] is under-conservative, with a mean P_{EXP}/P_{EC5} of 1.92.

Table 17: Comparison of experimental strengths with design strengths

Assembly	Test	Specimen	Steel thickness (mm)	Timber thickness (mm)	d_f for screw	F_{EXP} (kN)	F_{EXP}/F_{EC5}	Failure mode
One screw	1	S08-T15	8	15	6.93	6.4	2.06	D
	2	S08-T30	8	30	6.93	7.02	1.91	D
	3	S08-T45	8	45	6.93	6.5	1.42	E
	4	S12-T15	12	15	6.93	5.75	1.85	C
	5	S12-T30	12	30	6.93	8.1	2.20	D
	6	S12-T45	12	45	6.93	8.54	1.86	E
	7	S16-T15	16	15	6.93	6.55	2.11	C

	8	S16-T30	16	30	6.93	5.85	1.59	D
	9	S16-T45	16	45	6.93	6.64	1.45	E
	10	S20-T15	20	15	6.93	6.27	2.02	D
	11	S20-T30	20	30	6.93	7.79	2.12	D
	12	S20-T45	20	45	6.93	5.53	1.21	E
Two screws	13	S08-T15	8	15	6.93	9.47	1.71	C
	14	S08-T30	8	30	6.93	9.54	1.46	D
	15	S08-T45	8	45	6.93	14.19	1.74	E
	16	S12-T15	12	15	6.93	10.9	1.97	D
	17	S12-T30	12	30	6.93	13.11	2.00	D
	18	S12-T45	12	45	6.93	14.62	1.79	E
	19	S16-T15	16	15	6.93	10.89	1.97	C
	20	S16-T30	16	30	6.93	13.42	2.05	C
	21	S16-T45	16	45	6.93	12.52	1.54	D
	22	S20-T15	20	15	6.93	15.14	2.73	D
	23	S20-T30	20	30	6.93	15.39	2.35	D
	24	S20-T45	20	45	6.93	12.87	1.58	D
Three screws	25	S08-T30	8	30	6.93	24.01	2.68	E
	26	S08-T45	8	45	6.93	24.17	2.17	E
	27	S12-T30	12	30	6.93	17.08	1.91	D
	28	S12-T45	12	45	6.93	23.09	2.07	E
	29	S16-T30	16	30	6.93	13.53	1.51	D
	30	S16-T45	16	45	6.93	23.5	2.11	E
	31	S20-T30	20	30	6.93	16.38	1.83	D
	32	S20-T45	20	45	6.93	21.32	1.91	E

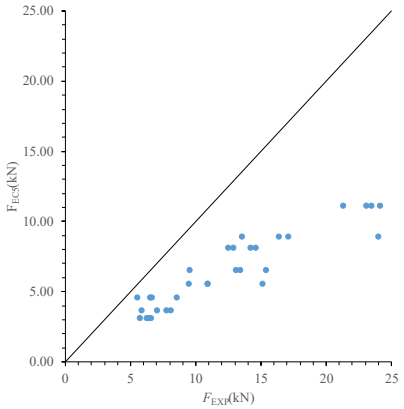

Figure 46 Comparison of results of Eurocode-5 with experimental results

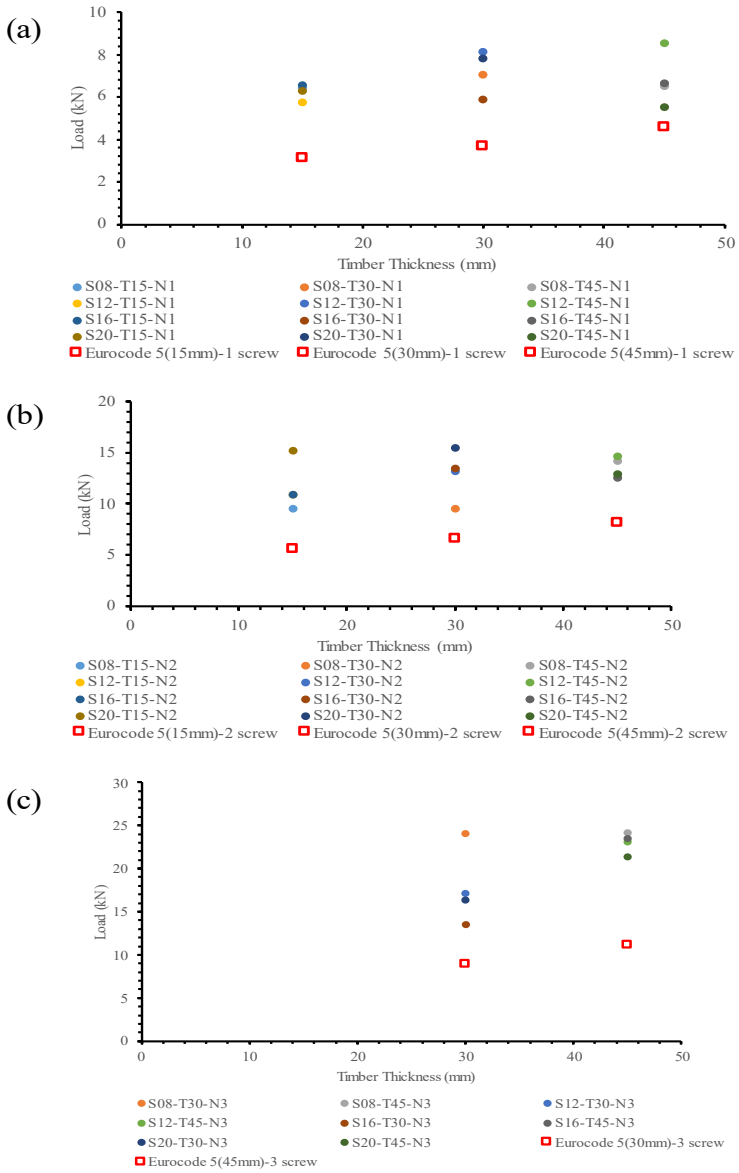

Figure 47 Eurocode 5 comparison with experimental test results for (a) One screw (b) Two screws

(c) Three screws

5.3 Proposed design equations

Based on the failure modes, the experimental test results were used to propose the modified design equation of timber to steel connection using self-drilling wing screws under lateral loading. The proposed equation has variables such as the characteristic yield moment of the screw ($M_{y,Rk}$), characteristic embedment strength (f_{hk}), diameter of screw (d), timber thickness(t_1), and characteristic withdrawal capacity of the fasteners ($F_{ax,\alpha,Rk}$).

For Failure mode C,

$$F_{v,Rk} = f^{1.69}_{h,k} d^{0.33} t^{0.97}$$

For Failure mode D,

$$F_{v,Rk} = f_{h,k} d t_1 \left[\sqrt{2 + \frac{4M_{y,Rk}}{f_{h,k} d t_1^{1.43}}} - 1.2\right] + \frac{F_{ax,Rk}}{1.98}$$

For Failure mode E,

$$F_{v,Rk} = 3.32\sqrt{M_{y,Rk} f_{h,k} d} + \frac{F_{ax,Rk}}{0.31}$$

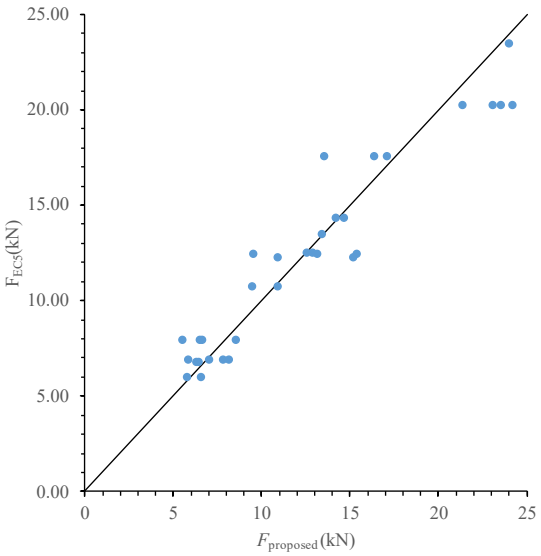

Figure 48 Comparison of results of the proposed equation with experimental results

A comparison was made using Eurocode 5, and proposed design equations with experimental results as shown in Figure 46 and Figure 48 respectively. Table 18 shows that the proposed equation could predict the shear capacity more favorably than the design equation obtained from Eurocode-5 with a coefficient of variation of 0.14 for $F_{EXP}/F_{proposed}$. As discussed in section 3.1.1, the stiffness and strength are quantified based on tests where Eurocode-5 prediction is over-conservative when compared to experimental test results.

Table 18 Comparison of experimental test results with Eurocode-5 and proposed design equations

Specimen	F_{EC5} (kN)	F_{EXP} (kN)	$F_{proposed}$ (kN)	F_{EXP}/F_{EC5}	$F_{EXP}/F_{proposed}$
S08-T15-N1	3.11	6.4	6.80	2.06	0.94
S08-T30-N1	3.68	7.02	6.90	1.91	1.02
S08-T45-N1	4.58	6.5	7.96	1.42	0.82
S12-T15-N1	3.11	5.75	5.97	1.85	0.96
S12-T30-N1	3.68	8.1	6.90	2.20	1.17
S12-T45-N1	4.58	8.54	7.96	1.86	1.07
S16-T15-N1	3.11	6.55	5.97	2.11	1.10
S16-T30-N1	3.68	5.85	6.90	1.59	0.85
S16-T45-N1	4.58	6.64	7.96	1.45	0.83
S20-T15-N1	3.11	6.27	6.80	2.02	0.92
S20-T30-N1	3.68	7.79	6.90	2.12	1.13
S20-T45-N1	4.58	5.53	7.96	1.21	0.69
S08-T15-N2	5.60	9.47	10.75	1.69	0.88
S08-T30- N2	6.63	9.54	12.43	1.44	0.77
S08-T45-N2	8.25	14.19	14.33	1.72	0.99
S12-T15-N2	5.60	10.9	12.24	1.95	0.89

S12-T30-N2	6.63	13.11	12.43	1.98	1.05
S12-T45-N2	8.25	14.62	14.33	1.77	1.02
S16-T15-N2	5.60	10.89	10.75	1.95	1.01
S16-T30-N2	6.63	13.42	13.51	2.02	0.99
S16-T45-N2	8.25	12.52	12.53	1.52	1.00
S20-T15-N2	5.60	15.14	12.24	2.70	1.24
S20-T30-N2	6.63	15.39	12.43	2.32	1.24
S20-T45-N2	8.25	12.87	12.53	1.56	1.03
S08-T30-N3	9.35	24.01	23.48	2.57	1.02
S08-T45-N3	11.64	24.17	20.23	2.08	1.19
S12-T30-N3	9.35	17.08	17.54	1.83	0.97
S12-T45-N3	11.64	23.09	20.23	1.98	1.14
S16-T30-N3	9.35	13.53	17.54	1.45	0.77
S16-T45-N3	11.64	23.5	20.23	2.02	1.16
S20-T30-N3	9.35	16.38	17.54	1.75	0.93
S20-T45-N3	11.64	21.32	20.23	1.83	1.05
			Average	1.87	1.00
			Standard Deviation	0.32	0.14

6 Conclusions and Future Study

6.1 Conclusion

This paper presents an experimental investigation aimed to study the structural behaviour of self-drilling wing screw connections designed from radiata pine timber and thick hot-rolled steel. An assessment of the structural performance of the composite connection was conducted through a series of material and shear tests.

The experimental tests conducted on the screw connection yielded multiple results. An initial experimental investigation was carried out on a 45 mm timber to 8 mm steel connection using different screw lengths and results show that the capacity remains constant with an average capacity of 6.5 kN.

Subsequently, two types of screws with similar specifications available in New Zealand were selected. When comparing the shear capacity using 45 mm timber to 8 mm steel, the capacity difference was 60% on average. It is evident that capacity and stiffness vary with each type of screw.

When investigating the effect of the screw axis, the capacity of timber to steel shear connection increases significantly by 140% when the screw is inclined at an angle of 45 degrees. This is because an axial component is developed when force is no more acting perpendicular to the screw axis.

From the experimental results of multiple screw connection tests, all the screw specimens failed in shear and timber thickness played a significant impact in determining the failure mode. For 2 screw connection, the average group effect reduces by 6.8% and 9.4% for 15 mm and 30 mm timber thickness, and an average rise of 1.3% in the group effect for a timber thickness of 45 mm. In 3 screw connections, the average group effect reduces by 17% for 30 mm timber thickness, and an average rise of 15% for 45 mm timber thickness.

In timber to steel shear test, as the timber thickness changes from 15 mm to 45 mm, capacity

increases on average for 1 screw and 2 screws by 17% and 32% respectively. However, for 3 screws as timber thickness increases from 30 mm to 45 mm capacity increases by 35%. Further discussing the effect of steel thickness for one screw, two screws, and three screws as steel thickness increases from 8 mm to 20 mm there is an average decrease in capacity by 14%, 9%, and 11% respectively.

The failure modes were analysed by varying the thickness of the timber and the strain contour was determined using Digital Image Correlation (DIC) for timber thicknesses of 15 mm, 30 mm, and 45 mm, corresponding to Failure Mode C, Failure Mode D, and Failure Mode E, respectively. The steel thickness was examined using a microscope for thicknesses of 8 mm, 12 mm, 16 mm, and 20 mm. It was observed that when the timber thickness is 30 mm, regardless of the steel thickness, the screw breaks due to shear without causing any damage to the steel surface. The Eurocode-5 [24] does not have provisions for predicting the shear strength of self-drilling wing screws in timber-to-steel connections. This is visible as the predicted capacity is under conservative by 90%. To address this issue, new equations are provided based on Failure mode C, Failure mode D, and Failure mode E.

Failure mode C

$$\mathrm{F_{v,Rk}} = f^{1.69}{}_{\mathrm{h,k}} d^{0.33} t^{0.97}$$

Failure mode D

$$\mathrm{F_{v,Rk}} = \mathrm{f_{h,k} d t_1} \left[\sqrt{2 + \frac{4\mathrm{M_{y,Rk}}}{\mathrm{f_{h,k} d t_1^{1.43}}}} - 1.2 \right] + \frac{\mathrm{F_{ax,Rk}}}{1.98}$$

Failure mode E

$$\mathrm{F_{v,Rk}} = 3.32 \sqrt{\mathrm{M_{y,Rk} f_{h,k} d}} + \frac{\mathrm{F_{ax,Rk}}}{0.31}$$

6.2 Limitation

These are the limitations of the current study

- The research is confined to specific grades of steel and timber.
- Due to the drilling capacity of the screw, the study was restricted to a single screw diameter.
- The proposed equation is based on the failure modes. The equation provides shear capacity but is not suitable for the initial prediction of failure modes. Therefore further research should be conducted using FEA analysis using parameters like different grades of steel, different screw arrangements, and different timber materials for further evaluation of connection strength.

6.3 Future Study

Future research on the behaviour of shear connections in structural steel with timber can be carried out in the following ways, according to the experimental investigation presented in this paper.

• Additional grades and varieties of timber, besides SG08 H3.2 timber, can be utilized to assess the structural behaviour of the structural steel-to-timber connection using experimental methods and Finite Element Analysis (FEA).

• The investigation on screw arrangement is limited to three screws, however, more exploration can be carried out by incorporating additional screws and experimenting with other screw spacing.

• The experimental investigation revealed that the screw axis is a significant factor as shown in Section 4.3. However, further research is required to examine the parametric impact of various timber thicknesses, multiple screws, and varying screw axis.

• The research was conducted using a monotonic load scenario. Further studies can be conducted to understand the seismic behaviour of connection in cyclic loading.

7 Acknowledgments

Firstly, I would like to express my deep gratitude to my first supervisor Dr Arthur Zhiyuan Fang, for his advice, assistance, guidance, and patience.

Also, I would like to express my sincere appreciation to Dr Krishanu Roy, and Professor James Lim for their expertise, thoughtful advice, and constant encouragement.

My best thanks to Jerry MA from Wurth for supplying all the Screws, structural steel sheets, and tools for this research.

I want to thank Dr. Dan Bompa for his advice on my interpretation of research data.

I want to thank my guide, Dinesh Lakshmanan Chandramohan, for his valuable input on the test design for my research.

I want to thank my friends Shubham Tiwari, Kushal Ghosh, Anu Antony, Gagan Sengundham Dinesh, Vivekanandan Shivaji, Harsh Birwadkar, Puviyarasan Velayudham.

I want to express my gratitude to my family, my father K.R.Mohanswamy, and my mother Veena. B.R., and my brother Bhargava.M for their support and motivation to complete this project.

Finally, I would like to thank the University of Waikato technicians Sophia Rodrigues, Jonathan van Harselaar, Denis Jouan, Peter Higgins, and Bradley Scott for their help and assistance during laboratory testing.

8 References

[1] M. He, F. Lam, J. Yang, S. Zhang, Wood Structural Design. China Construction Industry Press, 2008.

[2] Y. Sun, X. Yang, On the development prospect of Chinese wood structural architecture, Building Materials Decoration. 6 (2011) 22–26.

[3] Z. Yuan, Y. Sun, Thermal insulation materials for wood structures, Decoration of Building Materials. 6 (2015) 23–25.

[4] Z. Wang, Y. Wang, Y. Cao, Z. Gao, Measurements of the Shear Modulus of Materials by the Free-Plate Torsional Mode Shape Method, J. Test. Eval. 47 (2) (2019) 1163–1181.

[5] Y. Cao, M. Li, Z. Wang, Y. Wang, Z. Gao, Dynamic Testing and Analysis of Poisson's Ratio of Lumbers Based on the Cantilever-Plate Bending Mode Shape Method, J. Test. Eval. 47 (4) (2019) 2540–2550.

[6] D. Denouwe, M. Adamah, F. Eric, B. Abdelhamid, Experimental study of the mechanical behaviour of timber-concrete shear connections with threaded reinforcing bars, Eng. Struct. 172 (2018) 997–1010.

[7] H. Li, G. Wu, Q. Zhang, A. Deeks, J. Su, Ultimate bending capacity evaluation of laminated bamboo lumber beams, Constr. Build. Mater. 160 (2017) 365–375.

[8] H. Zhang, H. Li, I. Corbi, O. Corbi, G. Wu, C. Zhao, T. Cao, AFRP influence on parallel bamboo strand lumber beams, Sensors. 18 (9) (2018) 2854.

[9] P. Shang, Y. Sun, D. Zhou, K. Qin, X. Yang, Experimental study of the bending performance of hollow glulam beams, Wood and Fiber Science. 50 (1) (2018) 3–19.

[10] H. Li, Z. Qiu, G. Wu, O. Corbi, L. Wang, I. Corbi, C. Yuan, Slenderness ratio effect on eccentric compression performance of parallel strand bamboo lumber columns, Journal of Structural Engineering ASCE. 145 (8) (2019) 04019077.

[11] H. Li, R. Liu, R. Lorenzo, G. Wu, L. Wang, Eccentric compression properties of laminated

bamboo lumber columns with different slenderness ratios. Proceedings of the Institution of Civil Engineers - Structures and Buildings. 172(5) (2019) 315-326.

[12] C. Tan, H. Li, D. Wei, R. Lorenzo, C. Yuan, Mechanical performance of parallel bamboo strand lumber columns under axial compression: experimental and numerical investigation, Constr. Build. Mater. 231 (2020) 117168.

[13] L. Tian, Y. Kou, J. Hao, Axial compressive behaviour of sprayed composite mortar–original bamboo composite columns, Constr. Build. Mater. 215 (2019) 726–736.

[14] L. Tian, Y. Kou, J. Hao, Flexural behaviour of sprayed lightweight composite mortar-original bamboo composite beams: experimental.

[15] A. Hassanieh, H. Valipour, M. Bradford, Load-slip behaviour of steel-cross laminated timber (CLT) composite connections, J. Constr. Steel Res. 122 (2016) 110–121.

[16] Žegarac Leskovar, V., & Premrov, M. (2021). A review of architectural and structural design typologies of multi-storey timber buildings in Europe. *Forests*, *12*(6), 757.

[17] R. Yang, H. Li, R. Lorenzo, M. Ashraf, Y. Sun, and Q. Yuan, "Mechanical behaviour of steel timber composite shear connections," Construction and Building Materials, vol. 258, 2020, doi: 10.1016/j.conbuildmat.2020.119605.

[18] A. Hassanieh, H. R. Valipour, and M. A. Bradford, "Experimental and analytical behaviour of steel-timber composite connections," *Construction and Building Materials*, vol. 118, pp. 63-75, 2016, doi: 10.1016/j.conbuildmat.2016.05.052.

[19] A. L. Y. Ng, H. H. Lau, Z. Fang, K. Roy, G. M. Raftery, and J. B. P. Lim, "The behaviour of cold-formed steel and Belian hardwood self-tapping screw connections," presented at the Cold-Formed Steel Research Consortium Colloquium, 2022.

[20] A. L. Y. Ng, H. H. Lau, Z. Fang, K. Roy, G. M. Raftery, and J. B. P. Lim, "Experimental studies of timber to cold-formed steel connections with self-drilling screws," *Structures*, vol. 49, pp. 492-507, 2023, doi: 10.1016/j.istruc.2023.01.111.

[21] Y. De Santis and M. Fragiacomo, "Timber-to-timber and steel-to-timber screw connections: Derivation of the slip modulus via beam on elastic foundation model," Engineering Structures, vol. 244, 2021, doi: 10.1016/j.engstruct.2021.112798.

[22] A. Hassanieh, H. R. Valipour, and M. A. Bradford, "Composite connections between CLT slab and steel beam: Experiments and empirical models," Journal of Constructional Steel Research, vol. 138, pp. 823-836, 2017, doi: 10.1016/j.jcsr.2017.09.002.

[23] P. Kyvelou, L. Gardner, and D. A. Nethercot, "Design of Composite Cold-Formed Steel Flooring Systems," Structures, vol. 12, pp. 242-252, 2017

[24] EN-1995-1-1 (2004) Eurocode 5. Design of timber structures—part 1-1: general-common rules and rules for buildings. European Committee for Standardisation, Brussels, Belgium.

[25] Vella, N., Gardner, L., & Buhagiar, S. (2020, April). Experimental analysis of cold-formed steel-to-timber connections with inclined screws. In *Structures* (Vol. 24, pp. 890-904). Elsevier.

[26] ASTM A370, Standard Test Methods and Definitions for Mechanical Testing of Steel Products, American Society of Testing Materials, ASTM, West Conshohocken, PA, 2019.

[27] ASTM D2395-17, Standard Test Methods for Density and Specific Gravity (Relative Density) of Wood and Wood-Based Materials, ASTM International

[28] ASTM D4442-20, 'Test Methods for Direct Moisture Content Measurement of Wood and Wood-Based Materials', ASTM International.

[29] Standards New Zealand (1993). NZS 3603: 1993 Timber Structures Standard. Standards New Zealand, Wellington, New Zealand

[30] CEN, N. (2006). EN10002-1-Tensile testing of metallic materials-Part 1: Method of test at ambient temperature. *European Committee for Standardization*

[31] EN ISO 6892-1:2009, Metallic materials – Tensile testing – Part 1: Method of test at room

temperature, (ISO 6892-1:2009); English version EN ISO 6892-1:2009, Beuth Verlag, Berlin, December 2009

[32] ASTM F1575 Standard Test Method for Determining Bending Yield Moment of Nails.

[33] ASTM. "Test Methods for Mechanical Fasteners in Wood, D1761-06." West Conshohocken, PA: ASTM International, 2006a.

[34] ASTM D5764 Standard Test Method for Evaluating Dowel-Bearing Strength of Wood and International Journal of Engineering & Technology 209 Wood-Based Products. American Society of Testing and Materials Designation D5764-23a.

[35] Wurth New Zealand Ltd, Auckland New Zealand.

[36] American Society for Testing and Materials, ASTM E8/E8M-21: Standard Test Methods for Tension Testing of Metallic Materials. 2021.

[37] M.R. Bambach, K.J.R. Rasmussen, Behaviour of self-drilling screws in light-gauge steel construction, J. Struct. Eng. ASCE 133 (6) (2007) 895–898.

[38] D. Denouwe, M. Adamah, F. Eric, B. Abdelhamid, Experimental study of the mechanical behaviour of timber-concrete shear connections with threaded reinforcing bars, Eng. Struct. 172 (2018) 997–1010.

[39] Khorsandnia Nima, Valipour Hamid R, Crews Keith. Experimental and analytical investigation of short-term behaviour of LVL–concrete composite connections and beams. Constr Build Mater 2012;37:229–38

[40] Xiao, Y., & Ishikawa, T. (2005). Bearing strength and failure behaviour of bolted composite joints (part I: Experimental investigation). *Composites science and technology*, *65*(7-8), 1022-1031.

[41] Ramirez-Jimenez, C. R., Papadakis, N., Reynolds, N., Gan, T. H., Purnell, P., & Pharaoh, M. (2004). Identification of failure modes in glass/polypropylene composites by means of the primary frequency content of the acoustic emission event. *Composites Science and*

Technology, *64*(12), 1819-1827.

[42] Timbolmas, C., Bravo, R., Rescalvo, F. J., Villanueva, P., & Portela, M. (2023). Digital image correlation and numerical analysis of CFRP-poplar timber interface subjected to modified single shear test. *Composite Structures*, *320*, 117188.

[43] He, Z., Zheng, G., Luo, Q., Li, Q., & Sun, G. (2024). Fatigue life improvement mechanisms of CFRP/Al hybrid joints–Load sharing study using a digital image correlation technique. *Composite Structures*, *327*, 117625.

[44] Shi, D., Demartino, C., Li, Z., & Xiao, Y. (2023). Axial load–deformation behaviour and fracture characteristics of bolted steel to laminated timber and glubam connections. *Composite Structures*, *305*, 116486.

[45] A. Hassanieh, H. Valipour, M. Bradford, Experimental and numerical study of steel-timber composite (stc) beams, J. Constr. Steel Res. 122 (2016) 367–378.

[46] Milewska, A. (2018). *Power-actuated fasteners in single shear* (Doctoral dissertation, ResearchSpace@ Auckland).

[47] Rogers, C. A., & Hancock, G. J. (1999). Screwed connection tests of thin G550 and G300 sheet steels. *Journal of Structural Engineering*, *125*(2), 128-136.

[48] LaBoube, R. A., & Sokol, M. A. (2002). Behaviour of screw connections in residential construction. *Journal of structural engineering*, *128*(1), 115-118.

[49] Standards Australia. (2010). AS 1720.1 - 2010 Timber Structures Part 1: Design Methods. Sydney, Australia: Standards Australia.

[50] Lu, L., Wang, D., Wang, W., Wu, H., Ding, K., Darkwah, K. K., & Yan, H. (2022, January). Shear bearing capacity of Self-drilling screw group connections of CFS sheets. In *Structures* (Vol. 35, pp. 160-171). Elsevier.

[51] Roy, K., Lau, H. H., Ting, T. C. H., Masood, R., Kumar, A., & Lim, J. B. (2019). Experiments and finite element modelling of screw pattern of self-drilling screw connections

for high strength cold-formed steel. *Thin-Walled Structures*, *145*, 106393

Appendix A Shear test for single screw connection

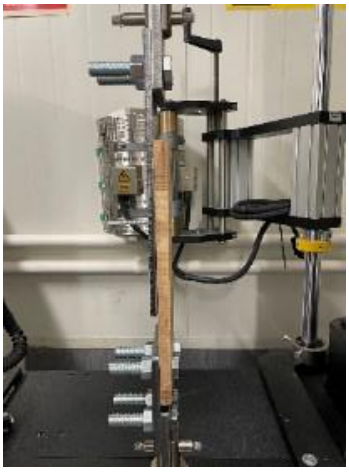

(a)Test setup

(b)Post-tested samples

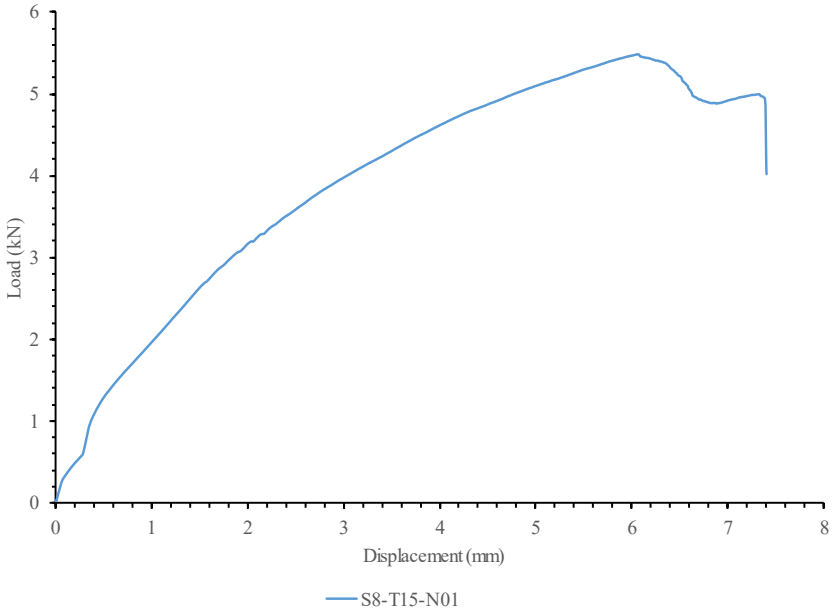

(c)Load v/s displacement curve for single screw of 8mm steel and 15mm timber

Figure 49 Test result of S08-T15-N01

(a)Test setup

(b) Post-tested samples

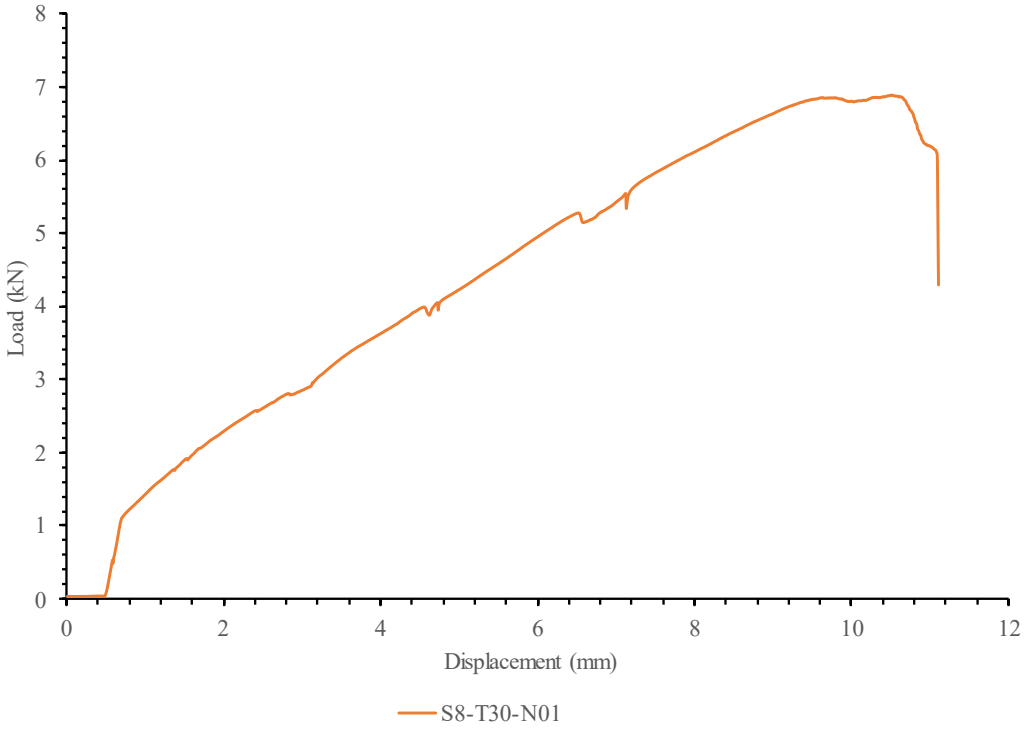

(c) Load v/s displacement curve for single screw of 8mm steel and 30mm timber

Test result of S08-T30-N01

(a)Test setup

(b) Post-tested samples

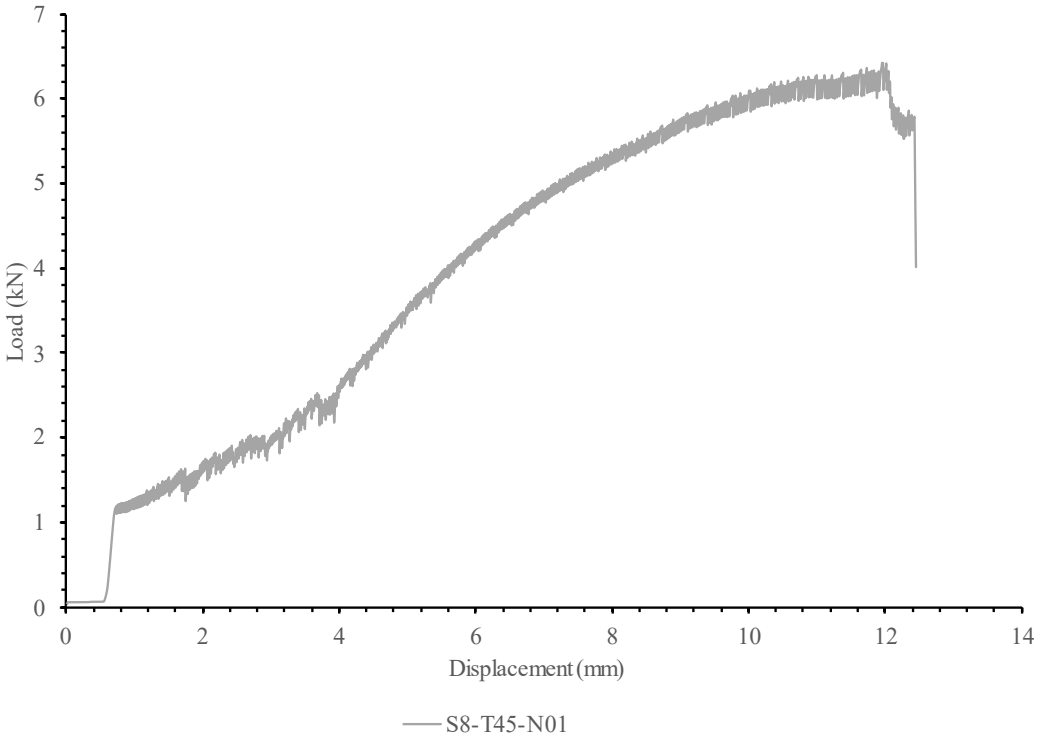

(c) Load v/s displacement curve for single screw of 8mm steel and 45mm timber

Figure 50 Test result of S08-T45-N01

(a)Test setup

(b)Post-tested samples

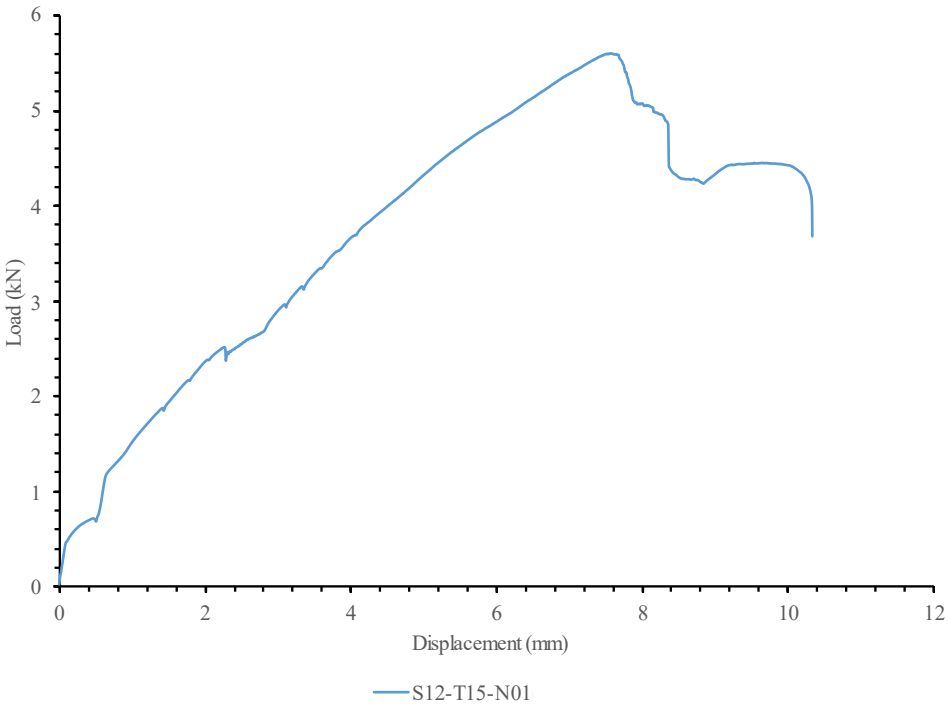

(c)Load v/s displacement curve for single screw of 12mm steel and 15mm timber

Figure 51 Test result of S12-T15-N01

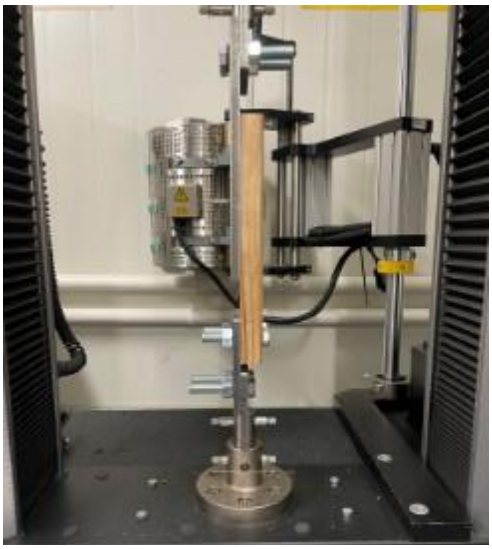

(a)Test setup

(b)Post-tested samples

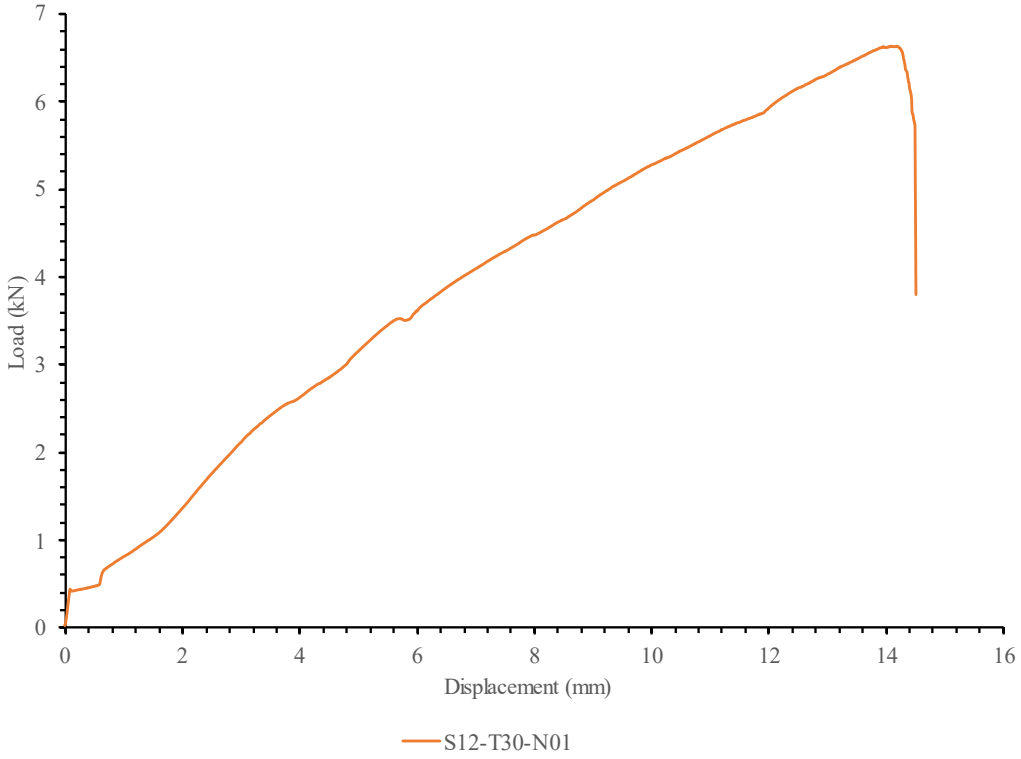

(c)Load v/s displacement curve for single screw of12mm steel and 30mm timber

Figure 52 Test result of S12-T30-N01

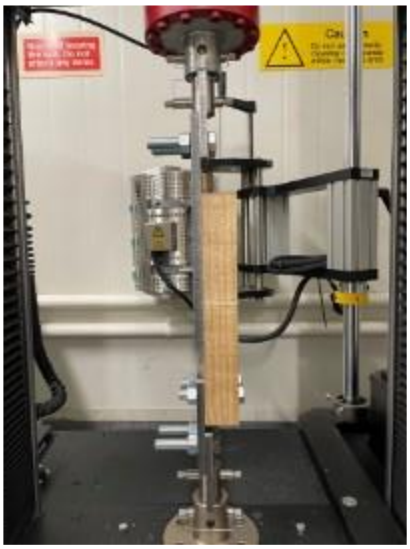

(a)Test setup

(b)Post-tested samples

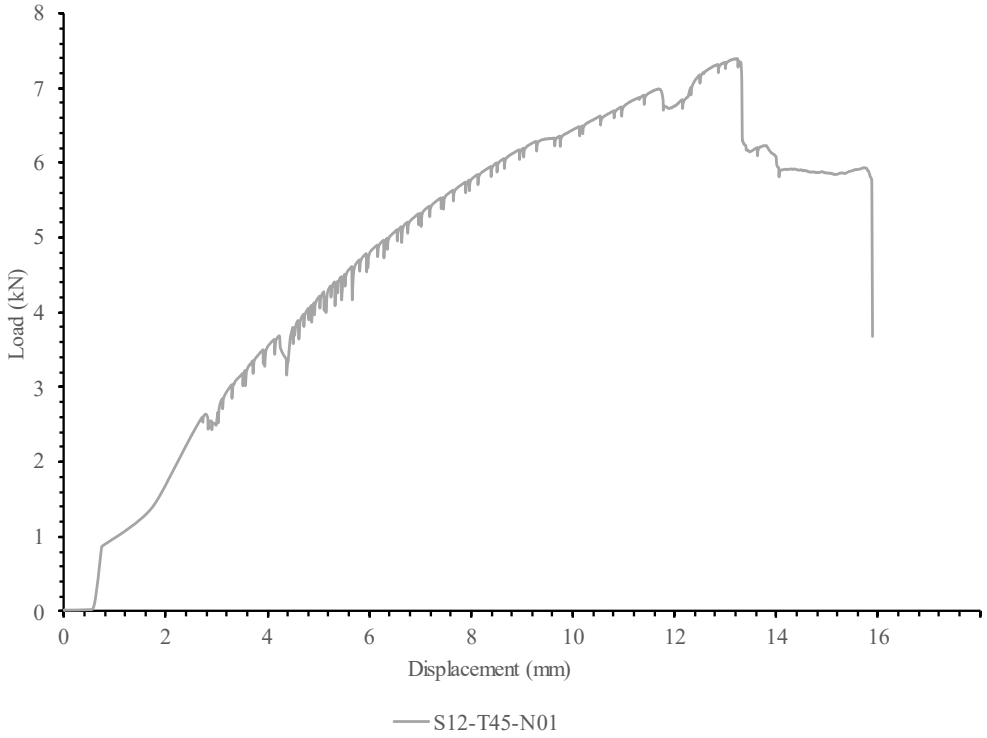

(c)Load v/s displacement curve for single screw of 12mm steel and 45mm timber

Figure 53 Test result of S12-T45-N01

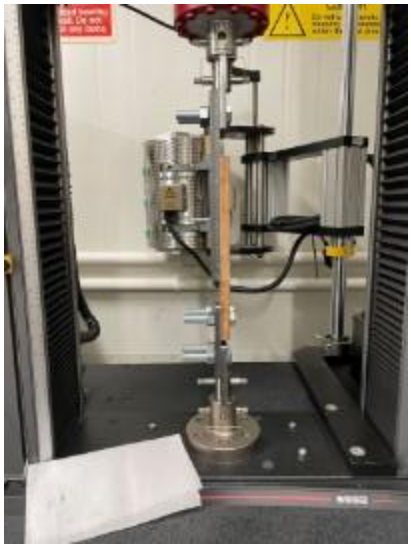

(a)Test setup

(b)Post-tested samples

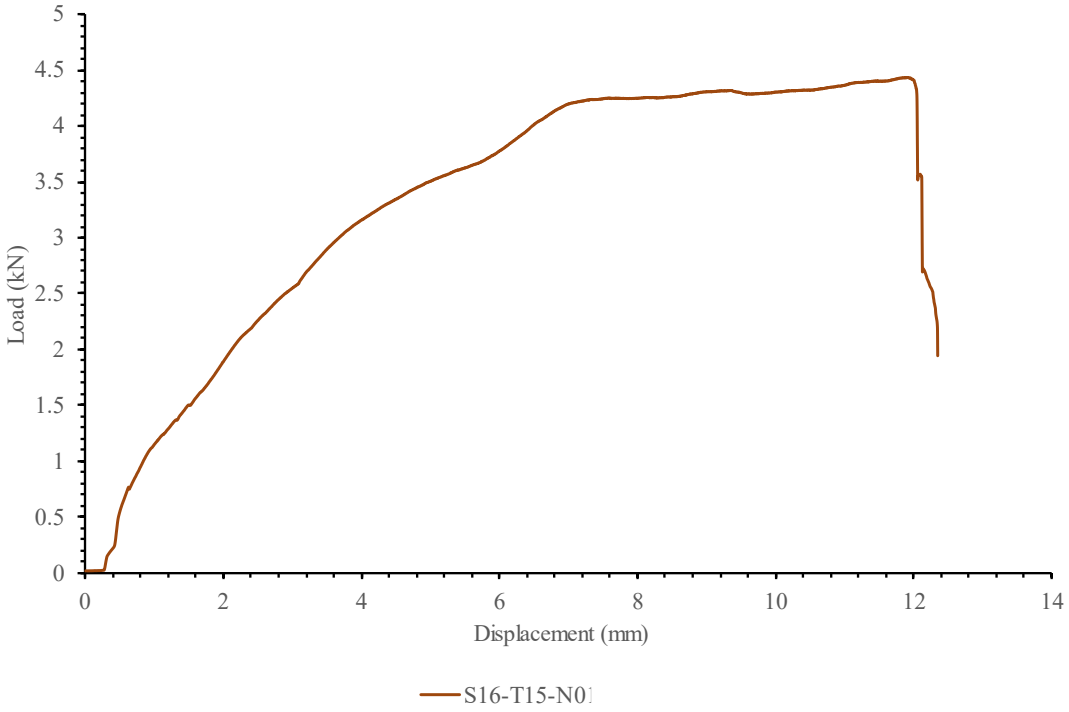

(c)Load v/s displacement curve for single screw of 16mm steel and 15mm timber

Figure 54 Test result of S16-T15-N01

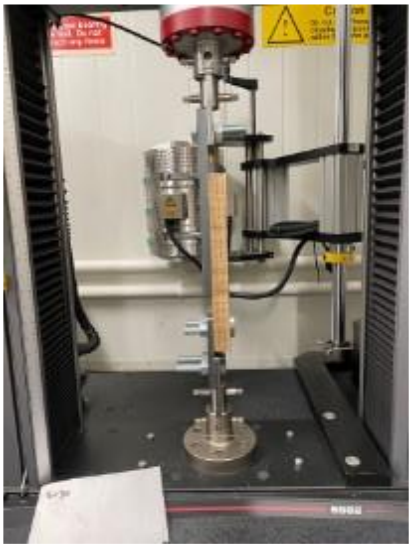

(a)Test setup

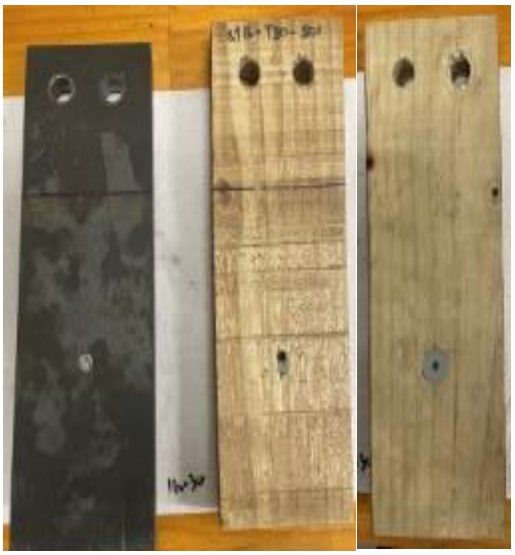

(b)Post-tested samples

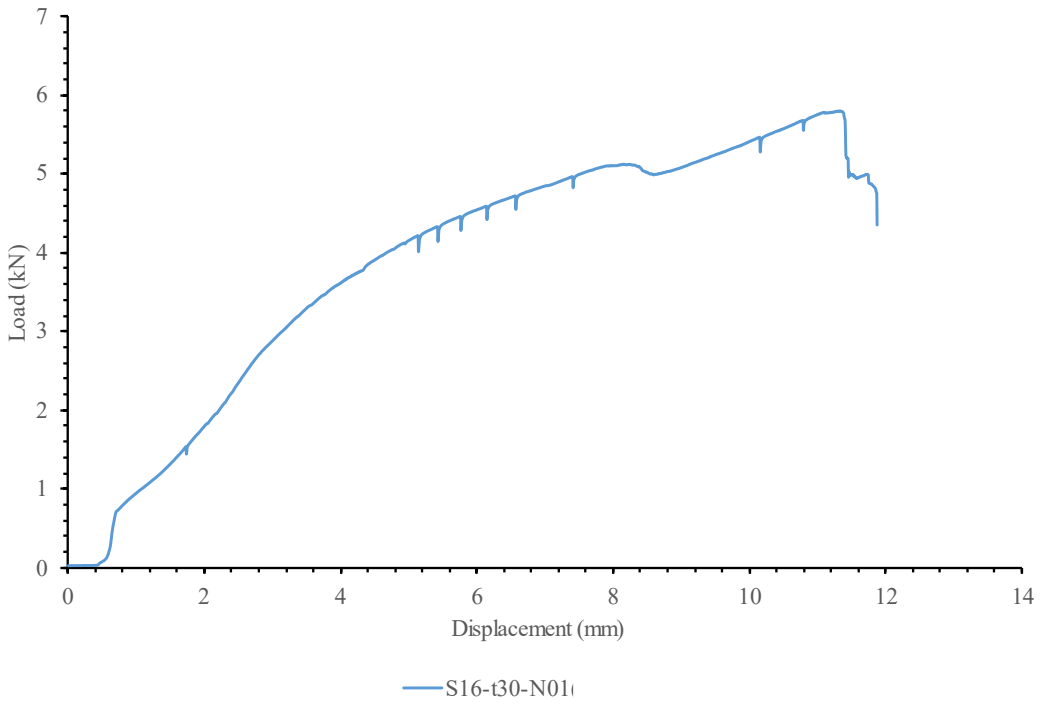

(c)Load v/s displacement curve for single screw of 16mm steel and 30mm timber

Figure 55 Test result of S16-T30-N01

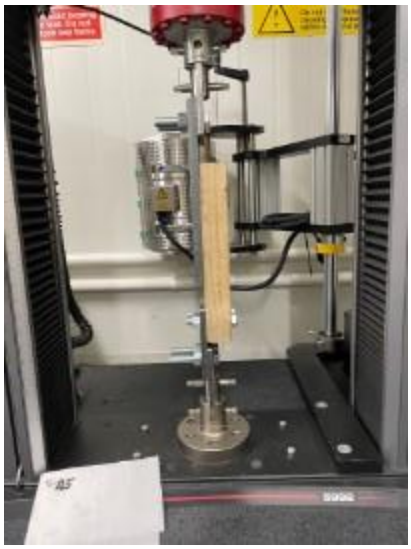

(a)Test setup

(b)Post-tested samples

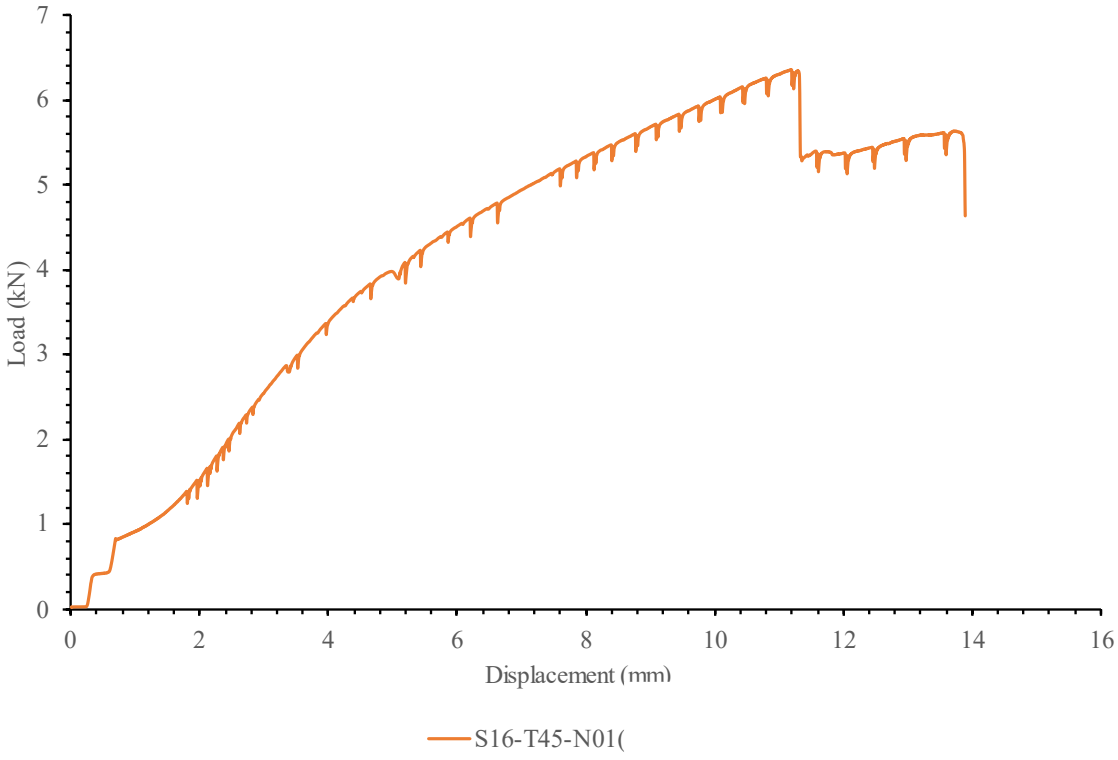

(c)Load v/s displacement curve for single screw ofl 6mm steel and 45mm timber

Figure 56 Test result of S16-T45-N01

(a)Test setup

(b)Post-tested samples

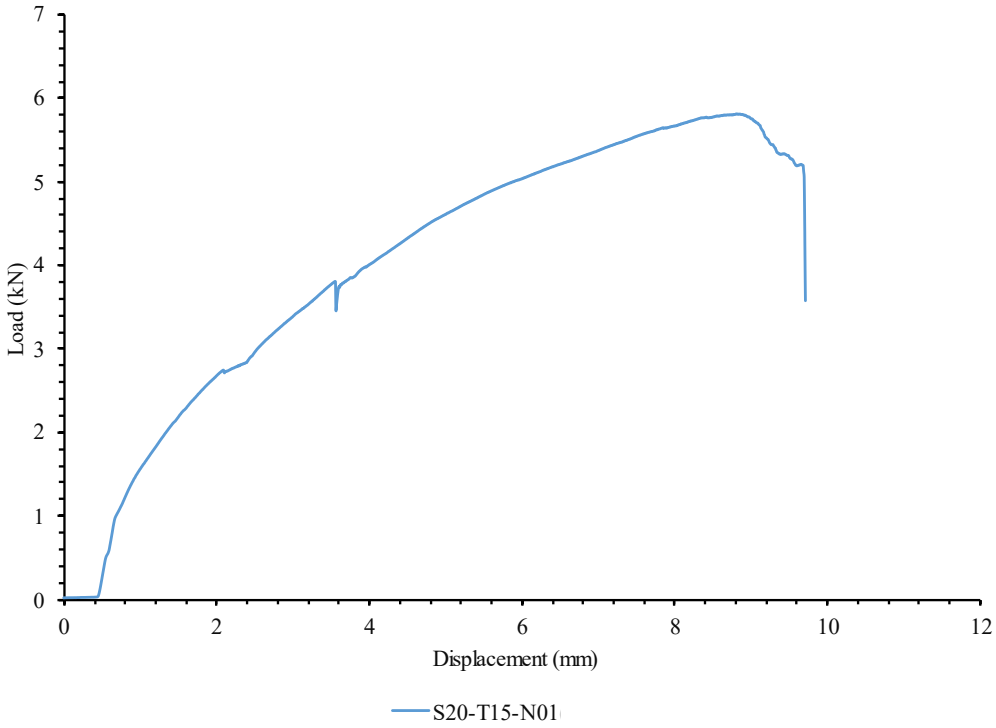

(c)Load v/s displacement curve for single screw of 20mm steel and 15mm timber

Figure 57 Test result of S20-T15-N01

(a)Test setup

(b)Post-tested samples

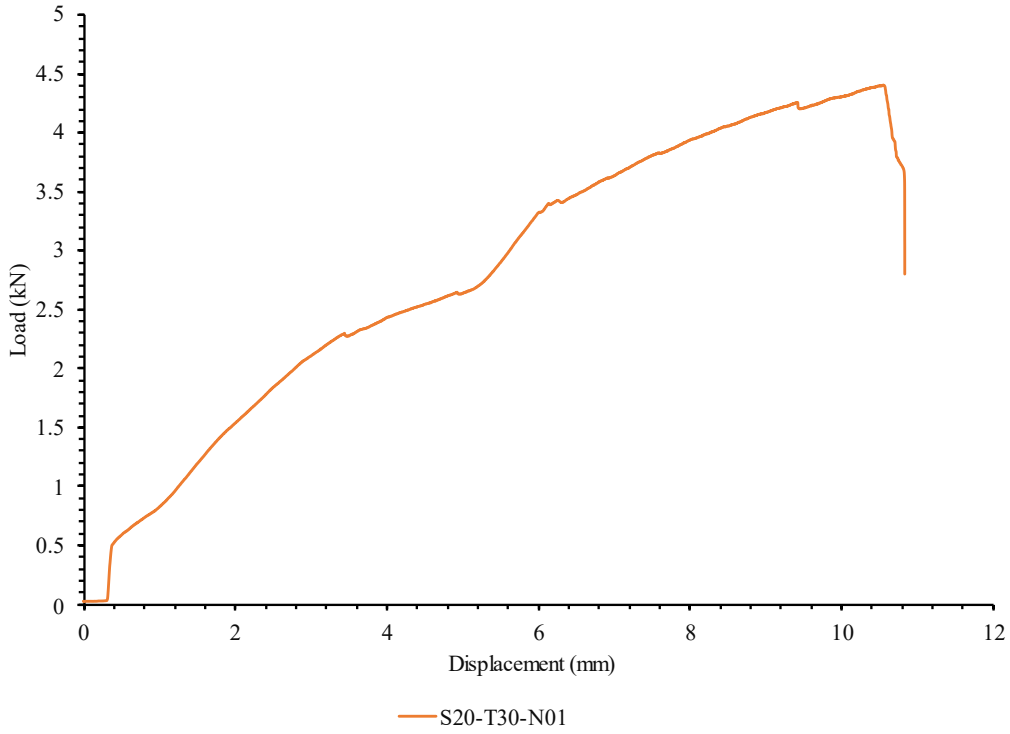

(c)Load v/s displacement curve for single screw of 20mm steel and 30mm timber

Figure 58 Test result of S20-T30-N01

(a)Test setup

(b)Post-tested samples

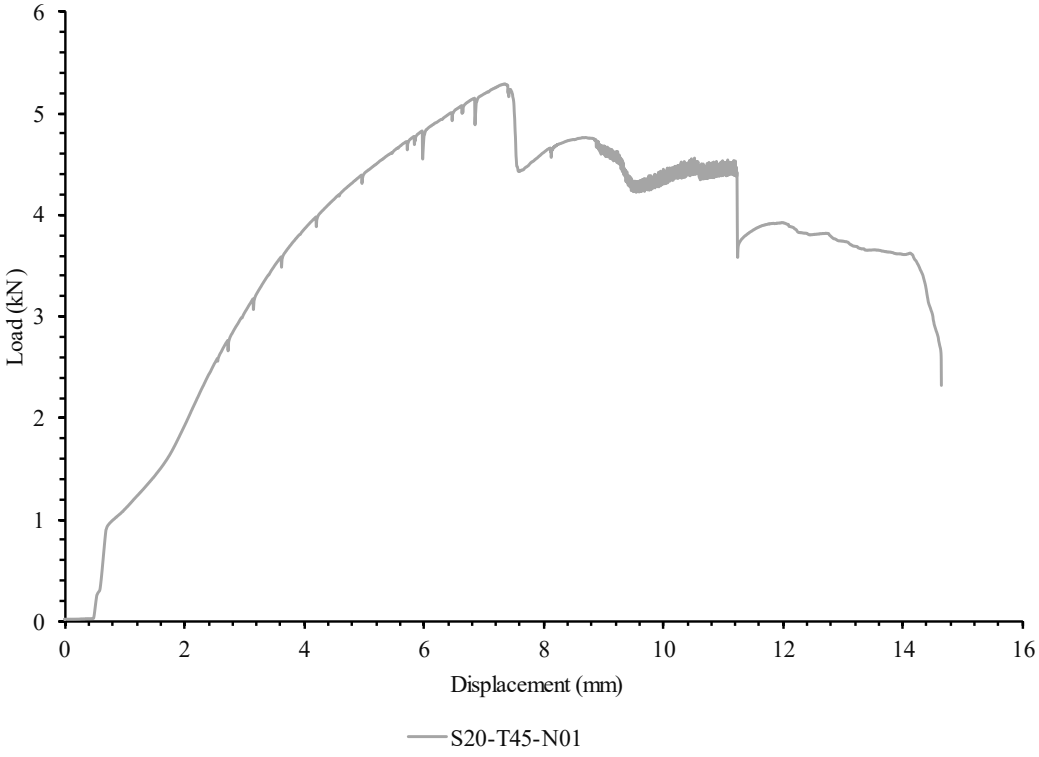

(c)Load v/s displacement curve for single screw of 20mm steel and 45mm timber

Figure 59 Test result of S20-T45-N01

Appendix B Shear test for two screw connection

(a)Test setup

(b) Post-tested samples

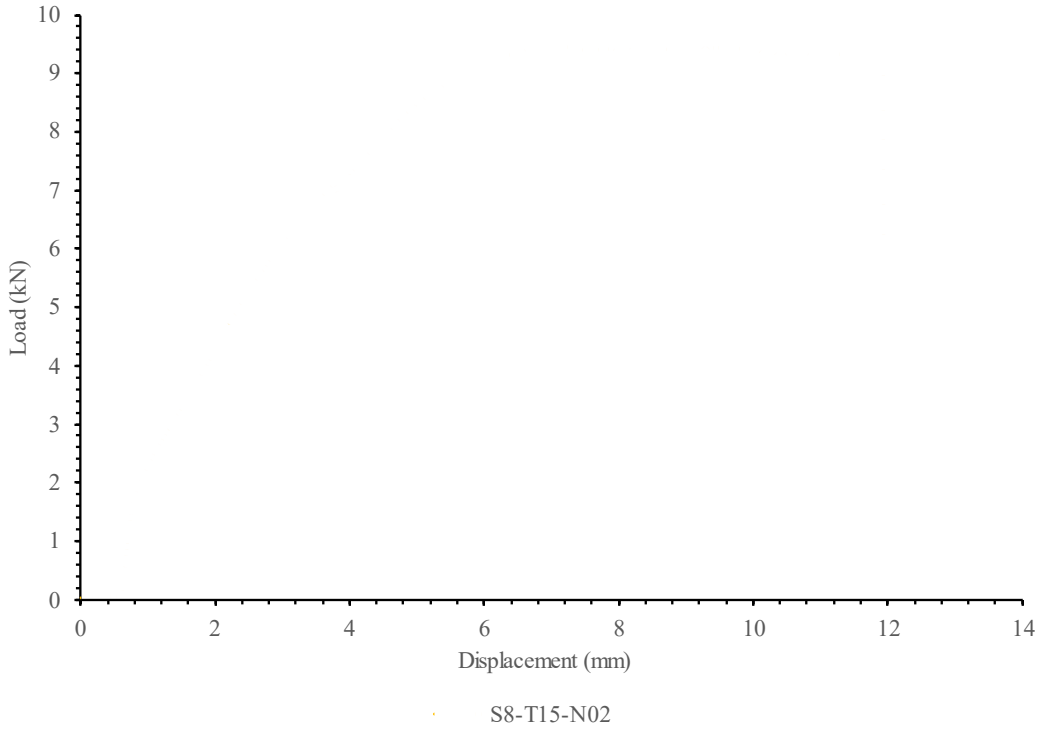

(c) Load v/s displacement curve for two screw of 8mm steel and 15mm timber

Figure 60 Test result of S08-T15-N02

(a)Test setup

(b) Post-tested samples

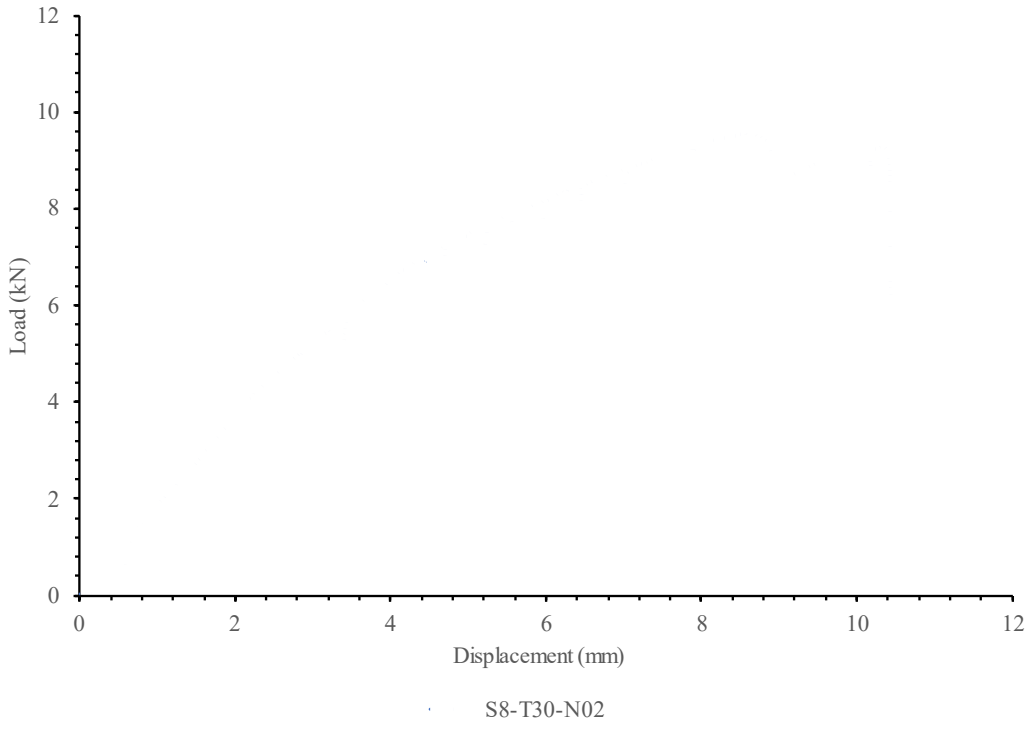

(c) Load v/s displacement curve for two screw of 8mm steel and 30mm timber

Figure 61 Test result of S08-T30-N02

(a)Test setup

(b) Post-tested samples

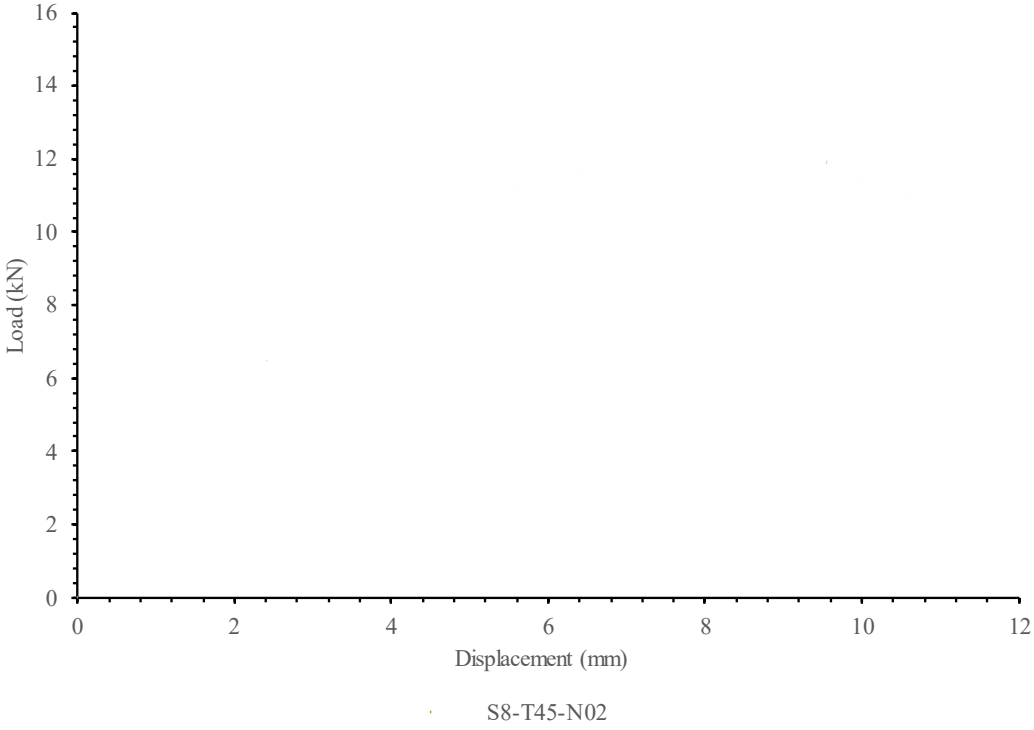

(c) Load v/s displacement curve for two screw of 8mm steel and 45mm timber

Figure 62 Test result of S08-T45-N02

(a)Test setup

(b)Post-tested samples

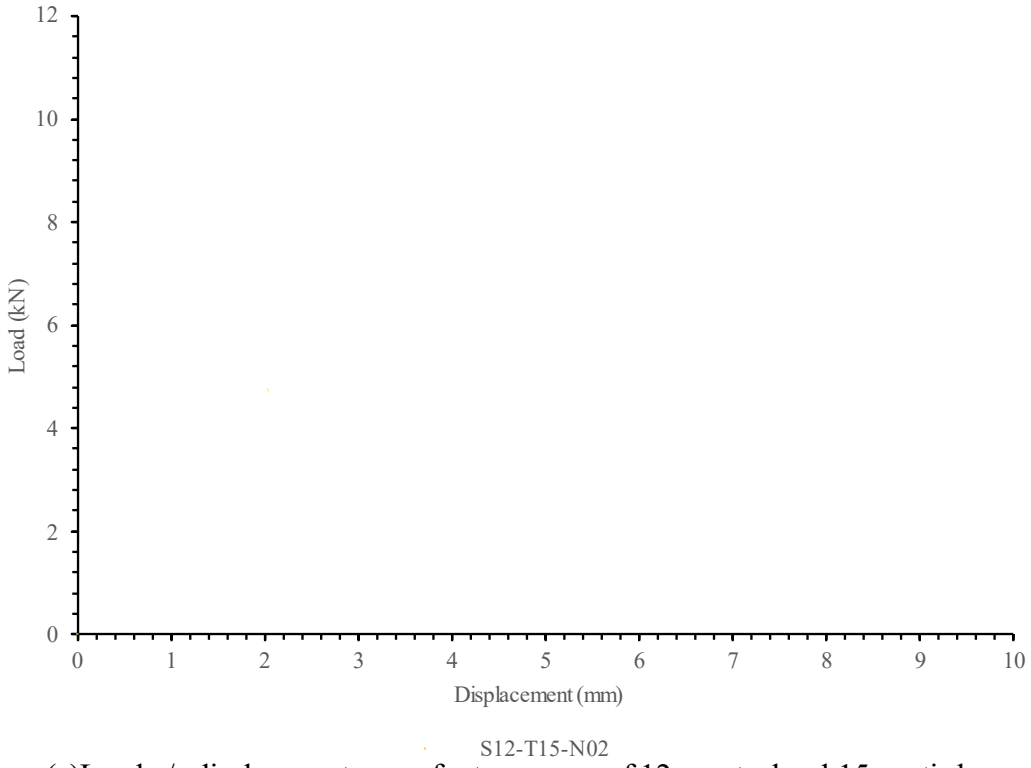

(c)Load v/s displacement curve for two screw of 12mm steel and 15mm timber

Figure 63 Test result of S12-T15-N02

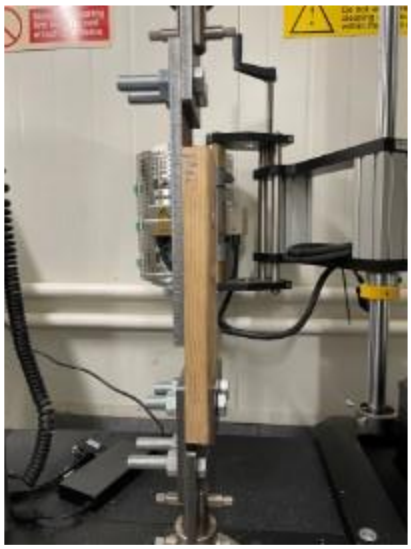

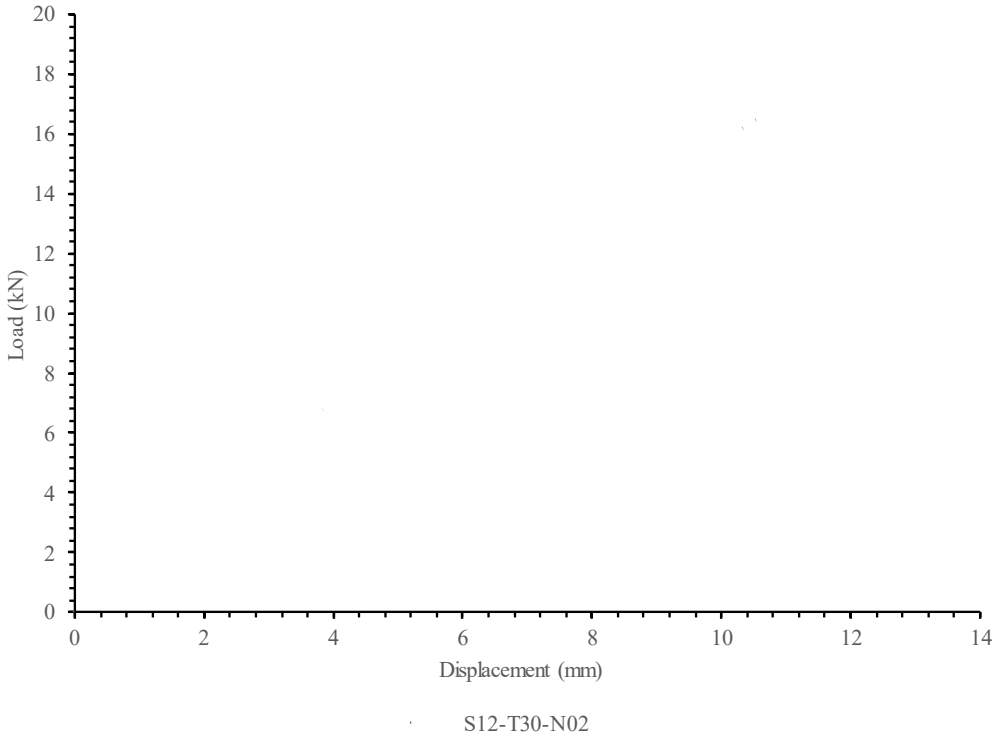

Figure 64 Test result of S12-T30-N02

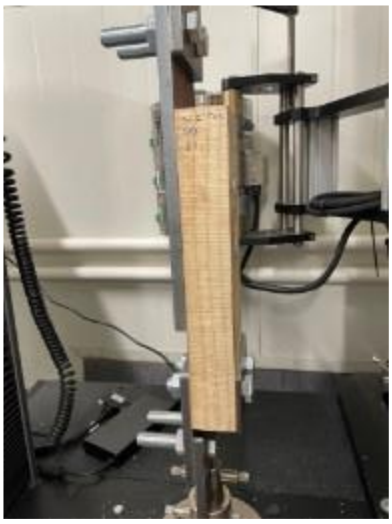

(a)Test setup

(b)Post-tested samples

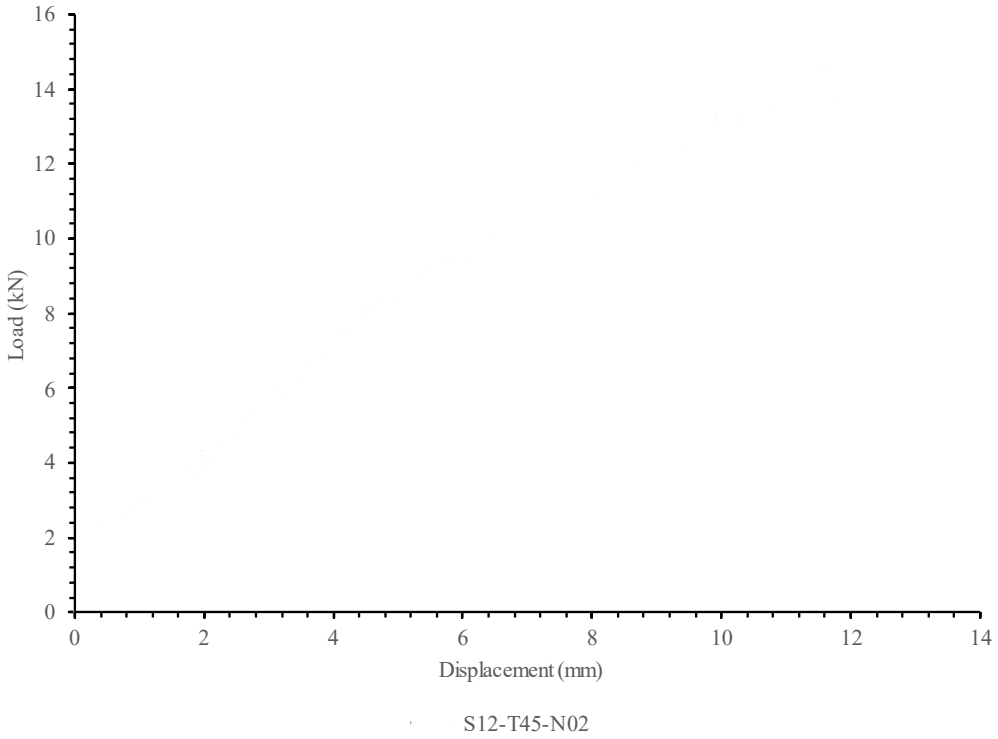

(c)Load v/s displacement curve for two screw of 12mm steel and 45mm timber

Figure 65 Test result of S12-T45-N02

(a)Test setup

(b)Post-tested samples

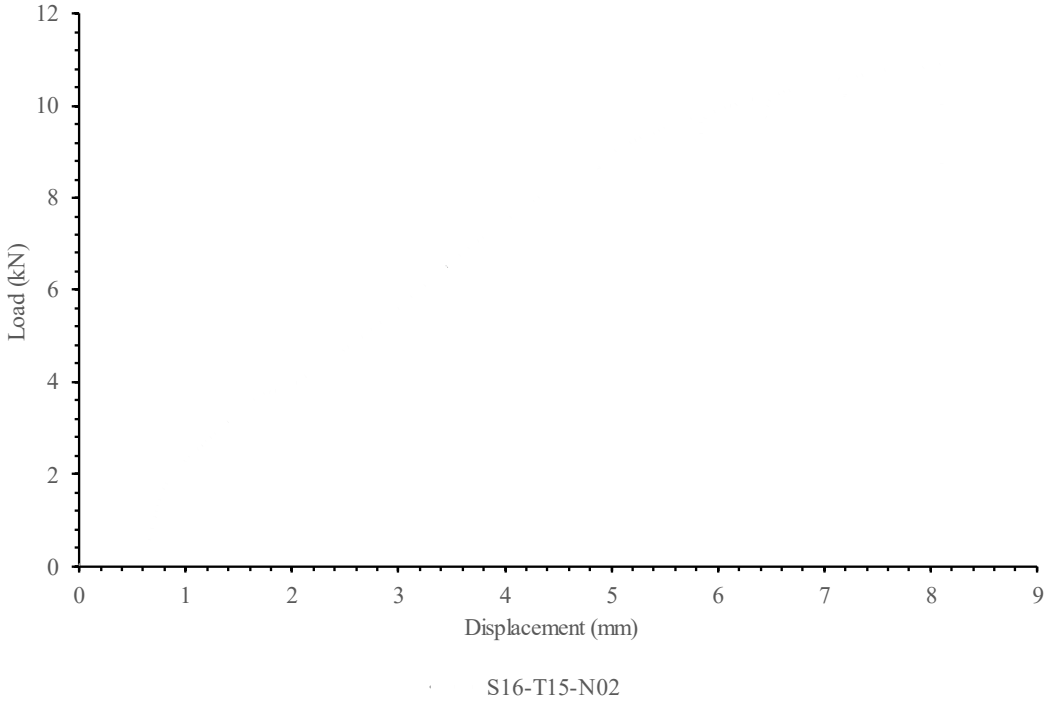

(c)Load v/s displacement curve for two screw of 16mm steel and 15mm timber

Figure 66 Test result of S16-T15-N02

(a)Test setup

(b)Post-tested samples

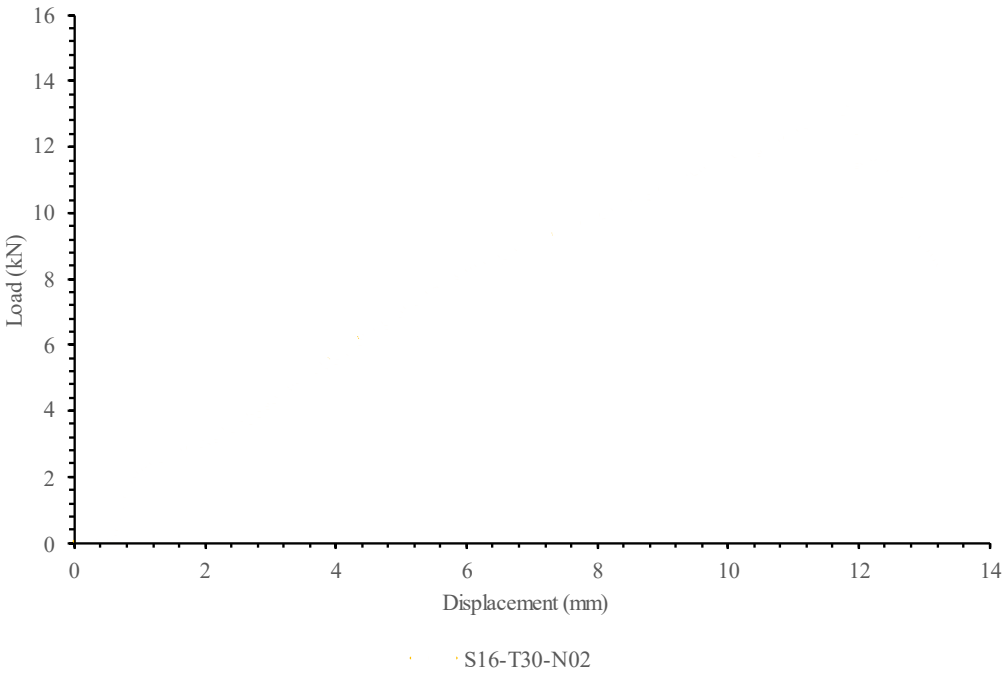

(c)Load v/s displacement curve for two screw ofl 6mm steel and 30mm timber

Figure 67 Test result of S16-T30-N02

(a)Test setup

(b)Post-tested samples

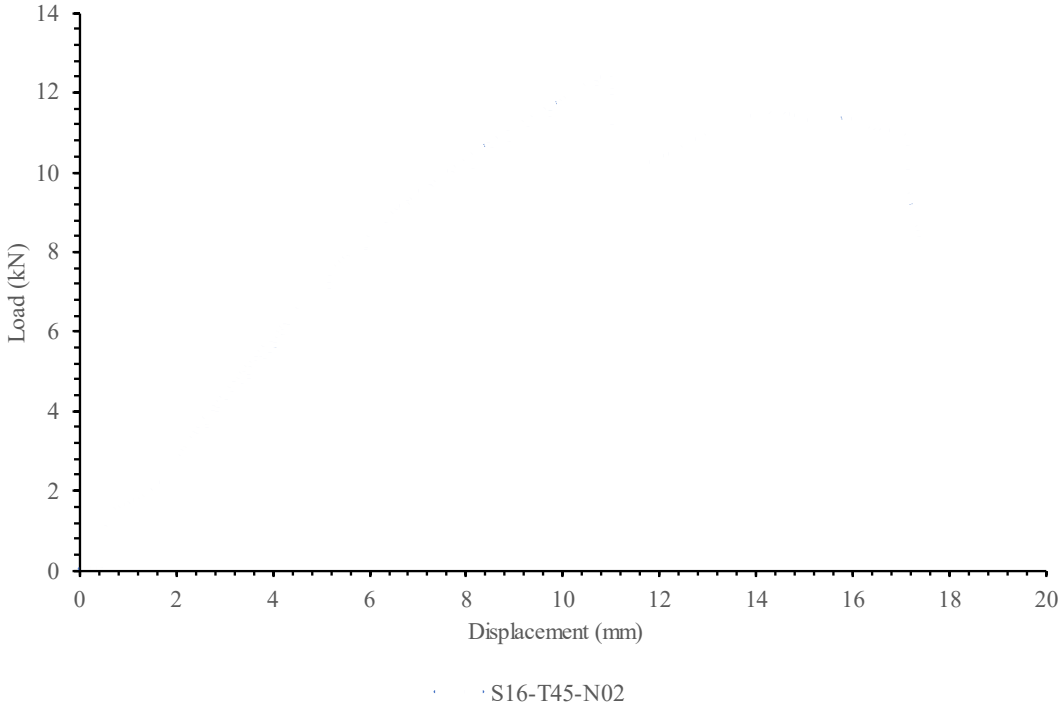

(c)Load v/s displacement curve for two screw of 16mm steel and 45mm timber

Figure 68 Test result of S16-T45-N02

(a)Test setup

(b)Post-tested samples

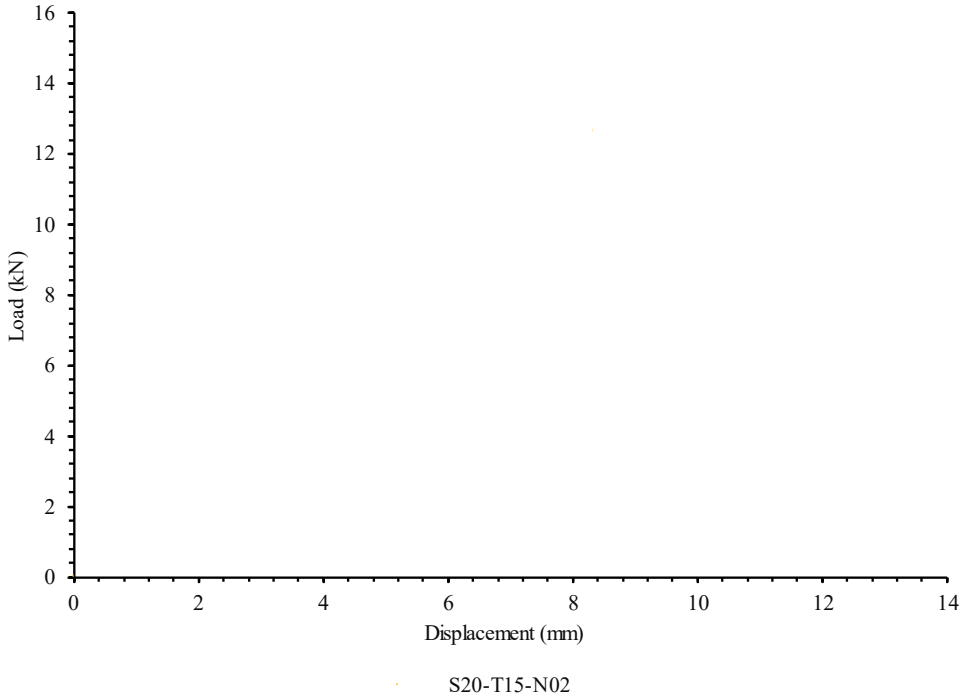

(c)Load v/s displacement curve for two screw of 20mm steel and 15mm timber

Figure 69 Test result of S20-T15-N02

(a)Test setup

(b)Post-tested samples

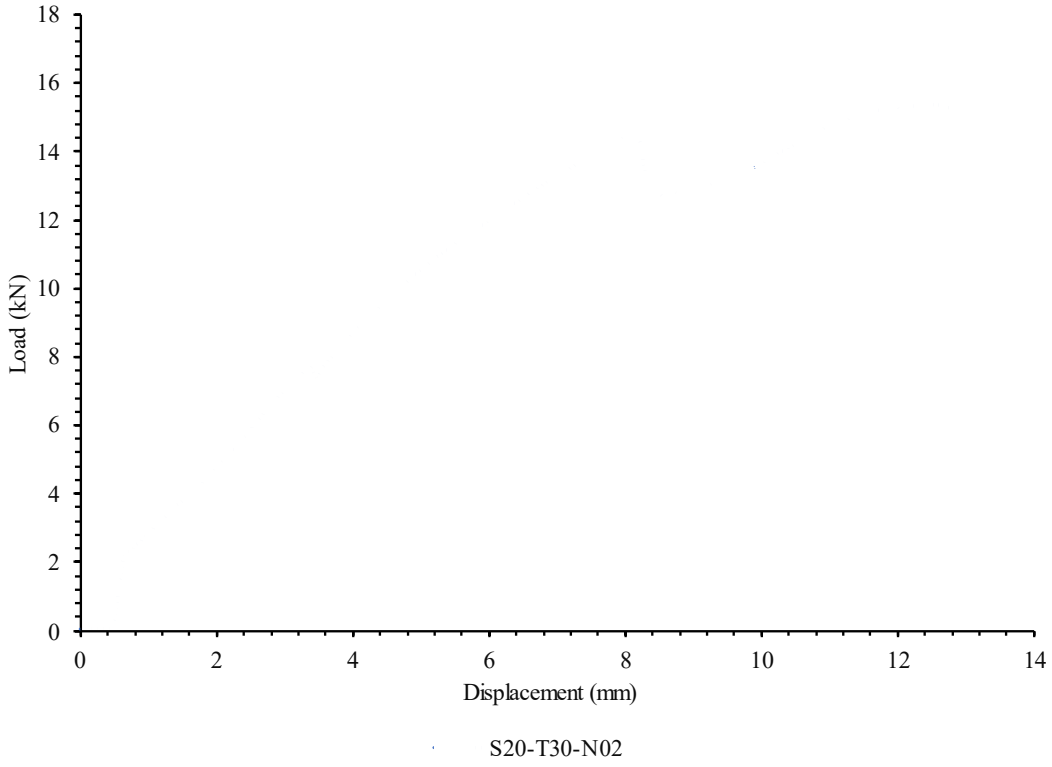

(c)Load v/s displacement curve for two screw of 12mm steel and 30mm timber

Figure 70 Test result of S20-T30-N02

(a)Test setup

(b)Post-tested samples

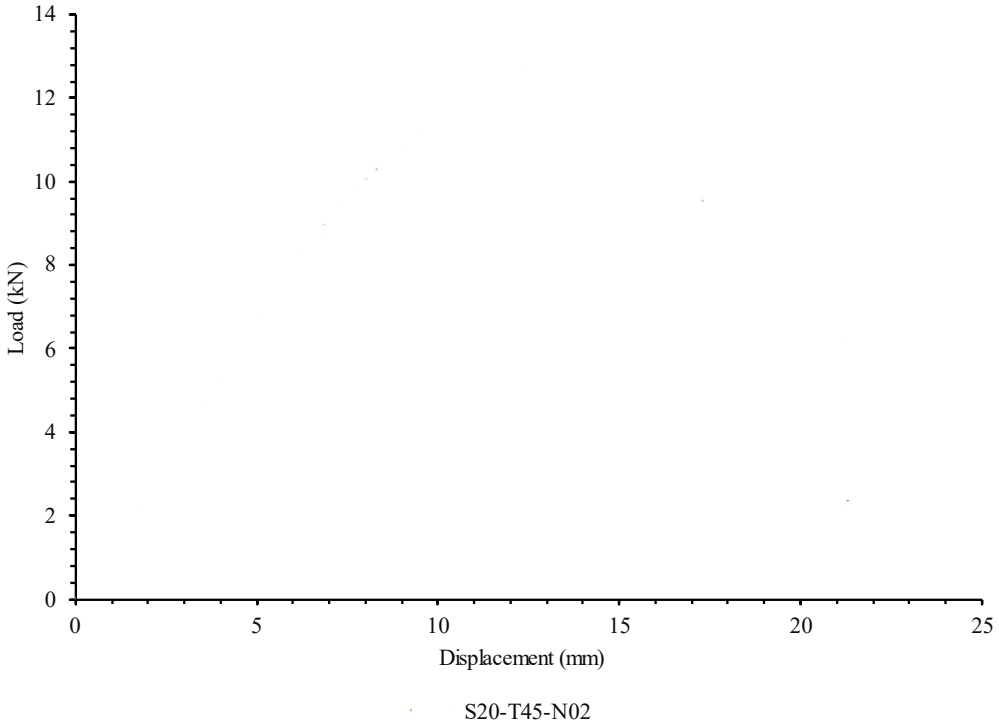

(c)Load v/s displacement curve for two screw of 20mm steel and 45mm timber

Figure 71 Test result of S20-T45-N02

Appendix C Shear test for three screw connection

(a)Test setup

(b) Post-tested samples

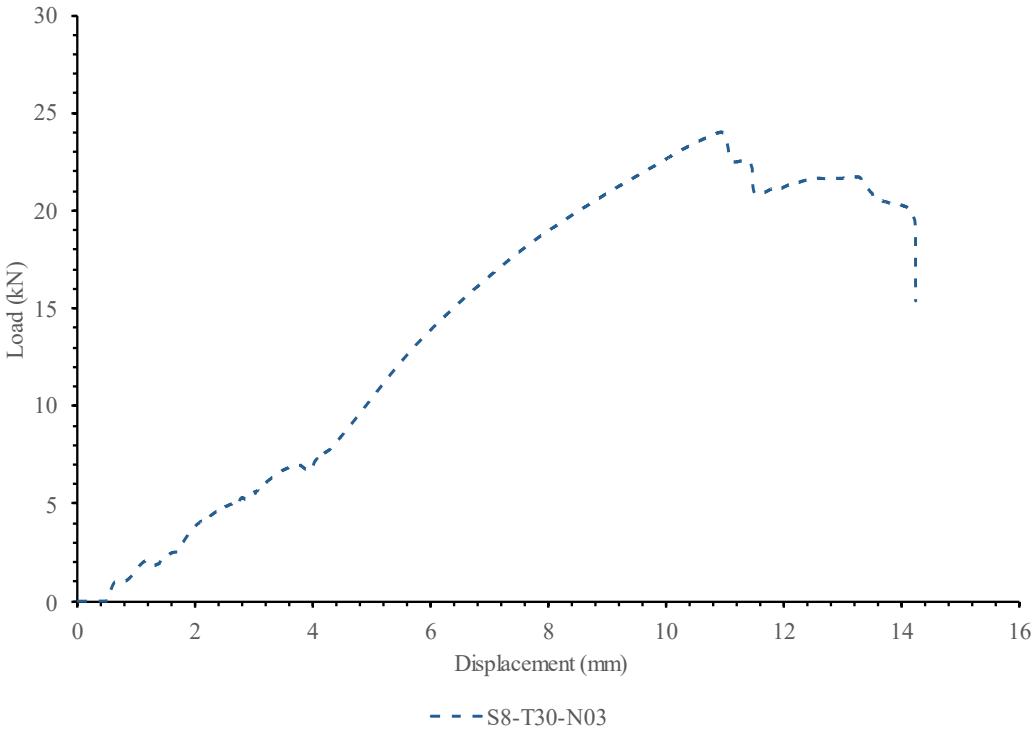

(c) Load v/s displacement curve for three screw of 8mm steel and 30mm timber

Figure 72 Test result of S08-T30-N03

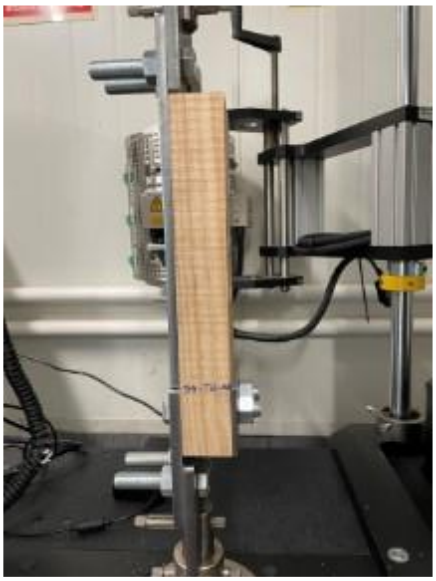

(a)Test setup

(b) Post-tested samples

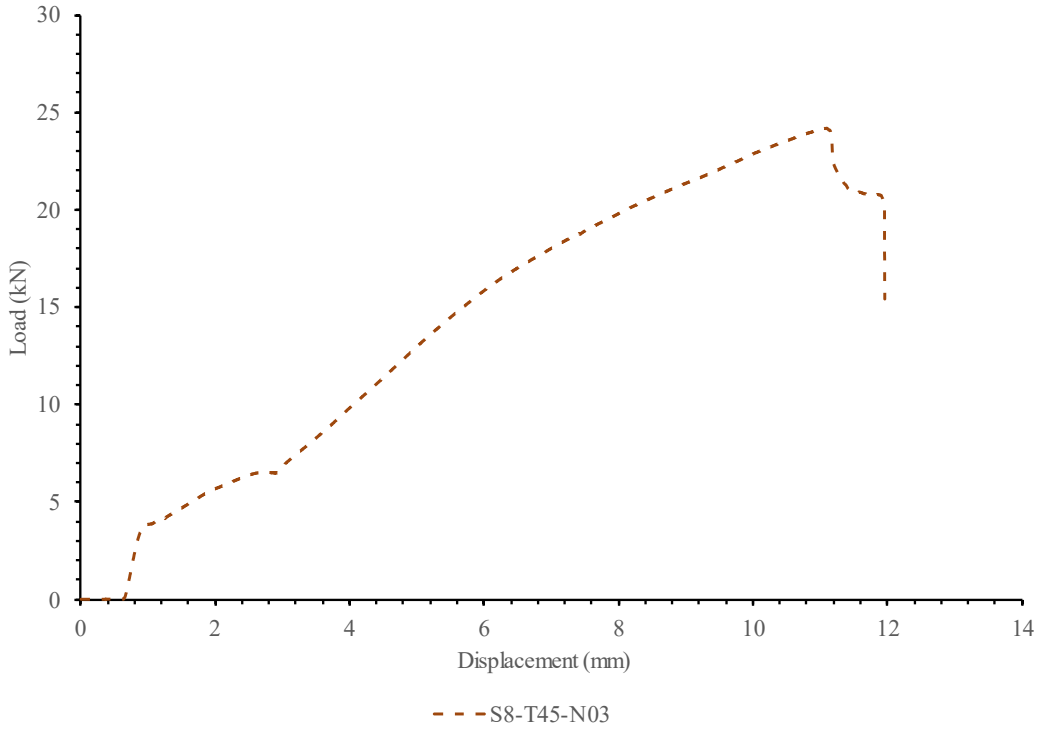

(a) Load v/s displacement curve for single screw of 8mm steel and 45mm timber

Figure 73 Test result of S08-T45-N03

(a)Test setup

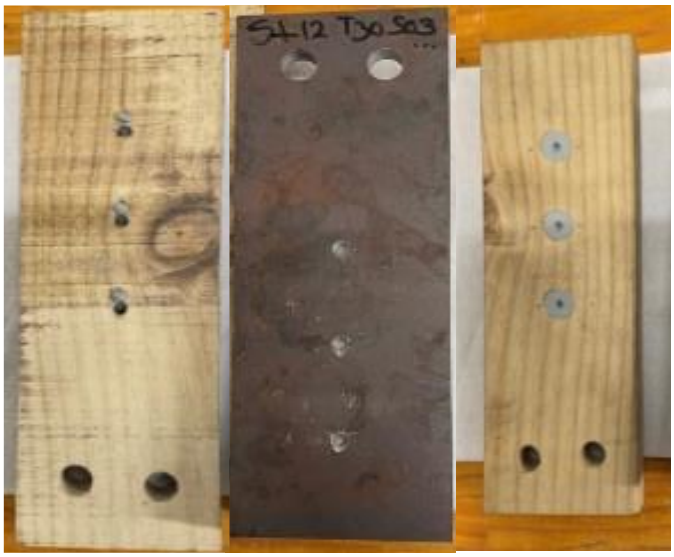

(b)Post-tested samples

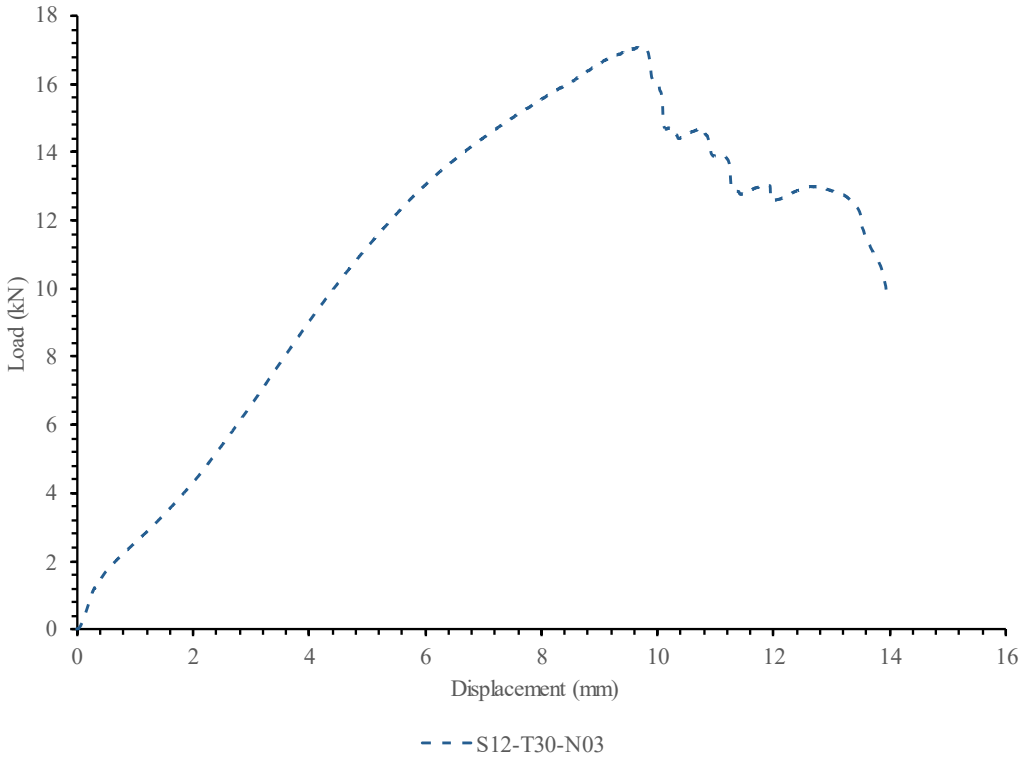

(c)Load v/s displacement curve for three screw of 12mm steel and 30mm timber

Figure 74 Test result of S12-T30-N03

(a)Test setup

(b)Post-tested samples

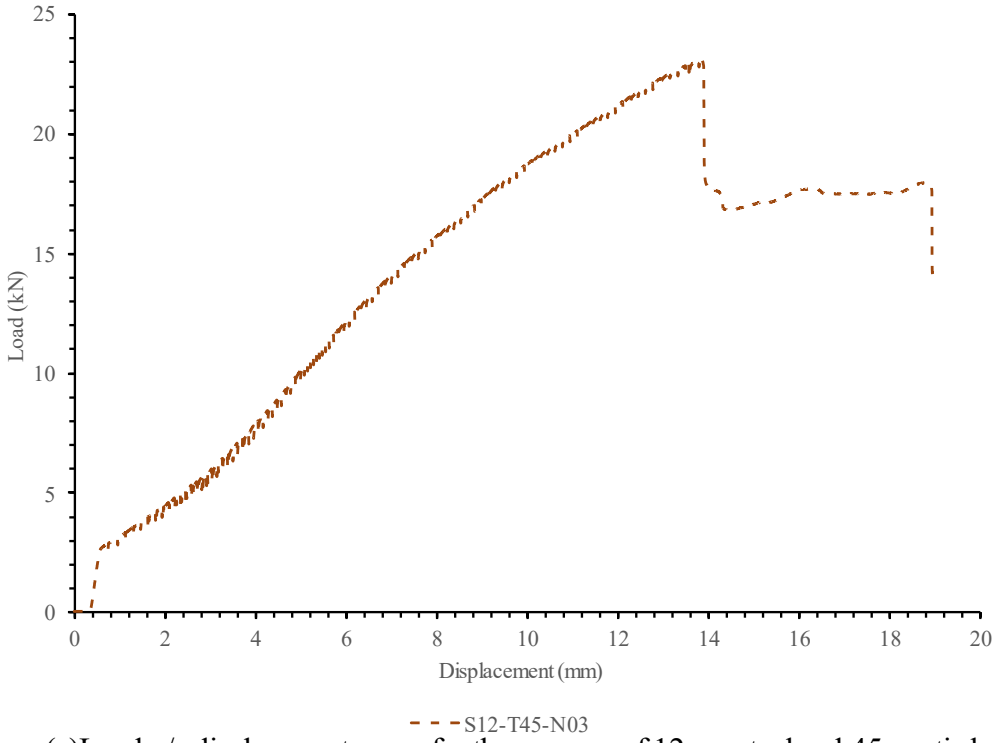

(c)Load v/s displacement curve for three screw of 12mm steel and 45mm timber

Figure 75 Test result of S12-T45-N03

(a)Test setup

(b)Post-tested samples

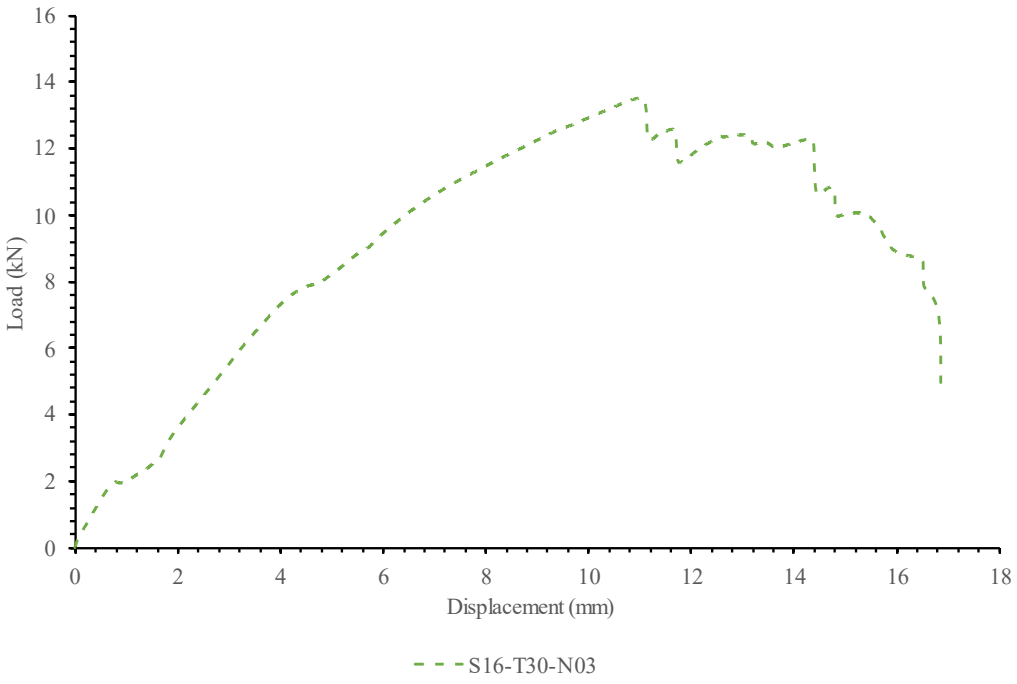

(c)Load v/s displacement curve for three screw of 16mm steel and 30mm timber

Figure 76 Test result of S16-T30-N03

(a)Test setup

(b)Post-tested samples

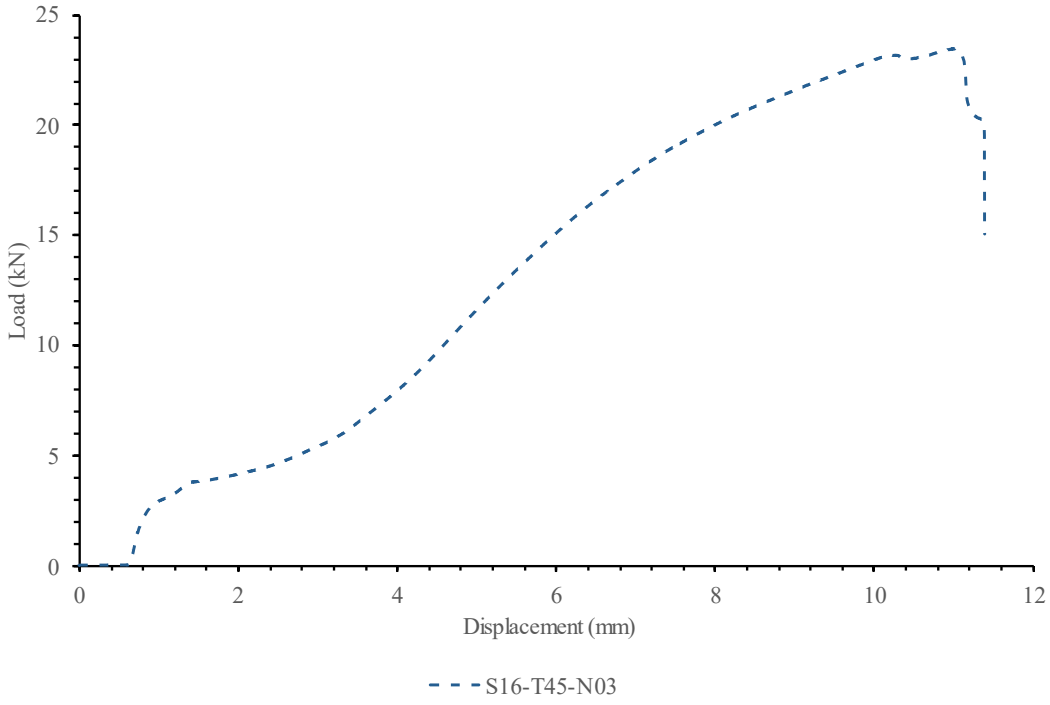

(c)Load v/s displacement curve for three screw of 16mm steel and 45mm timber

Figure 77 Test result of S16-T45-N03

(a)Test setup

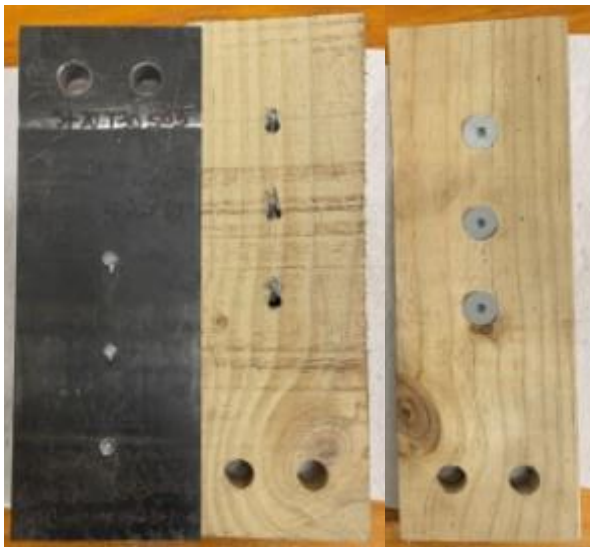

(b)Post-tested samples

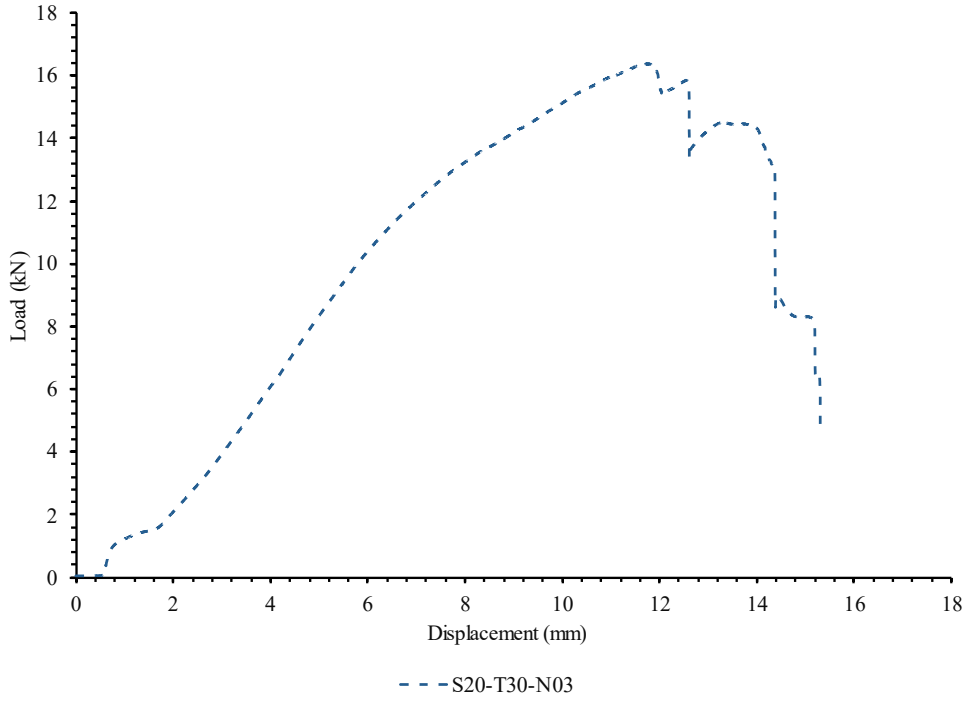

(c)Load v/s displacement curve for three screw of 20mm steel and 30mm timber

Figure 78 Test result of S20-T30-N03

(a)Test setup

(b)Post-tested samples

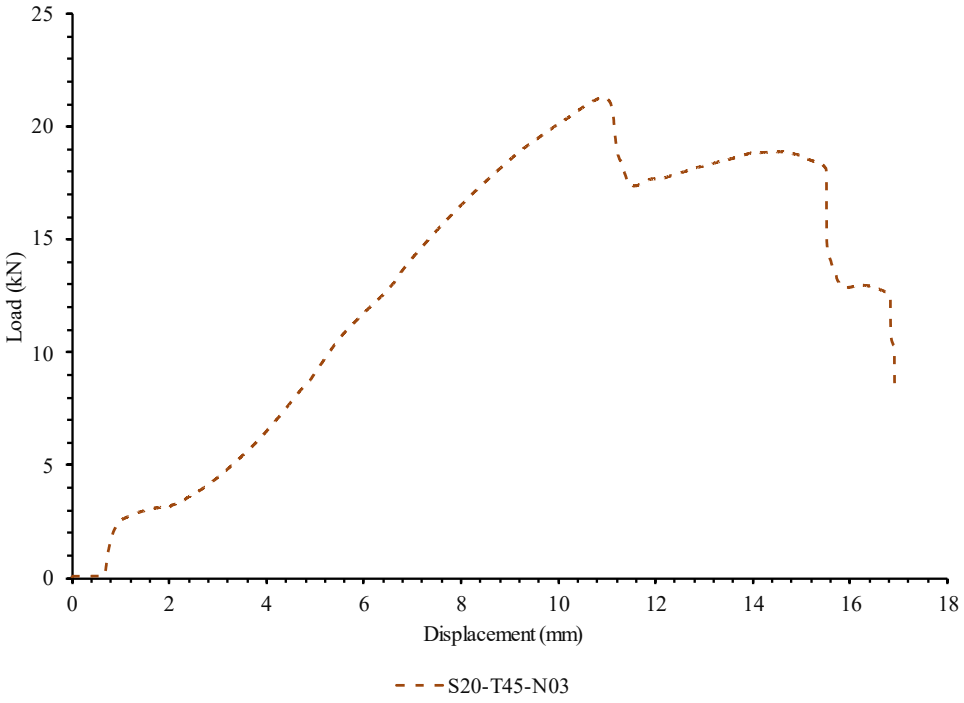

(c)Load v/s displacement curve for three screw of 20mm steel and 45mm timber

Figure 79 Test result of S20-T45-N03

Appendix D Shear test for 110 mm length single screw connection screw connection

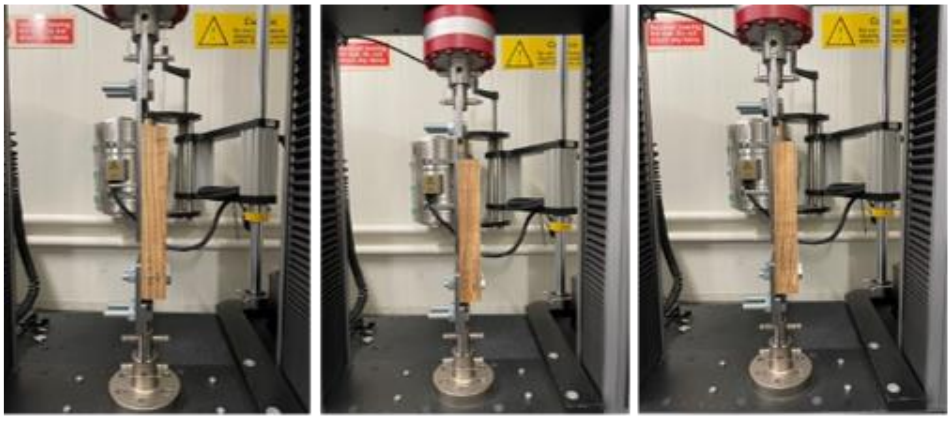

(a)Test setup

(b)Post-tested samples

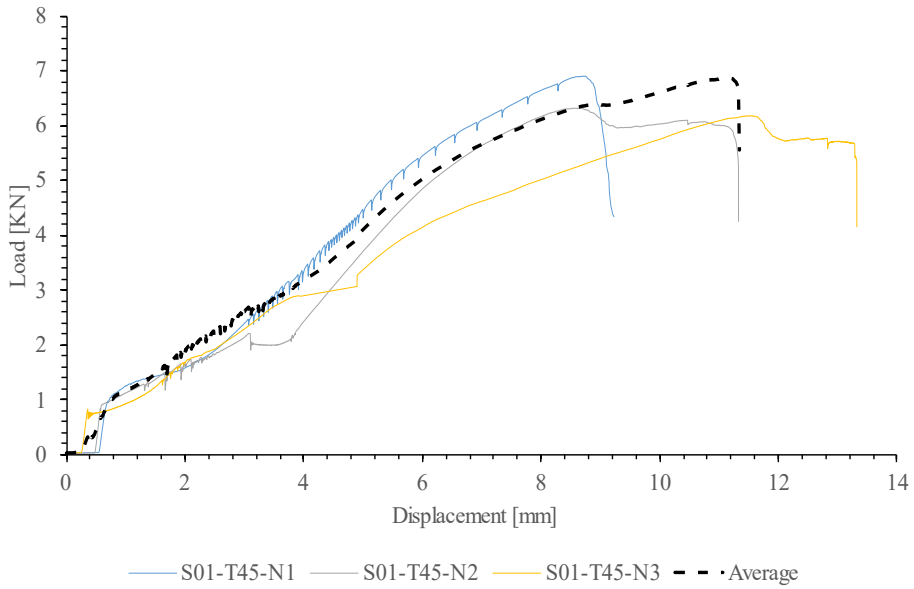

Figure 80 Test result of S08-T45-N01-110 mm screw

Appendix E Shear test for incline screw connection

(a)Test setup

(b)Post-tested samples

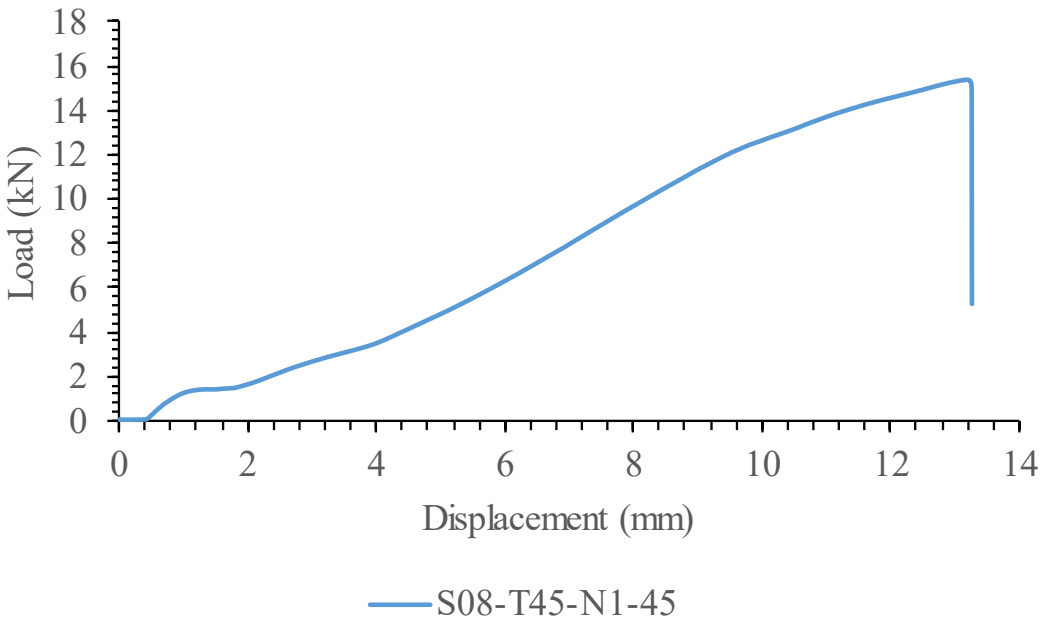

(c)Load v/s displacement curve for 45 -degree incline screw of 8mm steel and 45mm timber

Figure 81 Test result of S08-T45-N01-45

(a)Test setup (b)Post-tested samples

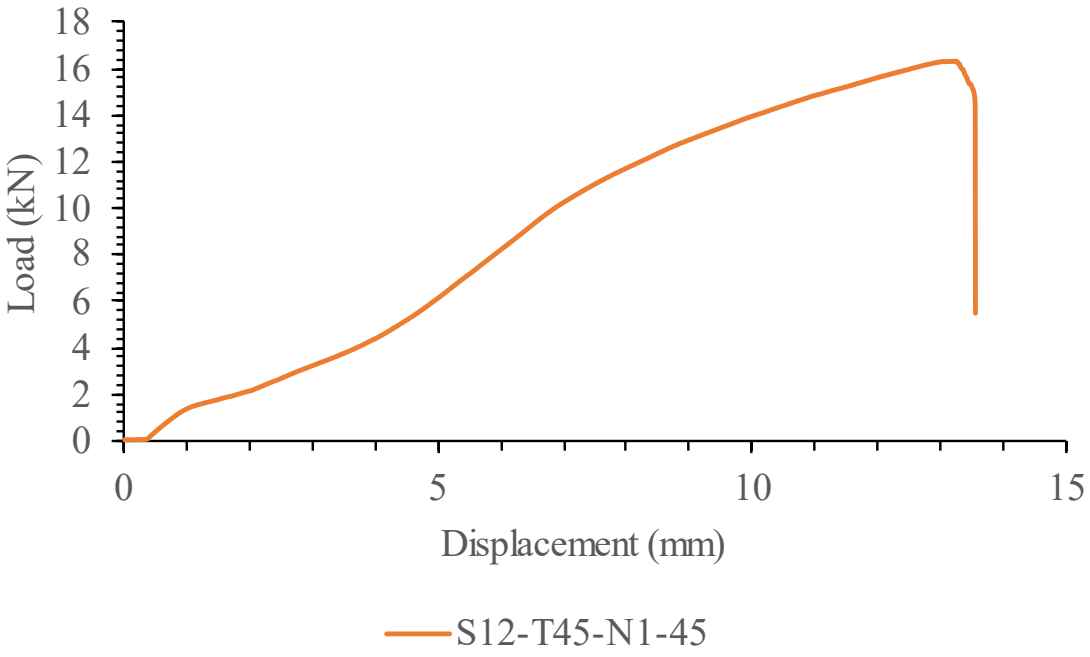

(c)Load v/s displacement curve for 45 -degree incline screw of 12mm steel and 45mm timber

Figure 82 Test result of S12-T45-N01-45

(a)Test setup

(b)Post-tested samples

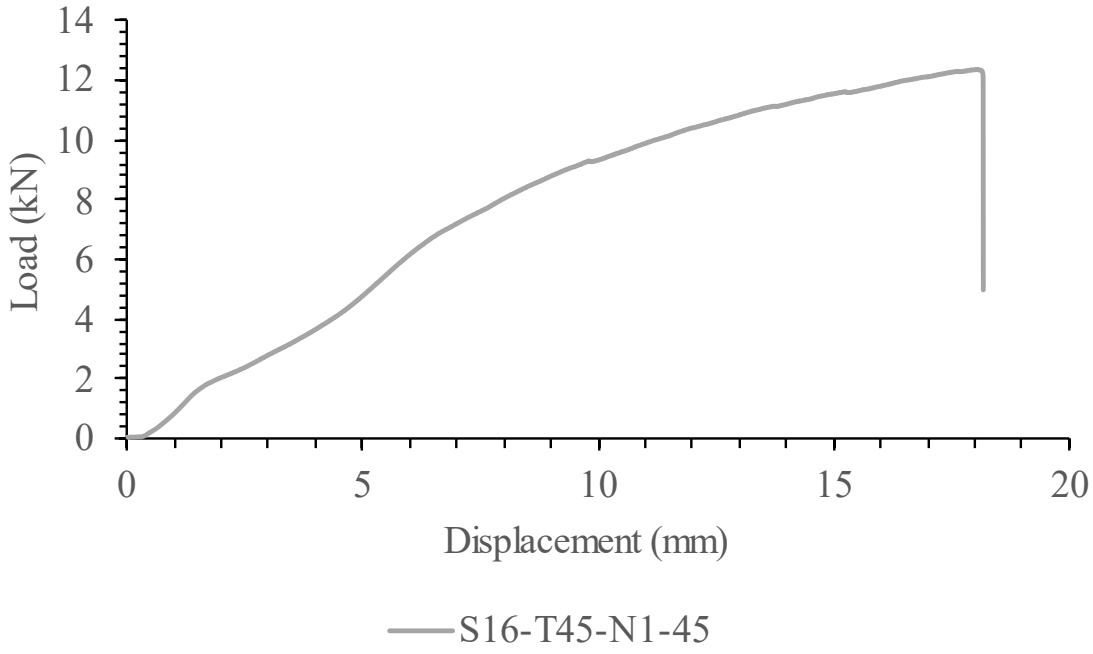

(c)Load v/s displacement curve for 45 -degree incline screw of 16mm steel and 45mm timber

Figure 83 Test result of S16-T45-N01-45

(a)Test setup

(b)Post-tested samples

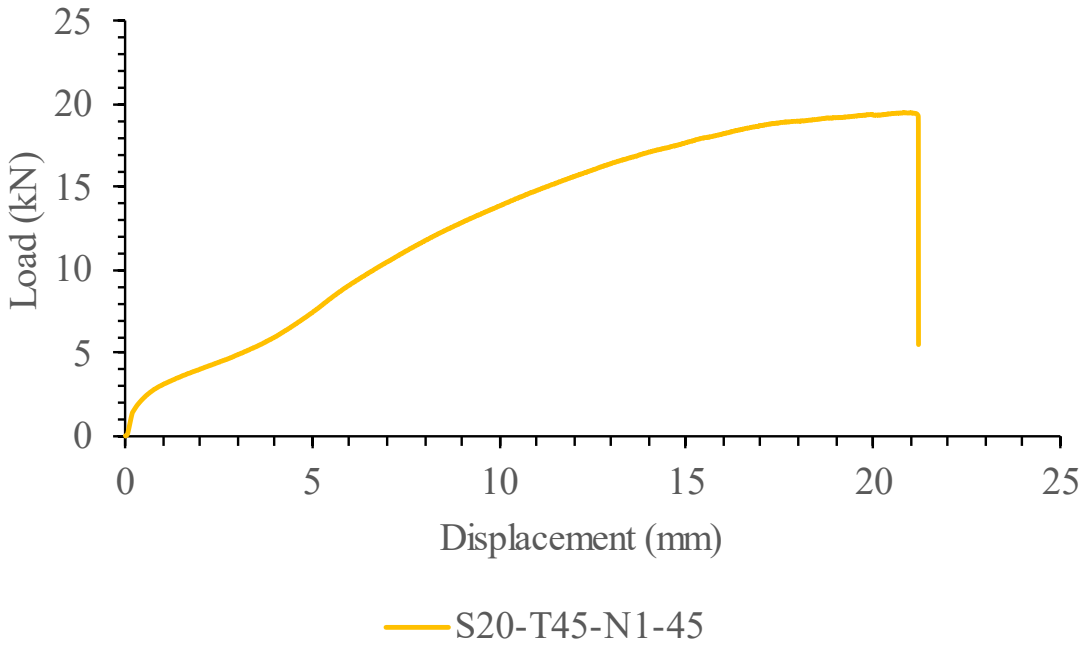

(c)Load v/s displacement curve for 45 -degree incline screw of 20mm steel and 45mm timber

Figure 84 Test result of S20-T45-N01-45

Appendix F Eurocode 5 design equation

$$F_{v,Rk} = \begin{cases} 0.4 f_{h,k} t_1 d & (a) \\ 1.15\sqrt{2M_{y,Rk} f_{h,k} d} + \frac{F_{ax,Rk}}{4} & (b) \\ f_{h,k} d t_1 & (c) \\ f_{h,k} d t_1 \left[\sqrt{2 + \frac{4M_{y,Rk}}{f_{h,k} d t_1^2}} - 1\right] + \frac{F_{ax,Rk}}{4} & (d) \\ 2.3\sqrt{M_{y,Rk} f_{h,k} d} + \frac{F_{ax,Rk}}{4} & (e) \end{cases} \quad (1)$$

Where,

$$F_{ax,\alpha,Rk} \begin{cases} f_{ax,k} d t_{pen} \\ f_{head,k} {d^2}_h \end{cases} \quad (2)$$

$$f_{ax,k} = 20 \times 10^{-6} \rho_k^2 \quad (3)$$

$$f_{head,k} = 70 \times 10^{-6} \rho_k^2 \quad (4)$$

$$M_{y,Rk} = 0.45 f_u d^{2.6} \quad (5)$$

$$f_{h,k} = 0.082(1 - 0.01d)\rho k \quad (6)$$

Density of timber ρk = 494.97 kg/m^3

Tensile Strength of wire = 569.49 N/mm^2

Screw head diameter = 20 mm

Screw nominal diameter = 6.3 mm

Effective Diameter d_{ef} = 5.4 mm

Characteristic yield moment of the screw

$M_{y,Rk} = 0.45 f_u d^{2.6}$

$M_{y,Rk} = 20555.23$ N.mm

Embedment strength in timber

$f_{h,k} = 0.082(1-0.01d)\rho k$

$f_{h,k} = 38.40$ N/mm^2

Characteristic withdrawal strength

$f_{ax,k} = 20\times10^{-6} \times \rho_k^2$

$f_{ax,k} = 4.90$ kg/m^3

$f_{head,k} = 70\times10^{-6} \times \rho_k^2$

$f_{head,k} = 17.15$ kg/m^3

Table 19 Characteristic withdrawal capacity calculation

Timber thickness(mm)	T_p (pont side penetration length) (mm)	$f_{ax,k}\ dt_{pen}$	$f_{head,k}d^2_h$	$F_{ax,Rk}$
15	43	1137.76	6859.87	1137.76
30	28	740.87	6859.87	740.87
45	13	343.97	6859.87	343.97

Table 20 Shear capacity calculation based on Eurocode-5

Timber thickness(mm)	Mode C (N)	Mode D (N)	Mode E (N)	Shear Capacity(N)	Corresponding failure mode
15	3110.06	3207.16	5032.63	3110.06	C
30	6220.12	3682.75	5218.1	3682.75	D
45	9330.18	4582.01	5304.1	4582.01	D

Table 21 Load carring capacity calculation for multiple screw based on Eurocode-5

Number of screws	Timber thickness(mm)	n_{ef}	F_{vrk} (N)	F_{vefrk} (N)
1	15	1	3110.06	3110.06
1	30	1	3682.75	3682.75
1	45	1	4582.01	4582.01
2	15	0.85	3110.06	5287.1
2	30	0.85	3682.75	6260.68
2	45	0.85	4582.01	7789.42
3	15	0.85	3110.06	7930.65
3	30	0.85	3682.75	9391.01
3	45	0.85	4582.01	11684.1

Appendix G Proposed design equation

For Failure mode C,

$$F_{v,Rk} = f^{1.69}_{h,k} d^{0.33} t^{0.97}$$

For Failure mode D,

$$F_{v,Rk} = f_{h,k} d t_1 \left[\sqrt{2 + \frac{4 M_{y,Rk}}{f_{h,k} d t_1^{1.43}}} - 1.2 \right] + \frac{F_{ax,Rk}}{1.98}$$

For Failure mode E,

$$F_{v,Rk} = 3.32 \sqrt{M_{y,Rk} f_{h,k} d} + \frac{F_{ax,Rk}}{0.31}$$

Where,

$$F_{ax,\alpha,Rk} \begin{cases} f_{ax,k} d t_{pen} \\ f_{head,k} d^2{}_h \end{cases} \quad (2)$$

$$f_{ax,k} = 20 \times 10^{-6} \rho_k^2 \quad (3)$$

$$f_{head,k} = 70 \times 10^{-6} \rho_k^2 \quad (4)$$

$$M_{y,Rk} = 0.45 f_u d^{2.6} \quad (5)$$

$$f_{h,k} = 0.082(1 - 0.01d)\rho k \quad (6)$$

Density of timber ρk = 494.97 kg/m^3

Tensile Strength of wire = 569.49 N/mm^2

Screw head diameter = 20 mm

Screw nominal diameter = 6.3 mm

Effective Diameter d_{ef} = 5.4 mm

Characteristic yield moment of the screw

$M_{y,Rk} = 0.45 f_u d^{2.6}$

$M_{y,Rk}$ = 20555.23 N.mm

Embedment strength in timber

$f_{h,k} = 0.082(1-0.01d)\rho k$

$f_{h,k}$ = 38.40 N/mm^2

Characteristic withdrawal strength

$f_{ax,k} = 20\times10^{-6} \times \rho_k^2$

$f_{ax,k}$ = 4.90 kg/m^3

$f_{head,k} = 70\times10^{-6} \times \rho_k^2$

$f_{head,k}$ = 17.15 kg/m^3

Table 22 Characteristic withdrawal capacity calculation

Timber thickness(mm)	T_p (pont side penetration length) (mm)	$f_{ax,k}\ dt_{pen}$	$f_{head,k}d^2_h$	$F_{ax,Rk}$
15	43	1137.76	6859.87	1137.76
30	28	740.87	6859.87	740.87
45	13	343.97	6859.87	343.97

Table 23 Shear capacity calculation based on proposed equation

	Specimen	N_{ef}	$f_{\{h,k\}}$ in N/mm2	$M_{(y,Rk)}$	$F_{(ax,\alpha,Rk)}$	Failure capacity (N)
Failure mode C	S12-T15-N1	1.00	38.40	20550.33	1137.76	5906.34
	S16-T15-N1	1.00	38.40	20550.33	1137.76	5906.34
	S08-T15-N2	1.80	38.40	20550.33	1137.76	5906.34
	S16-T15-N2	1.80	38.40	20550.33	1137.76	5906.34
	S16-T30-N2	1.80	38.40	20550.33	740.87	7407.68
Failure mode D	S08-T15-N1	1.00	38.40	20550.33	1137.76	6774.08
	S08-T30-N1	1.00	38.40	20550.33	740.87	6862.79
	S12-T30-N1	1.00	38.40	20550.33	740.87	6862.79
	S16-T30-N1	1.00	38.40	20550.33	740.87	6862.79
	S20-T15-N1	1.00	38.40	20550.33	1137.76	6774.08
	S20-T30-N1	1.00	38.40	20550.33	740.87	6862.79
	S08-T30- N2	1.80	38.40	20550.33	740.87	6862.79
	S12-T15-N2	1.80	38.40	20550.33	1137.76	6774.08
	S12-T30-N2	1.80	38.40	20550.33	740.87	6862.79
	S16-T45-N2	1.80	38.40	20550.33	343.97	6905.20
	S20-T15-N2	1.80	38.40	20550.33	1137.76	6774.08
	S20-T30-N2	1.80	38.40	20550.33	740.87	6862.79
	S20-T45-N2	1.80	38.40	20550.33	343.97	6905.20
	S12-T30-N3	2.54	38.40	20550.33	740.87	6862.79
	S16-T30-N3	2.54	38.40	20550.33	740.87	6862.79

	S20-T30-N3	2.54	38.40	20550.33	740.87	6862.79
Failure mode E	S08-T45-N1	1.00	38.40	20555.23	343.97	7956.36
	S12-T45-N1	1.00	38.40	20555.23	343.97	7956.36
	S16-T45-N1	1.00	38.40	20555.23	343.97	7956.36
	S20-T45-N1	1.00	38.40	20555.23	343.97	7956.36
	S08-T45-N2	1.80	38.40	20555.23	343.97	7956.36
	S12-T45-N2	1.80	38.40	20555.23	343.97	7956.36
	S08-T30-N3	2.54	38.40	20555.23	740.87	9230.35
	S08-T45-N3	2.54	38.40	20555.23	343.97	7956.36
	S12-T45-N3	2.54	38.40	20555.23	343.97	7956.36
	S16-T45-N3	2.54	38.40	20555.23	343.97	7956.36
	S20-T45-N3	2.54	38.40	20555.23	343.97	7956.36